THE UNIVERSITY OF CALGARY

CARBON AND OXYGEN ISOTOPE COMPOSITIONS OF TREE RINGS FROM A RECENT *Tamarix aphylla* SPECIMEN, DEATH VALLEY, CALIFORNIA

by

Zhong Chen

A THESIS

SUBMITTED TO THE FACULTY OF GRADUATE STUDIES

IN PARTIAL FULFILLMENT OF THE REQUIREMENTS FOR THE
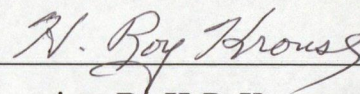
DEGREE OF MASTER OF SCIENCE

DEPARTMENT OF PHYSICS AND ASTRONOMY

CALGARY, ALBERTA

JUNE, 1996

THE UNIVERSITY OF CALGARY
FACULTY OF GRADUATE STUDIES

The undersigned certify that they have read, and recommend to the Faculty of Graduate Studies for acceptance, a thesis entitled, "Carbon and Oxygen Isotope Compositions of Tree Rings from a Recent *Tamarix aphylla* Specimen, Death Valley, California" submitted by Zhong Chen in partial fulfillment of the requirements for the degree of Master of Science.
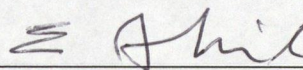
Supervisor, Dr. H. R. Krouse
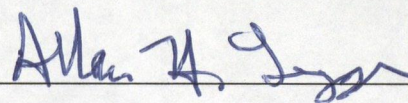Department of Physics and Astronomy

Dr. R. B. Hicks
Department of Physics and Astronomy

Dr. E. F. Milone
Department of Physics and Astronomy

Dr. A. H. Legge
Biosphere Solutions, Calgary

Date _August 06, 1996_

Abstract

Carbon and oxygen isotope abundances were determined in tree rings of a 50 year old specimen of *Tamarix aphylla* from Death Valley, California. The data could be best interpreted in terms of three growth stages. The third stage could be divided into three intervals. These stages coincide with those deduced independently from the $\delta^{34}S$ values of sulfur in tree rings by Yang *et al* (1996).

After correction for changes in atmospheric CO_2 due to fossil fuel combustion, good correlations were found among the five year running averages of $\delta^{13}C$ values, ring width, and precipitation for the three intervals of Stage III. For Stage II, good correlation was only found between $\delta^{13}C$ values and precipitation.

Changes in physiological behavior and isotope data reflect sources of water. Early roots were only in the vadose zone but as the tree grew, they penetrated the water table.

Acknowledgements

To my father, Xican Chen

and

my mother, Caiyun Chen

TABLE OF CONTENTS

LIST OF TABLES

LIST OF FIGURES

CHAPTER 1 INTRODUCTION

1.1 Motivation, Objectives, and Scope of the Study

Among the many triumphs of stable isotope research over the past four decades has been the recognition of three different photosynthetic pathways in different plant groups using carbon isotope data. In addition to the better understanding of fundamental internal plant processes, there have been many applications including food web studies, diets of ancient peoples, food adulteration, and historical changes in atmospheric CO_2 due to fossil fuel combustion. An important question being currently addressed by a few researchers is how the carbon isotope compositions of tree rings relate to past climate.

There is growing global concern about the increase in area of arid and semi-arid regions of the world. The survival of vegetation in the associated unfavorable environment, e.g. soil with high salt content and low rainfall, is an important research topic.

A slab cut from a trunk of a recent *Tamarix aphylla* specimen which grew over 50 years in Death Valley, California, became available to the Stable Isotope Laboratory at the University of Calgary. This provided an exciting research opportunity to pursue the objectives of determining how the stable isotope compositions of carbon and oxygen in recent growth rings of a tree growing under such adverse conditions relate to past climate and other parameters. An associated objective was to deduce from correlations between isotope data and other available parameters, how growth characteristics such as stomatal behavior and root development changed during the life of the tree.

1.2 Stable Isotopes

Isotopes are defined as atoms which have the same number of protons but a different number of neutrons. Isotopes can be divided into stable and unstable (radioactive) species. The term "stable" is relative, depending on the detection limits of radioactivity decay times. In many cases, one isotope is predominant, the others being present in minor relative concentrations. For example, in the earth's atmosphere, $^{16}_{8}O$ accounts for 99.75 % , $^{17}_{8}O$ for 0.037 % and $^{18}_{8}O$ for 0.204 % of the total oxygen in O_2.

1.2.1 Stable isotopic composition notation

The absolute abundance of an isotope (e.g., ^{18}O concentration) or absolute abundance ratios (e.g., $^{18}O/^{16}O$) are difficult to determine with sufficient accuracy for practical applications. In most investigations, it is sufficient to work with relative isotopic abundances (as described below). Relative abundances can be measured with much better precision than the accuracy obtainable in measuring absolute values.

The isotopic composition of a certain sample is usually expressed with the differential notation, in units of permil ($^0/_{00}$) or parts per thousand:

$$\delta\chi(\%_0) = \left[\frac{R_{sample}}{R_{standard}} - 1\right] * 1000 \qquad (1.1)$$

where χ can be D, ^{13}C, ^{18}O etc., and usually

$$R = \frac{the\ number\ of\ heavy\ atoms}{the\ number\ of\ light\ atoms} \qquad (1.2)$$

i.e., D/H, $^{13}C/^{12}C$, $^{18}O/^{16}O$ in the sample or standard.

For hydrogen and oxygen isotopes, SMOW (Standard Mean Ocean Water), a mixture of oceanic samples, was historically the internationally accepted reference. Because the supply was soon exhausted, this reference was replaced by one prepared under the guidance of the International Atomic Agency in Vienna and designated V-SMOW.

The measurements of $^{18}O/^{16}O$ abundance ratios are usually carried out with a mass spectrometer using CO_2 gas which can be easily prepared from a variety of materials and conveniently transferred cryogenically in vacuum systems.

The historical standard for stable carbon isotope composition measurement was CO_2 gas obtained by reacting a Belemnite fossil from the Peedee Formation of Carolina, U.S.A. with 100 percent phosphoric acid, and termed PDB. In modern practice, carbonate references based on a V-PDB scale have been circulated by the IAEA, Vienna. Carbon isotope abundances are also analyzed using CO_2 in gas mass spectrometers.

Another useful definition in stable isotope research is the "fractionation factor", α. It is defined as the ratio of the R values for two chemical compounds A and B or different physical states of the same compound (e.g., liquid and vapor):

$$\alpha_{A-B} = \frac{R_A}{R_B} \qquad (1.3)$$

In dealing with carbon stable isotope fractionation in plants, the term isotope discrimination, Δ, is used, defined by

$$\Delta = 1000 * (1 - R_{product} / R_{source}) \tag{1.4}$$

From this definition and Eq. 1.1, discrimination can be written as

$$\Delta = \frac{\delta_{source} - \delta_{product}}{1 + \delta_{source} / 1000} \tag{1.5}$$

1.2.2 Stable isotope fractionation

Isotope fractionation refers to the altering of isotope abundances during chemical and physical processes as the consequence of differences in nuclidic masses. Because the isotopes for a given element have the same number and arrangement of electrons, then chemical behaviors are very similar. However due to the mass differences of isotopes, isotopic compounds differ in their physicochemical properties (e.g., reaction rates, diffusion rates).

The magnitude of isotope fractionation increases with the relative mass difference between isotopes ($\Delta m / \bar{m}$). Therefore mass-dependent isotope abundance variations in nature are significant for the light elements, e.g., H, B, C, N, O and S. Since these elements participate in biologically and/or geologically important reactions, they are often studied isotopically.

The main phenomena producing isotope fractionations are isotope exchange reactions and kinetic processes.

Isotope exchange may involve different molecules or different phases of the same molecule. A typical isotope exchange reaction can be written as:

$$aA_1 + bB_2 \overset{\rightarrow}{\underset{\leftarrow}{}} aA_2 + bB_1 \qquad (1.6)$$

where the subscripts 1 and 2 refer to the light and heavy isotopes respectively of the element of interest; "a" and "b" are the number of moles of molecules "A" and "B" that have exchanged the isotopes. The isotopic equilibrium constant, K, may be expressed in terms of the partition functions Q of the various species (Urey, 1947; Bigeleisen and Mayer, 1947):

$$K = \frac{\dfrac{Q_{A_2}}{Q_{A_1}}}{\dfrac{Q_{B_2}}{Q_{B_1}}} \qquad (1.7)$$

and α is related to the equilibrium constant K by :

$$\alpha = K^{1/n} \qquad (1.8)$$

where n is the number of atoms exchanged.

A kinetic isotope effect occurs when the rate constants of a chemical reaction are isotopically dependent. During unidirectional chemical conversions, the lighter isotope species usually react faster and the isotope fractionation may be expressed as the ratio of the isotopic rate constants:

$$A_1 + B \xrightarrow{k_1} x_1 + \ldots \quad \ldots$$

(1.9)

$$A_2 + B \xrightarrow{k_2} x_2 + \ldots \quad \ldots$$

(1.10)
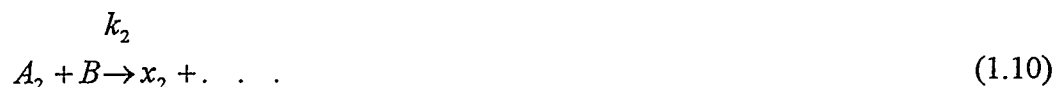
Here the lighter isotopic molecule A_1 with a rate constant k_1 competes with the heavier isotopic molecule A_2, with a rate constant, k_2. Using the "absolute reaction rate theory" with the concept of an "activated complex" developed by Eyring(1935), Bigeleisen (1949) formulated the theory of kinetic isotopic effects in such unidirectional conversions. The ratio of rate constants for the reaction may be written as:

$$\frac{k_1}{k_2} = \frac{\frac{Q_2}{Q_1}}{\frac{Q_2^*}{Q_1^*}} * \frac{V_{1L}^*}{V_{2L}^*}$$

(1.11)

The terms Q_2/Q_1 and Q_2^*/Q_1^* are ratios of isotopic partition functions for the reactants and activated complexes respectively. This expression omits the transmission coefficient and Wigner tunneling correction of absolute rate theory. The term V_{1L}^*/V_{2L}^* is the ratio of isotopic frequencies which can be expressed as an isotopic mass ratio characteristic of bond rupture in the activated state.

CHAPTER 2   STABLE C AND O ISOTOPE FRACTIONATION
IN PLANTS

Many species of continental plants on the earth can be divided into three different categories on the basis of their photosynthetic pathways: C_3 (Calvin-Benson), C_4 (Hatch-Slack) and CAM (Crassulacean acid metabolism). Historically, identification of these pathways was aided by the fractionation of carbon isotope during photosynthesis (e.g., Bender, 1968; Tregunna et al, 1970; Smith and Epstein, 1970; Bender, 1971). Analogous studies have been extended to other elements (H, N, O) (e.g., Libby, 1972; Epstein et al, 1976; Gray and Thompson, 1976, 1977; Burk and Stuiver, 1981).

2.1 Photosynthesis and Carbon Stable Isotope Discrimination in Plants

Photosynthesis in plants occurs on land and in water. For the former, the carbon source is atmospheric CO_2. Its $\delta^{13}C$ value has steadily decreased over time because of burning of fossil fuels ($\delta^{13}C \sim -26\ ^0/_{00}$). From 1956 to 1982, $\delta^{13}C$ has decreased from $-6.7\permil$ (concentration 314 ppm) to $-7.9\permil$ (concentration 342 ppm) (Keeling et al, 1979; Mook et al, 1983). In aqueous systems, dissolved carbonate species constitute the carbon source with $\delta^{13}C$ values near $0\permil$ in the ocean but ranging down to $-20\permil$ in freshwater.

2.1.1 Photosynthetic pathways

The fractionation of carbon isotopes during photosynthesis involves several distinct biochemical and physical processes that compete for control of CO_2 fixation. These processes have different tendencies to discriminate between ^{12}C and ^{13}C. The overall discrimination of a particular plant depends upon the photosynthetic mechanism

and in turn on the collective processes. Most models used to calculate the stable carbon isotope discrimination during photosynthesis are based on a simplified two-step sequence. In the first step (biophysical), atmospheric carbon dioxide, $[CO_2]_a$, diffuses into the plant and becomes internal carbon dioxide, $[CO_2]_i$. This step is reversible. The second step is the irreversible carboxylation reaction where CO_2 (or dissolved carbonate) is used to form the first carboxylation product $R - CO_2^-$

$$[CO_2]_a \underset{k_2}{\overset{k_1}{\underset{\leftarrow}{\rightarrow}}} [CO_2]_i \xrightarrow{k_3} R - CO_2^- \tag{2.1}$$
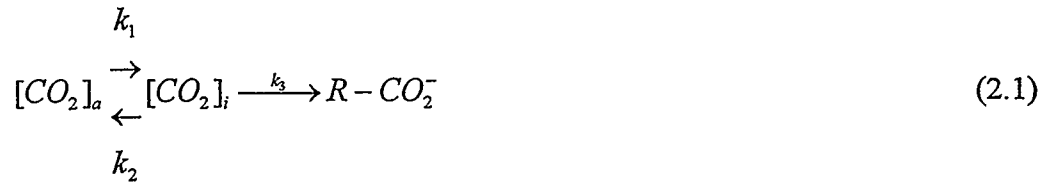
The constants k_1 and k_2 refer to rates of atmospheric CO_2 diffusion into and from the plant respectively. k_3 is the rate constant for enzymatic fixation (carboxylation), which may vary among plants and depends on environmental factors for a given species.

The first step involves the differential diffusivities of CO_2 containing ^{12}C and ^{13}C through the stomate. The diffusivity, D_{12}, of a gas designated "1" in another designated "2", depends on molecular shapes and interaction potentials and is also inversely proportional to the square root of the reduced masses of gases 1 and 2 (Mason and Marrero, 1970).

$$D_{12} \propto \left(\frac{m_1 m_2}{m_1 + m_2} \right)^{-1/2} \tag{2.2}$$

The isotopic discrimination, a, associated with diffusion of CO_2 in air is 4.4‰ since the diffusivity of $^{13}CO_2$ is less than that of $^{12}CO_2$ in air (Craig, 1953).

Plants are separated into three different categories according to the different enzymes used in the second step (biochemical).

C_3 plants: These include trees, cereals, sugar beets etc. C_3 plants incorporate CO_2 by carboxylation of ribulose bisphosphate (RuBP). The carbon isotope discrimination during CO_2 incorporation in C_3 plants is determined principally by ribulose bisphosphate carboxylase. The fractionation associated with k_3 may vary from -17‰ to -40‰. The $\delta^{13}C$ values of C_3 plants can vary from -20‰ to -35‰ (Ehleringer, 1989). Since *Tamarix aphylla* undergoes C_3 photosynthesis, the C_3 pathway is described in more detail in the next section.

C_4 plants: These include certain grasses, sugar cane, corn etc.. Phosphoenolpyruvate (PEP) is the enzyme used in the second step for C_4 plants. PEP appears not to discriminate against ^{13}C. Therefore, in C_4 plants, carbon fixation is principally limited by the rate of CO_2 diffusion to the site of fixation. The $\delta^{13}C$ values of C_4 plants can vary from -7 to -15‰ (Ehleringer, 1989).

Crassulacean acid metabolism (CAM) plants: These include succulents such as cacti. CAM plants may either fix atmospheric carbon in the manner of C_3 plants (by use of ribulose bisphosphate carboxylase) or in a C_4-like sequence in which phosphoenolphyruvate is carboxylated, then reduced in the dark forming malate which accumulates in vacuoles. In the following light period, the malate is decarboxylated and the CO_2 thus formed is fixed by ribulose bisphosphate carboxylase. The $\delta^{13}C$ values of CAM plants can vary from -10 to -22‰ (Ehleringer, 1989).

2.1.2 Calvin-Benson (C_3) cycle

A condensed version of the Calvin-Benson cycle is given in Fig. 2.1. The key energetic reactions in this cycle are the reduction of the carboxyl group to the aldehyde group at the C_3 level, and the phosphorylation of ribulose phosphate to the CO_2 acceptor ribulose bisphosphate. There are three major reactions to complete one cycle: (1) the carboxylation of RUDP to form PGA; (2) the reduction of PGA to TP; and (3) the regeneration of RUDP via RU5P. The CO_2 fixation by ribulose bisphosphate carboxylase produces two 3-phosphoglyceric acid molecules which are formed via an extremely unstable C_6 compound. TP serves not only as the starting point for the synthesis of carbohydrates including starch, sugar, and cellulose, but also for fatty acid and amino acid synthesis.

2.1.3 Model for carbon isotope fractionation during C_3 photosynthesis

2.1.3.a Definition of stomatal conductance

Stomata are minute openings which may number in the thousands cm^{-2} in the epidermis. Their function is exchange of gases between the plant and surrounding environment, the important transfers being exhalation of H_2O and O_2 and intake of CO_2.

The stomatal conductance of the leaf and boundary layer to transfer of a certain gas, g (mol $m^{-2}s^{-1}$), was defined by Cowan (1977):

$$g = \frac{D}{lV} \tag{2.3}$$
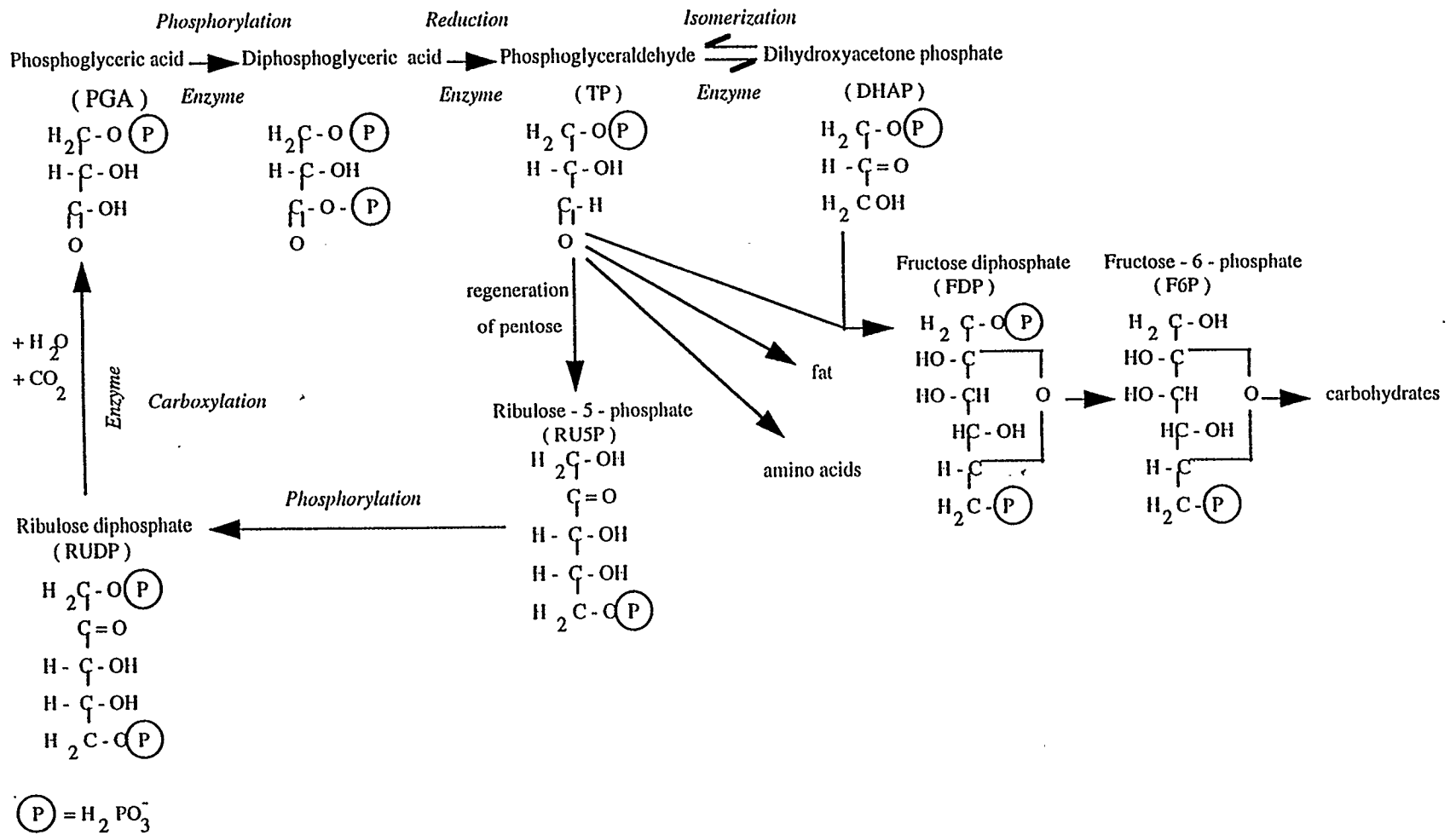
Fig. 2.1 Condensed version of the Calvin cycle (from Deines, 1980)

where D (m^2s^{-1}) = the diffusion coefficient for the gas, V (m^3mol^{-1}) = the molar volume of the gas, and l (m) = the effective path length for diffusion of the gas through the stomatal pore. This equation has been written incorrectly in Mott and Parkhurst (1991). It is noted that other dimensional quantities (e.g. area) may appear on the left side of the definition dependent upon units used for flux (rate of diffusion) but the units for D remain the same.

Usually the stomatal density and pore depth can be assumed to be constant for a given type of leaf. Then the effective path length is primarily a function of stomatal aperture, with small apertures causing longer effective path lengths.

2.1.3.b Model of Farquhar *et al.* (1982)

Several models have been used to describe the fractionation of the carbon isotopes during photosynthesis (e.g. Deleens *et al.*, 1983; Farquhar, 1983; Hattersley, 1982; Peisker, 1985; Reibach and Benedict, 1977). The model established by Farquhar *et al.*(1982) is described below.

The model assumes that of all the steps involved in photosynthesis, the carbon isotope fractionation is determined by two (1) the differential diffusivities of CO_2 containing ^{12}C and ^{13}C through the stomata and, (2) the enzymatic fixation in the carboxylation reaction. The isotope discrimination, a, associated with the differential diffusivities is 4.4 $^0/_{00}$. The value for discrimination in the carboxylation reaction designated "b", ranges from 27 to 30 $^0/_{00}$.

The source of the biochemical discrimination against ^{13}C in C_3 plants lies with the primary carboxylating enzyme, ribulose-1,5-bisphosphate carboxylase (Park and Epstein, 1960) which discriminates against ^{13}C because of the intrinsically lower reactivity of ^{13}C

(Melander and Saunders, 1979). Isotope discrimination by the enzymes may vary with pH, temperature, and metal ion concentrations (O'Leary, 1978). Phosphoenolpyruvate (PEP) carboxylase (as in C_4 and CAM species) appears not to discriminate against ^{13}C, but diffusional and recarboxylation factors play an important role in determining the isotopic composition. Little further discrimination occurs after photosynthesis within the leaf, except during lipid metabolism (DeNiro and Epstein, 1977). It is for this reason that the carbon isotope composition of a tree ring can be related to conditions in a contemporary leaf during photosynthesis.

The molar flux density, A (mol m^{-2}s^{-1}) of $^{12}CO_2$ into the plant from the atmosphere is given by:

$$A = g(p_a - p_i)/P \qquad (2.4)$$

where g is the conductance of the boundary layer and stomatal pores to the diffusion of $^{12}CO_2$, p_a and p_i are the partial pressures of $^{12}CO_2$ in the external atmosphere and in the intercellular spaces, respectively, and P (same units as p_i) is the atmospheric pressure. Equation 2.4 is Fick's first law as can be readily seen by substituting for g from Equation 2.3.

The gradient of concentration of CO_2 from the intercellular spaces to the chloroplasts (where photosynthesis occurs) is assumed to be negligible in comparison to that along the stomatal path. Hence the rate of carboxylation was considered to be first order with respect to p_i (Farquhar et al. 1980)

$$A = k p_i \qquad (2.5)$$

The quantities "A" in Equations 2.4 and 2.5 are equivalent i.e. all CO_2 reaching the chloroplasts undergoes carboxylation.

Solving Eq. 2.5 for p_i, one can eliminate p_i from Eq. 2.4 and Eq. 2.5 giving

$$A = \frac{kg/P}{k+g/P} p_a \qquad (2.6)$$

Analagous equations with primes placed on appropriate quantities, can be written for the diffusion and carboxylation of $^{13}CO_2$.

$$A' = g'(p'_a - p'_i)/P \qquad (2.7)$$

$$A' = k'p'_i \qquad (2.8)$$

$$A' = \frac{k'g'/P}{k'+g'/P} p'_a \qquad (2.9)$$

where the prime refers to $^{13}CO_2$. We also have the following equations

$$g' = g(1 - a/1000) \qquad (2.10)$$

$$k' = k(1 - b/1000) \qquad (2.11)$$

Using the definition of isotopic discrimination given in Equation 1.4 and replacing $R_{product}$ by A'/A and R_{source} by p'_a/p_a gives:

$$\Delta = \left(1 - \frac{A'/A}{p'_a/p_a}\right) * 1000 \qquad (2.12)$$

Dividing Equation 2.9 by Equation 2.6 gives an expression for $(\Delta/\,A)/(\,p'_a/p_a)$. Then substituting for g and k in terms of g' and k' from Equations 2.10 and 2.11 in that expression, leads to the following expression for the discrimination:

$$\Delta = \frac{k'a + g'b/P}{k'+g'/P} \qquad (2.13)$$

From Equation 2.7 we can replace g' by $A\,P/(p'_a - p'_i)$ and from Equation 2.8 this becomes:

$$g' = \frac{k'p'_i P}{p'_a - p'_i} \qquad (2.14)$$

Substituting this into Equation 2.13, we have:

$$\Delta = a + (b-a)p'_i/p'_a \qquad (2.15)$$

Finally, using the definition of isotopic discrimination given in Equation 1.4, and assuming $1+ \delta^{13}C_{atm} \approx 1$, we obtain the following equation:

$$\delta^{13}C = \delta^{13}C_{atm} - a - (b-a)p'_i/p'_a \qquad (2.16)$$

where $\delta^{13}C_{atm}$ and $\delta^{13}C$ are the stable isotope compositions of atmospheric CO_2 and plant respectively.

2.2 Application of Stable Carbon Isotope Abundance Variations to Ecophysiological Studies of Plants

Historically, to avoid the difficulties of chemical heterogeneity in wood samples (described in 2.2.1), a single component, cellulose, which remains relatively stable after its synthesis, was extracted. For hydrogen isotope studies, it was found necessary to remove all oxygen-bound hydrogens which are considered to be exchangeable since their D/H abundance ratio might have changed since the initial synthesis of cellulose(Epstein *et al.*, 1976). However, for oxygen and carbon stable isotope measurements, cellulose can be used directly.

Before the establishment of Farquhar *et al*'s C_3 photosynthetic model, stable carbon isotopes in tree rings were mainly applied to two areas: studies of the evolution of atmospheric CO_2 (e.g. Freyer and Wiesberg, 1973, 1975; Rebello and Wagener, 1976; Pearman *et al.*, 1976) and climate change (e.g. Grinsted *et al.*, 1979; LaMarche, 1974). More recently, stable carbon isotope data have also been used to study plant physiology (e.g. O'Leary, 1988; Farquhar *et al.*, 1989a,b; Ehleringer, 1989; Keeling, 1989; Guy *et al.*, 1989).

In this section, the chemical heterogeneity of wood is described followed by the applications of stable carbon isotopes in tree rings.

2.2.1 Chemical heterogeneity of plant material

Chemically, 95 to 98% of dried plant matter consists primarily of three different materials: cellulose, hemicellulose and lignin. The remaining 2-5% comprises low molecular weight compounds called extractives. Average chemical compositions of plant

material are given in Table 2.1. The amount of each component varies considerably between species and even in the same species in different environments.

Table 2.1 Average % chemical composition of plant material (from Thomas, 1977)

Polymers	SoftWoods	Hardwoods
Cellulose	42 ± 2	45 ± 2
Hemicellulose	27 ± 2	30 ± 5
Lignin	28 ± 3	20 ± 4
Extractives	3 ± 2	5 ± 3

As seen in Table 2.1, cellulose makes up to 42% to 45% of the wood. Cellulose is a polymer of anhydro-D-glucopyranose units linked by β-(1->4) glycosidic bonds. The number of glucose units varies in different natural celluloses. The basic unit of cellulose is the chair conformation shown in Fig. 2.2.
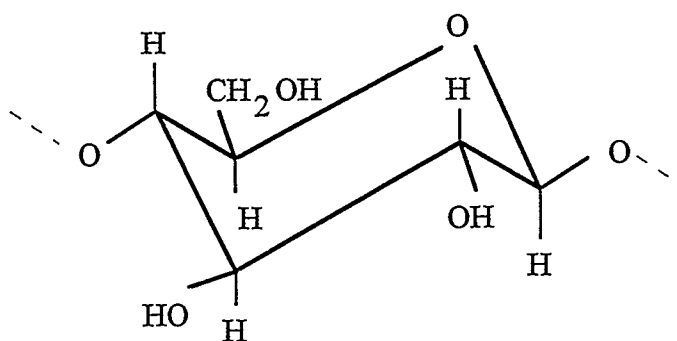
Fig. 2.2 Chair conformation of cellulose

Hemicellulose, which is also termed β-cellulose, is usually branched, whereas cellulose (which is also termed α-cellulose) is unbranched. Lignin is the major non-carbohydrate component of plant material.

2.2.2. Carbon isotopic composition of chemical components

Plant material consists of different components with different solubilities and extraction characteristics when treated with acids, bases, or organic solvents. Sugar, cellulose, and hemi-cellulose have $\delta^{13}C$ values close to the mean value of the plant. However, as seen in Fig. 2.3, there exists big differences in $\delta^{13}C$ values for different organic components, from lipid, which is -5.2±2.4‰, to pectin, which is +3.6±0.9‰ with respect to the total plant. The range in $\Delta^{13}C$ values for the lipid-plant fractionation is quite large since the lipid includes a variety of organic compounds which also have their own distinct isotopic compositions.

Since organic compounds in plants differ in concentration and isotopic composition in different plants and even differ in individual tree rings, $\delta^{13}C$ values from cellulose have been preferred over that of whole plants to derive climatic and other environmental information at the growth site.

2.2.3 Evolution of atmospheric CO_2

One of the most interesting problems is studying the historical change of the $\delta^{13}C$ value of atmospheric CO_2. Some researchers argued that it was feasible to obtain this information from the $\delta^{13}C$ values of tree rings since atmospheric CO_2 is the source for terrestrial plant photosynthesis. Change in the $\delta^{13}C$ value of atmospheric CO_2 over time should be recorded in tree rings. Dequasie and Grey (1970) and Farmer and Baxter (1974) found a trend of decreasing atmospheric $\delta^{13}C$ values with time based on analyses of total wood. Their results indicated nearly -2.6‰ change since the middle of the last century. Freyer and Wiesberg (1973, 1975) and Rebello and Wagener (1976) observed a
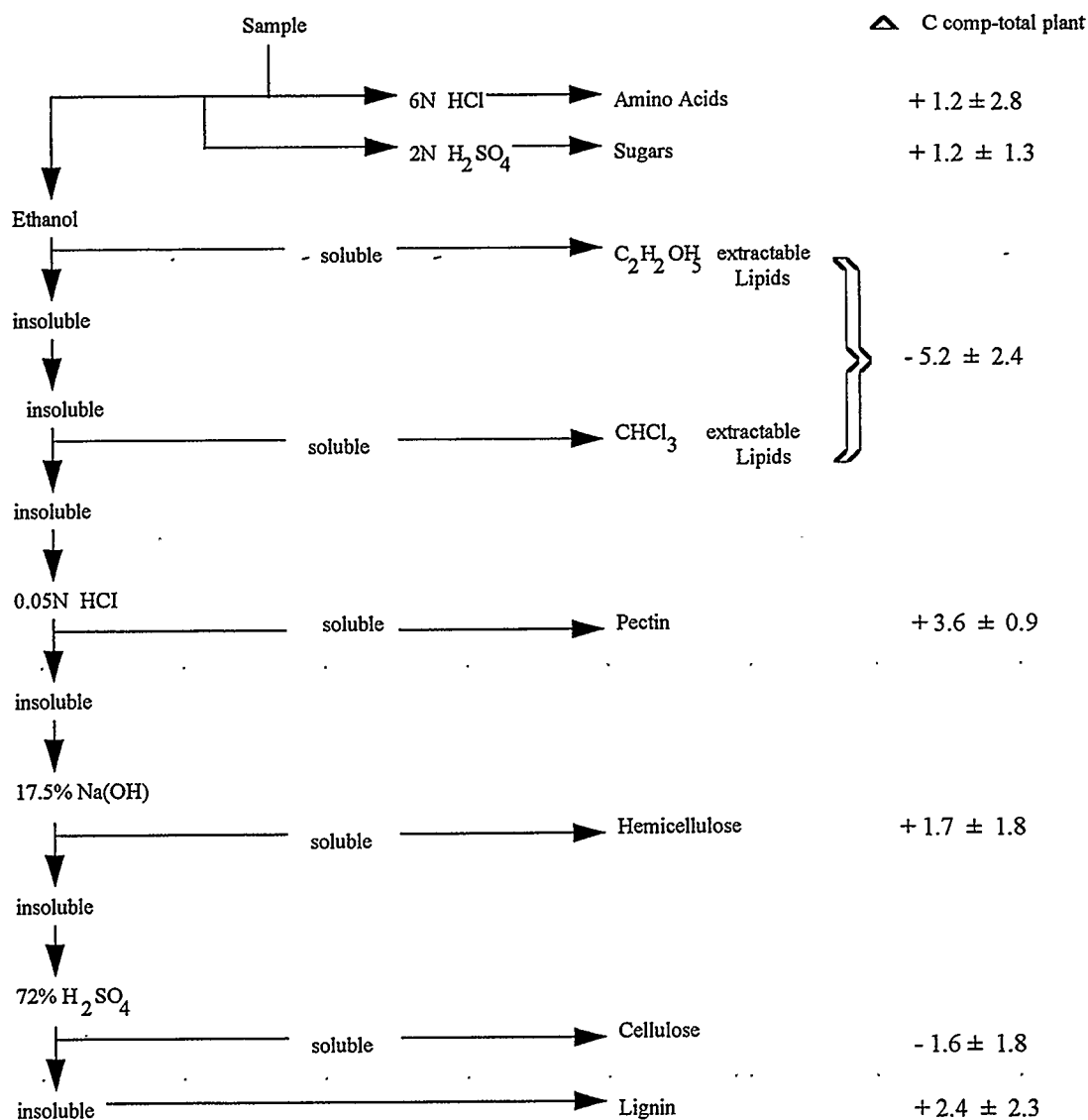
Fig. 2.3 The $\delta^{13}C$ values for different chemical components in plants (from Deines, 1980).

much smaller change on the bases of $\delta^{13}C$ analyses of tree ring cellulose. However, opposite trends were suggested in the work of Jansen (1962) and Galimov (1976).

More recently, on the basis of Eq. 2.13 established by Farquhar *et al.* (1982), Feng and Epstein (1995) argued that the $\delta^{13}C$ time series obtained from tree ring cellulose contain high-frequency variations and a long-term decreasing trend. The high-frequency signals can be effectively explained by variations in precipitation whereas the low-frequency variation is mostly related to changes in open atmospheric conditions, such as the concentration and the $\delta^{13}C$ values of CO_2. They used curve fitting to derive the low-frequency signal which appears to fit well with results obtained by other methods, such as direct $\delta^{13}C$ measurements of atmospheric CO_2 (Keeling, 1958; Keeling *et al.*, 1989) and measurement of the $\delta^{13}C$ values of CO_2 separated from gas bubbles in ice samples (Friedli *et al.*, 1986). Feng and Epstein (1995) deduced that between 1740 and 1988, the change in $\delta^{13}C$ value of atmospheric CO_2 is about -0.44‰ per decade, whereas the change measured by more direct means is only -0.26‰ per decade. The difference of -0.18‰ per decade can be attributed to the affect of changing concentration of atmospheric CO_2 on photosynthesis, which is equivalent to about -0.02 ‰/ppm (Feng and Epstein, 1995).

2.2.4 Dependence of stable carbon isotope fractionation upon environmental factors

Juvenile Effect: For photosynthesis, the main source of the carbon is atmospheric CO_2. Another source of CO_2, especially for young plants, is CO_2 respired by the plants and soil. The $\delta^{13}C$ value of this CO_2 source is lower than that of free atmosphere (~ -20‰, Keeling, 1958; Park and Epstein, 1960). The amount of this CO_2 used by the plant depends on the wind velocity and turbulence, growing stage of a plant and density of nearby vegetation. The effect of wind speed and turbulence are likely to vary seasonally or even daily. Reuse of the respired CO_2 from plant and soil may have long term effects on the $\delta^{13}C$ value of tree rings. This is called the Juvenile Effect. Usually young trees

growing under a canopy utilize more respired CO_2 and therefore $\delta^{13}C$ values increase with age during the first 20-50 years (Feng and Epstein, 1995).

Water Stress and Relative Humidity: Within 2%, c_i / c_a is equal to p'_i / p'_a, where c_i and c_a (unit-less) are the concentrations of intercellular and atmospheric CO_2 (Farquhar et al, 1982), Hence Eq. 2.16 can be written:

$$\delta^{13}C = \delta^{13}C_{atm} - a - (b-a)c_i / c_a$$
$$= \delta^{13}C_{atm} - a - (b-a) \, p_i/p_a \qquad (2.17)$$

where p_i and p_a hereafter are designated as the partial pressures of CO_2 in the intercellular space and atmosphere.

Furthermore

$$c_i = c_a - A / g \qquad (2.18)$$

and then

$$\delta^{13}C = \delta^{13}C_{atm} - a - (b-a)(c_a - A/g) / c_a \qquad (2.19)$$

Where A hereafter is designated as the rate of CO_2 assimilation by the plant and g is the conductance of the boundary layer and stomatal pores to the diffusion of CO_2 (also called leaf conductance).

When soil moisture levels decrease, a common response is simultaneous decreases in photosynthesis, transpiration, and leaf conductance. If supply of CO_2 decreases at a

faster rate under stress than the demand of CO_2 for photosynthesis, then p_i in Eq. 2.17 will decrease. This effect should be manifested as an increment of $\delta^{13}C$. Therefore, plants under water stress induced by low soil moisture have higher $\delta^{13}C$ values.

It has been found that plants in arid region have lower g and c_i under low humidity (Farquhar *et al.*, 1980). Therefore, under high temperature and low precipitation conditions (low humidity), higher $\delta^{13}C$ values are expected from Eqs. 2.18, and 2.19. Lipp *et al.* (1996) showed that the $\delta^{13}C$ value of tree rings of *Tamarix jordanis* growing in Israel is linearly correlated inversely to relative humidity.

Salinity: Smith and Epstein (1970) measured $\delta^{13}C$ values for a variety of C_3 and C_4 plants from salt marshes but made no correlation with salinity. In more localized environments, Guy *et al.* (1980) showed that for the halophytes *Salicornia virginia* and *Spartina foliosa*, increasing salt concentrations resulted in decreased isotope discrimination (i.e. higher $\delta^{13}C$ values in the plant) both in the field and in growth chambers. The total range of discrimination was 10‰. The explanation for this is that increasing salinity initiates a decrease in p_i (Seemann and Critchley, 1985).

Other Factors: It has been shown that many other factors affect carbon isotope discrimination during photosynthesis including light intensity, nutritional status of a plant, temperature, and air pollution. It has been observed that long-term exposure to air pollutants (e.g. ozone, sulfur dioxide) can decrease both leaf conductance and photosynthesis and therefore lower p_i and higher $\delta^{13}C$ values for the tree rings. Greitner and Winner (1988) found $\delta^{13}C$ values to increase with ozone exposure. In a field study, Mayer *et al.* (1994) did not find any significant differences in the $\delta^{13}C$ values of needles

from *Pinus contorta* Lond. × *Pinus* banksiand Lamb exposed to different long term levels of industrial SO_2 emissions.

2.3 Oxygen Isotope Fractionation in Plants

The incorporation and isotopic composition of oxygen in cellulose synthesized at the leaf can theoretically be attributed to the three different sources:

(1) oxygen from carbon dioxide.

(2) oxygen from water.

(3) oxygen input via photorespiration.

Although oxygen from the carbon dioxide is incorporated into carbohydrates during the carboxylation reaction, its oxygen isotope composition is of no consequence in determining that of cellulose. DeNiro and Epstein (1979) found similar oxygen isotope compositions for cellulose extracted from two sets of wheat plants grown in isotopically similar water, but with CO_2 having largely different $\delta^{18}O$ values. The third potential source of oxygen has not been extensively evaluated, but studies with labeled O_2 have shown that any labelling effect of O_2 via photorespiration may be lost during the Calvin cycle (Berry *et al.* 1978). The conclusion drawn is that water is the principal agent governing the oxygen isotope composition of cellulose. Several studies (Epstein *et al,* 1977; DeNiro and Epstein, 1981; Sternberg and DeNiro, 1983; Sternberg *et al,* 1984; Sternberg *et al,* 1986a) of several different plants , including plants having different photosynthetic modes, have shown that cellulose oxygen isotope ratios are always $27 \pm 3\ \permil$ higher for the plants than for the water at the site of synthesis.

It has been shown that fractionation of oxygen isotopes does not occur during uptake of soil water through the root and up the stem to the leaf (Gonfiantini *et al*, 1965; Zundel *et al*, 1978). The $\delta^{18}O$ value of leaf water increases because of evapotranspiration (Gonfiantini *et al*, 1965; Ferhi and Letolle, 1977; Lesaint *et al*, 1974). The extent of relative enrichment of $H_2^{18}O$ during evapotranspiration depends on, among other factors, particular physiological characteristics of each species.

How is oxygen from water incorporated into cellulose? Two models have been hypothesized. The first one proposes that prior to incorporation into the Calvin cycle, oxygen in carbon dioxide is at isotopic equilibrium with water in the leaf. Since the amount of water must be greater than that of CO_2, the $\delta^{18}O$ value of carbon dioxide entering the Calvin cycle will essentially be determined by the isotope composition of the water (Epstein *et al*, 1977). This model proposes that no further isotopic exchange occurs after the carbon dioxide is fixed into metabolites. The second model proposes that the oxygen isotope composition of plant cellulose is determined by the carbonyl hydration reaction, which can be expressed by the following equation (DeNiro and Epstein 1981):

$$R_2C = O + H_2O \leftrightarrow R_2C(OH)_2 \qquad (2.20)$$

Several lines of evidence indicate that this latter hypothesis may be correct (DeNiro and Epstein 1981). Sternberg and DeNiro (1983) observed that the $\delta^{18}O$ value of the carbonyl oxygen of acetone is 27‰ higher than that of the water with which it is in equilibrium. This result indicates that the carbonyl hydration reaction is sufficient to render the $\delta^{18}O$ value of cellulose 27‰ higher than that of the water at the site of synthesis. The evidence supporting the carbonyl hydration hypothesis was the observation that carbonyl oxygens of metabolic intermediates exchange with water *in vivo*. This was demonstrated by growing carrot tissue culture, *Acetobacter xylinum* (a cellulose-producing bacteria),

and germinating castor beans in the dark with waters having different $\delta^{18}O$ values (Sternberg *et al.* 1986). If no oxygen isotope exchanges occur after carbon dioxide fixation (as is proposed in the first model), then the $\delta^{18}O$ of the cellulose from these growth experiments should be constant, regardless of the $\delta^{18}O$ values of the water in which these cultures were grown, and match the $\delta^{18}O$ values of the substrate. Alternately, if the oxygen atoms of carbohydrate and water exchange during cellulose synthesis, the $\delta^{18}O$ value of cellulose from these cultures should be strongly correlated with $\delta^{18}O$ value of the water available for growth. The results corroborated the latter expectation: for example, carrot tissue cultures grown on sucrose acquired cellulose with $\delta^{18}O$ values which indicated that about 45 percent of the oxygen atoms in the metabolic pathway between sucrose and cellulose exchange with water. These observations indicate that the percentage of oxygen atoms that exchange with water is similar to the percentage of carbonyl oxygens in the substrate and subsequent intermediates during the pathway of cellulose synthesis. Further, the carbonyl oxygen atoms that exchanged with water during the synthesis of cellulose from glycerol have $\delta^{18}O$ values 27‰ higher than those of the water they exchanged with. This is consistent with the observed 27‰ enrichment in cellulose relative to the water available for growth. These results indicate that the oxygen isotope composition of cellulose may be determined by the carbonyl hydration reaction occurring at the three-carbon-sugar level.

CHAPTER 3 EXPERIMENTAL METHODS AND MASS SPECTROMETRY

3.1. Experimental Methods

3.1.1. Extraction of cellulose

Due to the chemical heterogeneity, three steps (Fig. 3.1) are necessary to extract pure cellulose (alpha-cellulose) from raw wood: (1) Preliminary Treatment, (2) Chloriting, and (3) Alkaline Treatment.

3.1.1.a. The preliminary treatment

The wood samples were ground to pass 40 mesh in a Wiley mill. Then about 3.0 g of sample were extracted in a Soxhlet apparatus with 75 ml : 150 ml benzene:ethanol for 24 hours followed by another 24-hour extraction with 95% ethanol (Green, 1963). A glass thimble instead of the usual paper thimble was used to hold the sample in the extraction apparatus to avoid introducing other cellulosic material. The purpose of this treatment is to remove benzene-ethanol soluble fractions, such as lipid and resin.

The sample was rinsed with 10 ml acetone three times followed by rinsing with distilled water and drying at room temperature.

tree ring samples

extracted with C_6H_6 and C_2H_5OH followed
by C_2H_5OH (24 hours, Soxhlet extractor)

insoluble   soluble, discarded

cellulose, lignin and   waxes, fats, oil, resin
hemicellulose   and other relatively
                                                   mobile components.

bleached and soaked in $NaClO_2$ +
CH_3COOH solution (70 ^0C)

insoluble   soluble, discarded

cellulose and hemicellulose   lignin

soaked in 18% NaOH

insoluble   soluble, discarded

cellulose   hemicellulose

Fig. 3.1 Extraction of Cellulose

3.1.1.b. Chloriting treatment

The sample was then put into a 225-ml Erlenmeyer flask with 100 ml distilled water. The flask was loosely stoppered with an inverted 25-ml Erlenmeryer flask. Then the 225-ml Erlenmeyer flask was placed in a temperature controlled water bath. After heating to 70 ^{0}C, about 0.4 ml of glacial acetic acid was added followed by about 0.9 g of technical-grade sodium chlorite. After about 50 minutes of heating at 70 ^{0}C, fresh portions of acetic acid and sodium chlorite were added on two occasions to produce a white to slightly yellow sample (Green, 1963). The sample was then filtered with a glass fritted Büchner funnel and washed with water.

During the above treatment, the lignin is chlorited and is washed away. It is essential to make the pH of the solution 3-4 for maximum chloriting (Green, 1963). Until this step, the sample is usually called hollocellulose and contains a lot of non-*alpha*-cellulose, termed *beta* and *gamma* cellulose. *Beta* and *gamma* cellulose which are alkali-soluble are now included in the general term - hemicellulose.

3.1.1.c. Alkaline treatment

In order to obtain relatively pure *alpha*-cellulose, the above sample was extracted with alkali to remove certain soluble carbohydrates which are mainly hemicellulose. It has been found that sodium hydroxide and lithium hydroxide are much more effective than potassium hydroxide in their relative extractive powers for the mannose-containing polysaccharides which are associated with hollocellulose. It is also known that these three solvents have nearly equal solvent powers over a wide range of concentrations for xylose, arabinose, galactose, and uronic acid-containing polysaccharides (Hamilton and Quimby,

1957). So 18% sodium hydroxide is used to remove the hemicellulose thereby obtaining nearly pure *alpha*-cellulose.

110 g of sodium hydroxide were dissolved in 500 ml of distilled water. Then the above sample was placed in 100 ml of this solution and stirred with a magnetic stirrer for at least 1·hour. The sample was filtered with a Büchner funnel (This step is quite time consuming) and washed with distilled water until the filtrate became neutral (not alkaline). Finally, water was removed from the sample in a freeze dryer over 24 hours.

3.1.2. Preparation of CO_2 for oxygen isotope composition measurement

The modifications of Edwards *et al* (1994) to a nickel pyrolysis technique (Thompson and Gray, 1977; Brenninkmeijer and Mook, 1981) have enchanced the efficiency of $\delta^{18}O$ analyses on μg samples of water and organic matter. The improved method uses resealable nickel "bombs" which permit greatly increased service life for the individual tubes (>50 cycles). This greatly reduces the experimental costs. e.g. in the Brenninkmeijer and Mook's method, cutting and welding of tubes was necessary prior to each sample analysis. This method has good reproducibility of $\delta^{18}O$ determinations ranging from ± 0.1 to $\pm 0.5\%$ for cellulose samples (Edwards *et al*, 1994). Therefore we adapted this method to measure the oxygen isotopic composition of cellulose samples.

3.1.2.a. Theoretical considerations of the nickel pyrolysis technique

The completion of the pyrolysis reaction is driven by the loss of hydrogen, which diffuses through the wall of the nickel tubes at high temperature. Therefore oxygen atoms

in cellulose are fully taken up in CO and CO_2 according to the following (unbalanced) general equations:

$$(CH_2O)_n \rightarrow CO + CO_2 + C + H_2 \qquad (3.1)$$

$$H_2O + C \rightarrow CO + CO_2 + C + H_2 \qquad (3.2)$$

It is shown that although there exist broad variations in the CO/CO_2 ratios in the pyrolysis reaction, the oxygen isotope composition of the CO_2 is independent of this ratio (Edwards *et al.*, 1994). Therefore it is not necessary to recover oxygen from CO to measure the oxygen isotopic composition of cellulose samples and the $\delta^{18}O$ -value of the sample can be obtained directly from the CO_2.

3.1.2.b. Description of pyrolysis apparatus

Pyrolysis bombs and the puncturing device were constructed in the Faculty of Science, Technical Services Machine Shop. About 10 cm length of nickel rod (1 cm O.D) was drilled but left closed at one end. The bomb is sealed with a Cajon NI-4-VCR-2-BL nickel disk squeezed between two raised circular seat rings (Fig. 3.2).

The puncturing device consists of three components machined from brass (Fig. 3.3). The discs are punctured by a replaceable sewing machine needle, secured with a set-screw. It is lowered easily by hand via the threads on the cap of the unit. Three O-rings provide vacuum-tight seals within the unit. A horizontal machined stainless-steel Rotulex-type fitting attached by silver soldering, allows connection a vacuum extraction line (Fig. 3.4).
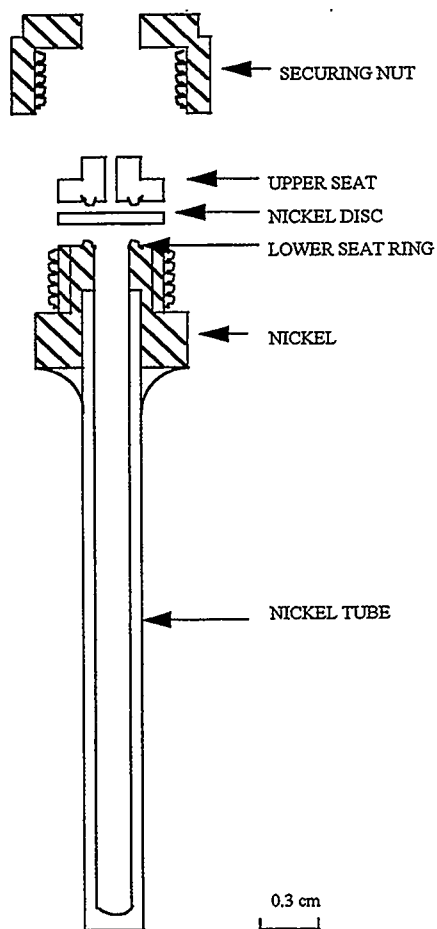
Fig. 3.2 Sketch of nickel pyrolysis bomb
(after Edwards *et al.*, 1994)
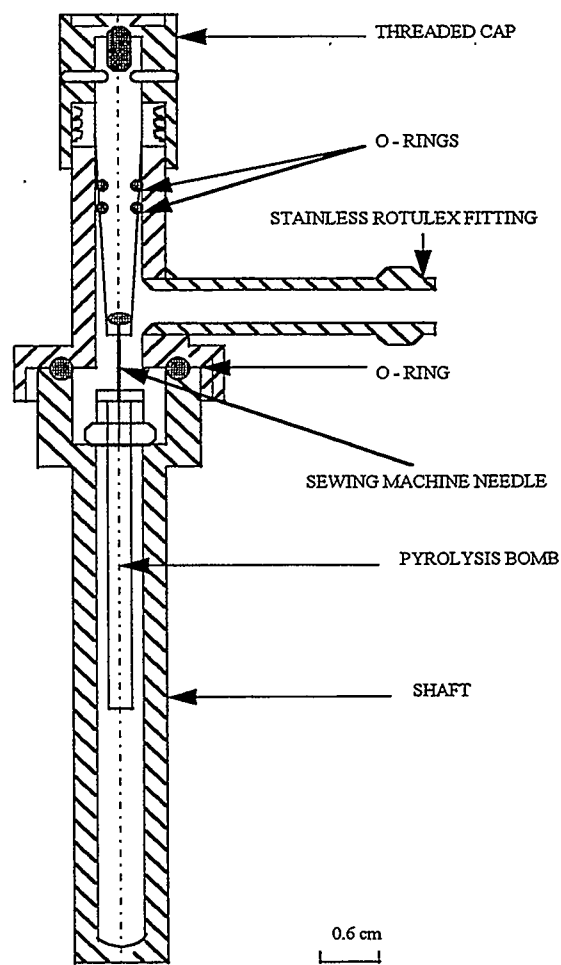
Fig. 3.3 Sketch of puncturing device
(after Edwards *et al.*, 1994)

3.1.2.c. Experimental procedure

(a) Bomb conditioning

Heating of the pyrolysis bombs causes oxidation of the outer surface of the nickel bombs. The oxide layers must be removed after each sample run to ensure a complete pyrolysis reaction during the next run. This is done by hand sanding with an abrasive pad.

After each run, the interior walls of the tube were cleaned using a cylindrical file. Three separate filings were interspersed by washing with acetone. Care must be taken not to score the beveled sealing surfaces.

(b) Loading the sample

The cellulose samples were weighed (20-60 mg) and put into the nickel tubes carefully. After loading up to 7 tubes, they were put into a specially designed wide mouthed jar with a rubber cap containing a valve. The jar was attached to a vacuum line for a period of at least twelve hours. This step ensured that any atmospheric water adsorbed by the cellulose was degassed.

The valve on the top of the jar was then closed. The jar was removed from the vacuum line and placed in a glovebox. After flooding the glovebox with argon for about 3 minutes, the valve on the jar was opened to the argon cylinder thus filling the jar and loaded nickel tubes with argon. Each nickel tube was transferred to a holder in the glovebox, being continually flushed with a stream of argon going through a pipette. Finally a nickel disc and nut were placed on the top of the nickel tube. The nut was first hand tightened and then tightened with a socket wrench so that the sealing rings were effectively pressed into the nickel disk.

(c) Baking

The bottom (nickel tube part) of sealed bombs were baked at 1050 ^{0}C for about 50 minutes in an electric resistance oven. The upper threaded parts with the nickel disk remained outside of the oven to maintain the integrity of the seal and to reduce the possibility of seizing of the threads. After air-cooling to room temperature, the bombs were ready for collection of CO_2.

(d) Collection of CO_2

The extraction line for collecting CO_2 is shown in Fig. 3.4. The heated section (Fig. 3.4) was set at 380 ^{o}C for about one hour in advance to permit thermal stabilization. The bottom portion of the puncturing device (for holding a nickel sample tube) was unscrewed and removed from the puncturing device. Care must be taken that the needle is in the raised position. A cooled pyrolysis nickel tube was lowered into the removed bottom portion (shaft). The bottom was screwed back on and the puncturing device evacuated by opening valves #1 and #2 in the extraction line (Fig. 3.4). When an adequate vacuum was obtained (usually after about 4 minutes of pumping), valve #1 was closed. Then the upper cap was carefully screwed down so that the needle punctured the nickel disk. The cap was raised slightly to allow the contained gases to diffuse through the hole. The gases were exposed to the heated section of the preparation line in order to decompose nickel carbonyl and possibly other gases which would condense with CO_2.

After about 5 minutes, valve #2 was closed and a dewar of liquid nitrogen placed around trap A. Valve #1 was opened to allow the CO_2 to condense in trap A (usually about 4-5 minutes). Valve #1 was closed and non-condensable gases were slowly bled off by alternately opening and closing valve #2.

Finally, valve #2 was closed and the liquid nitrogen dewar on trap A replaced with a methanol/dry ice bath. A dewar of liquid nitrogen was placed at the bottom of the Pyrex sample tube to condense CO_2 into it. After about 5 minutes. the Pyrex tube was collapsed, sealed and removed with a natural gas-O_2 torch. This step is easier if the upper part of the Pyrex tube has been previously constricted at atmospheric pressure (Fig. 3.4).
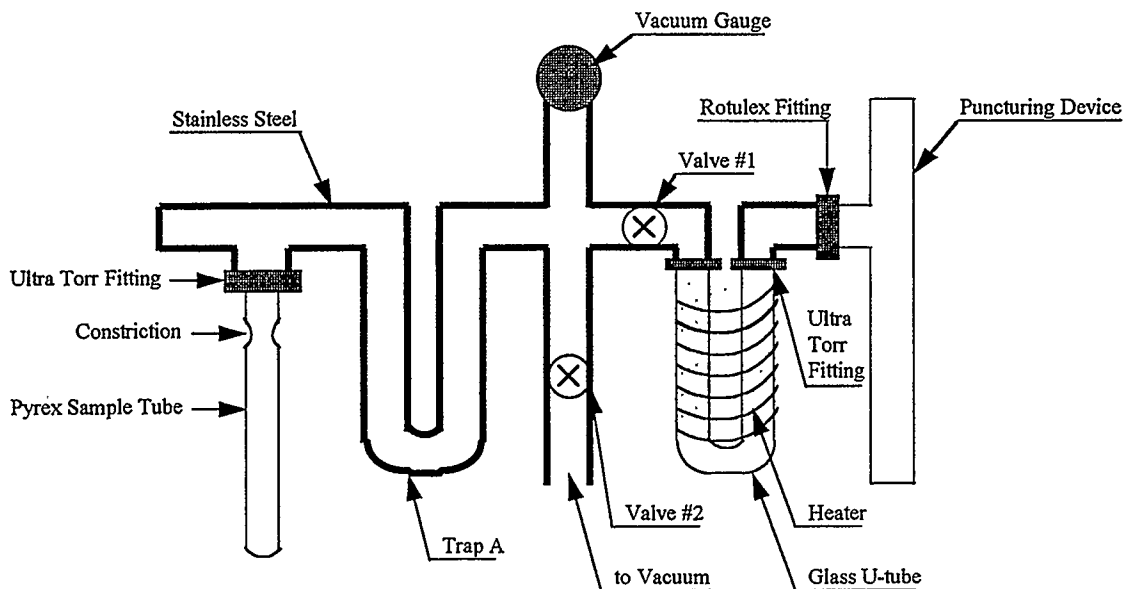
Fig. 3.4 CO₂ collection line

3.1.3 Preparation of CO_2 for carbon isotope abundance measurement

Traditionally, carbon isotope analyses of organic matter have been obtained by oxidation to CO_2 in a sample preparation system which provides cryogenic removal of H_2O, N_2, and O_2. In this investigation, the conventional approach was used as well as a Carlo Erba combustion unit (Elemental Analyzer) combined with a continuous flow mass spectrometer (See next section). The samples are combusted in tin cups which are dropped into a furnace at 1000 °C and through which He is flowing. A pulse of O_2 is introduced as the cup is dropped. Since oxidation of tin is exothermic, it is claimed that the combustion temperature may exceed 1600 °C. This high temperature minimizes production of nitrogen oxides (which should not be a problem with cellulose). In any case, a furnace with a tube containing copper is downstream from the combustion tube and converts nitrogen oxides to N_2 and CuO. Purification of gaseous products is further realized by a gas chromatograph built into the Elemental Analyzer. At the appropriate time, exiting CO₂ is directed into the mass spectrometer.

3.2 Mass Spectrometry

Mass spectrometric methods are by far the most effective means of measuring isotope abundances. A mass spectrometer separates charged atoms and molecules on the basis of the mass dependence of their motions in magnetic and/or electrical fields. A stable isotope mass spectrometer can be divided into four parts: (1) the inlet system, (2) the ion source, (3) the mass analyzer, and (4) the ion detector assembly.

A dual inlet system is used to alternately introduce a sample of unknown isotope composition and a reference gas. To avoid mass discrimination, viscous (as opposed to molecular) gas flow is used in the inlet system. The sample gas has a pressure of typically 5 cm Hg and is introduced to the source through a long ($\sim$ 1 m) capillary.

In the mass spectrometer, ions are formed in the source. Ions of gaseous samples are provided most reliably by electron bombardment. A beam of electrons, with energy of the order of 100 ev, effectively collide with outer electrons of molecules thereby removing them to produce positive ions. Then the ions are accelerated in an electric field through a potential difference V. When leaving the electric field, all ions possess essentially the same kinetic energy, according to the equation:

$$\frac{1}{2}mv^2 = qV \qquad (3.3)$$

A uniform magnetic field separates the ion beams emerging from the ion source according to their M/e (mass/charge) ratios. When an ion moves in a magnetic field, it will experience a force, $\vec{F} = q\vec{v} \times \vec{B}$. The ion moves in a circular orbit of radius r. If $\vec{B} \perp \vec{v}$ then F = qvB. By Newton's second law

$$qvB = Mv^2 / r \tag{3.4}$$

where v^2/r is centripetal acceleration. Eliminating v in Eq. 3.3 and Eq. 3.4 gives

$$r = \left(\frac{2VM}{q}\right)^{1/2} B^{-1} \tag{3.5}$$

According to Eq. 3.5, as the ion beam passes through the magnetic field, the ions are deflected into separate circular paths, the radii of which are proportional to the square root of M/e.

After passing through the magnetic field, the separated ions are collected in Faraday cups. Electron currents (10^{-11} to 10^{-9} A) flowing from ground to neutralize the positive ions in the cups are amplified and in our laboratory converted to voltages (~ 1 volt). The voltages corresponding to each isotopic ion current then undergo V to F conversion (1 volt = 10^5 Hz) followed by counting circuitry. Thus three ion currents corresponding to masses 44 ($^{12}C^{16}O_2^+$), 45 (mainly $^{13}C^{16}O_2^+$) and 46 (mainly $^{12}C^{18}O^{16}O^+$) are collected in three Faraday cups and presented as counts to the computer for calculating $\delta^{13}C$ and $\delta^{18}O$ values. Switching between the standard and sample gases is also computer controlled.

In conventional isotope ratio mass spectrometers (IRMS), less than 1 percent of the sample gas is consumed during analysis since a minimum amount had to be prepared to maintain viscous flow conditions. In continuous flow IRMS (CF-IRMS) the total gas sample produced is swept through the mass spectrometer source with He carrier gas. The presence of the latter assures viscous flow conditions. Simultaneous collection of the ion currents in three Faraday cups still occurs. However, the measurement procedure differs. The areas under the currents versus time plots (corresponding to the time that the sample

was swept through the source) are determined i.e. $\int I(t)dt$ or the total charge collected by each cup is determined. The result is that much smaller samples can be analyzed more quickly and the costs of chemicals and cryogenic baths substantially reduced.

For this thesis, a Micromass 903 mass spectrometer was used to measure oxygen and carbon stable isotope abundance ratios of manually prepared CO_2. The standard deviation of $\delta^{18}O$ and $\delta^{13}C$ measurements was better than ± 0.2 $^0/_{00}$. For carbon isotope abundance ratio measurements, a continuous flow Prism mass spectrometer was also used in combination with the Carlo Erba Elemental Analyser. The standard deviation of $\delta^{13}C$ measurements was less than ± 0.05 $^0/_{00}$.

Chapter 4 Results

A slab of *Tamarix aphylla* main trunk was obtained near Nevares Spring from Death Valley, California. Cellulose was extracted from wood samples corresponding to individual growth rings. In this chapter, the environmental setting of the sample site is described, followed by the measured isotope data and tests to see if and how they correlate to precipitation and ring width.

4.1 Environmental Setting of the Sample Site

Death Valley, California (latitude: $35°33'$ -$36°45'$ N; longtitude: $116°12'$ -$117°16'$ W), is the hottest and driest part of southwestern North America, lying south and west of the Colorado Plateau and extending westward to the Sierra Nevada Mountains. The valley is a young structural sag between two mountain blocks, the Panamint Range to the west and Black Mountains to the east (Fig 4.1). At present, the valley floor is 86 m below sea level, which is the lowest point of the inner North America continent. As one of the many desert basins between mountain ranges in the western United States, Death Valley is influenced by three very different environments: (1) high mountain ranges, (2) alluvial fan gravels sloping from the base of each range to the edge of (3) a broad salt encrusted mud flat - playa - salt pan complex. Winter temperatures on the valley floor are rarely down to the freezing point. Average summer temperatures are about $40°$ C and a maximum of $56.7°$ C has been recorded (after Yang *et al*, 1996).

Most of the precipitation for the Death Valley area falls from December to March. As seen in Table 4.1, the precipitation during the period starting from December of the previous year to March of the year under consideration is about 56% of the annual precipitation. The annual precipitation (January 1 to December 31) of this area ranges from 0 to 11.51 cm with an average of 5.12 cm (1944-1993). For such arid environments,
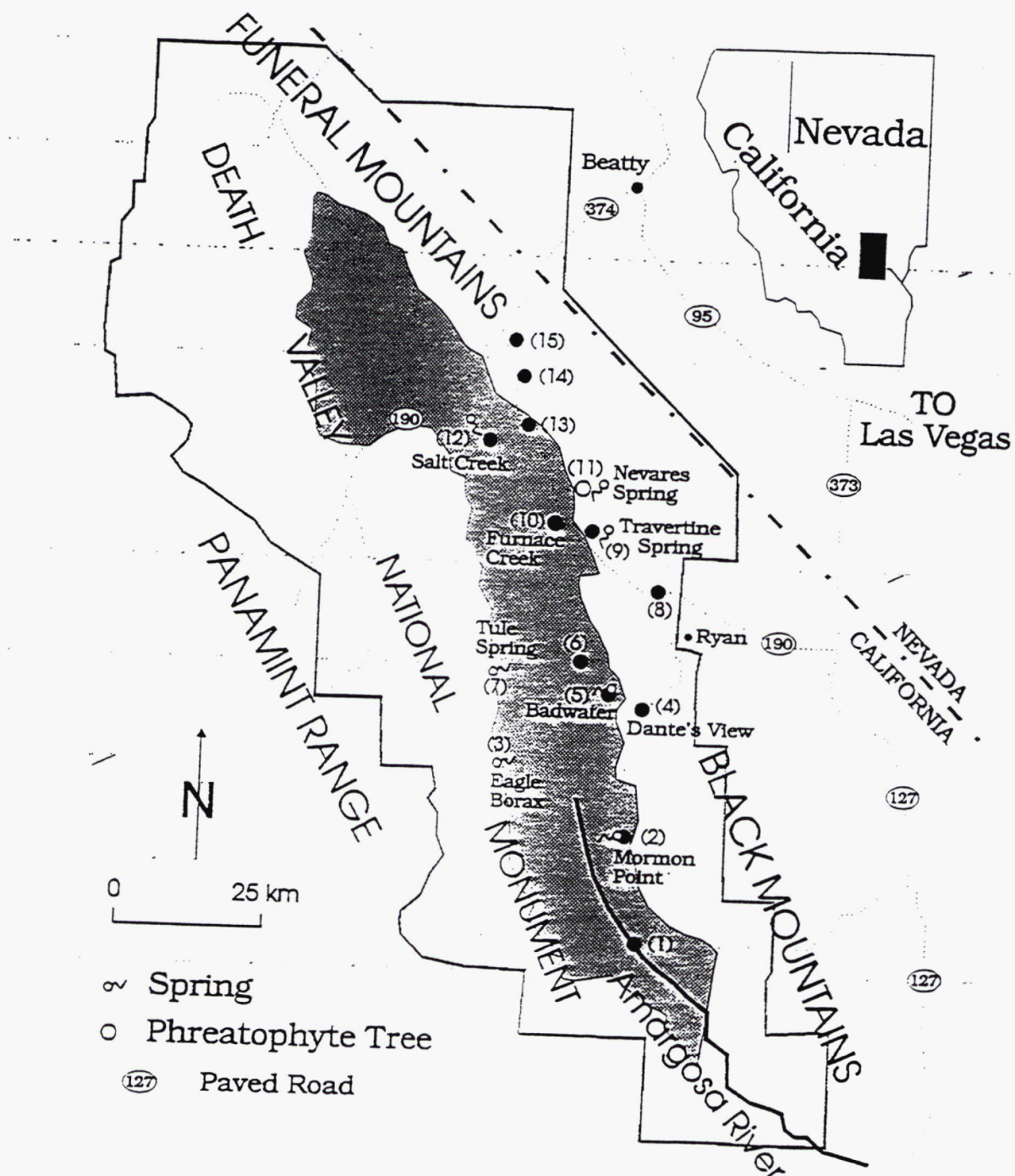
Fig. 4.1 Map of Death Valley, California and surroundings (after Yang *et al*, 1996)

Feng and Epstein (1995) used the concept of hydrological year. The hydrological year N is defined to be from October 1 of N-1 to September 30 of N. One reason for using the hydrological year is that the precipitation during the winter term(October to December) should affect the tree growth more during the following spring, since tree growth is slow during winter and fast during spring.

Tamarix aphylla was imported to the southwestern USA from the mediterranean. It can serve as a dune stablizer and windbreak (Robinson,1965; Baum, 1978). Its tap roots can reach down to 30 m depth and subsuperficial side roots may reach 50 m horizontally. The species can store large amounts of water in its roots and undergoes high evapotranspiration. Salt secretion is another typical feature of this tree, which leads to desalinization of deeper soil and increase of salinity in the upper layers.

On April 30, 1993, Yang *et al* (1996) obtained a cross-sectional slice of a *Tamarix aphylla* trunk (see Fig 4.1 for sample location) during a hydrogeological field investigation of Death Valley. The live tree had been cut down and totally removed two days earlier. The perimeter of the trunk near its base was about 260 cm with maximum and minimum diameters of 85 and 72 cm. Assuming that the tree rings are annual, this tree was about 50 years old at the time of cutting.

Cross sections of 2.0 cm wide × 9.0 cm thick for each tree ring were sampled from the *Tamarix aphylla* tree trunk and used for raw wood carbon isotope analysis and to extract cellulose using the method described in Chapter 3 for carbon and oxygen isotope analysis.

Table 4.1 Annual precipitation in the Death Valley area (precipitation data from Death Valley Park Office, obtained by Wenbo Yang, 1993).

Time (Year)	Dec - March (cm)	hydrological year (cm)	Annual (cm)
1944	5.51	6.43	6.32
1945	0.53	4.14	3.91
1946	1.73	4.42	8.89
1947	3.07	7.14	2.16
1948	1.37	2.21	0.48
1949	4.24	6.15	6.17
1950	0.13	3.23	3.10
1951	0.13	0.13	0.81
1952	5.28	6.86	8.56
1953	0.79	2.39	0.00
1954	3.60	5.51	7.42
1955	0.66	3.10	1.19
1956	0.00	2.13	2.13
1957	1.14	0.00	3.45
1958	1.83	6.78	4.75
1959	1.45	4.19	4.72
1960	4.78	4.83	3.91
1961	0.36	3.56	3.58
1962	1.68	2.82	1.96
1963	2.34	5.61	6.10
1964	0.20	3.02	2.67
1965	0.38	5.13	8.43
1966	1.75	5.38	2.01
1967	0.20	1.93	3.50
1968	3.05	5.82	4.11
1969	6.15	7.87	8.69
1970	3.45	4.39	5.82
1971	0.53	3.20	2.44
1972	1.60	3.30	5.72
1973	4.78	9.04	5.79
1974	4.29	6.55	8.81
1975	1.98	6.63	3.84
1976	6.10	9.73	10.69
1977	0.61	7.14	7.11
1978	9.02	11.09	10.24

Table 4.1 (Continued)

Time (Year)	Dec-March (cm)	Hydrological year (cm)	Annual (cm)
1979	4.24	4.78	4.47
1980	5.36	8.10	8.10
1981	1.93	2.01	4.50
1982	3.81	7.65	6.65
1983	7.52	11.58	11.51
1984	1.37	5.54	4.16
1985	0.13	1.32	2.21
1986	1.27	2.69	2.54
1987	3.56	4.55	9.50
1988	4.85	15.37	9.75
1989	0.38	1.24	1.14
1990	1.32	3.28	3.25
1991	2.54	3.23	3.86
1992	6.50	6.58	8.53
1993	8.53	8.92	6.40

4.2 Stable Carbon Isotope Composition of Cellulose and Raw Wood

4.2.1 Difference between the $\delta^{13}C$ values of raw wood and cellulose

The measured $\delta^{13}C$ values for the cellulose and raw wood are given in Table 4.2. In Fig. 4.2, the $\delta^{13}C$ values for cellulose and raw wood have been plotted against age. The $\delta^{13}C$ values of raw wood (-28.09 to -25.42 $^o/_{oo}$) attest to C_3 photosynthesis. The differences between the $\delta^{13}C$ values of cellulose and raw wood are plotted in Fig. 4.3. For a given sample, $\delta^{13}C_{cell} > \delta^{13}C_{wood}$.

As seen in Fig.4.2, the trend of change of the $\delta^{13}C$ values in raw wood is the same as that in cellulose but the differences range from as large as 2.03‰ down to 0.39‰ (Fig. 4.3).

As mentioned in Chapter 2, wood consists of many organic materials with variable different percentages and $\delta^{13}C$ values. This leads to the variations of the differences between the $\delta^{13}C$ values of raw woods and cellulose. For a year when this difference is large, one possible explanation is that there are higher percentage compositions of lignin and lipid, since their $\delta^{13}C$ values are the most negative found for chemical compounds in wood (Fig. 2.3).

Variations in the $\delta^{13}C$ values of total wood can be due to either or the combination of both of the following reasons: (a) variation of the percentage compositions of chemical components with different but fixed $\delta^{13}C$ values, and (b) variation of the $\delta^{13}C$ value over time for individual chemical components. It seems impossible to theoretically foretell the effects of environmental parameters on the chemical composition of wood. Therefore, it is impractical to draw any useful environmental information solely from the

Table 4.2 $\delta^{13}C$ values for Tamarix aphylla tree rings (raw wood and cellulose).

Radius (mm)	Age (Year)	$\delta^{13}C$ (permil,PDB) Raw Wood	$\delta^{13}C$ (permil,PDB) Cellulose
0.7	1944	-27.08	-25.67
1.6	1945	-28.09	-27.58
2.2	1946	-27.57	-26.79
2.9	1947	-26.57	-24.98
4.3	1948	-26.82	-26.33
5.2	1949	-26.68	-24.65
5.8	1950	-26.42	-24.88
6.6	1951	-26.26	-25.27
7.4	1952	-26.64	-24.93
8.2	1953	-27.47	-26.95
9.0	1953	-26.71	-24.89
9.7	1954	-26.95	-25.13
10.3	1954	-26.70	-25.70
11.0	1955	-25.51	-24.94
11.8	1956	-26.62	-25.43
12.9	1957	-27.79	-26.65
13.5	1958	-26.38	-25.29
14.1	1959	-26.15	-25.30
14.7	1960	-26.27	-25.62
15.1	1961	-26.70	-25.71
15.4	1962	-26.63	-25.30
15.8	1963	-26.84	-25.54
16.4	1964	-26.66	-25.36
16.8	1965	-26.54	-25.07
17.2	1966	-26.32	-25.36
17.6	1967	-27.08	-26.15
18.0	1968	-26.32	-25.68
18.9	1969	-26.83	-26.01
19.5	1970	-26.15	-26.12
20.0	1970	-25.51	-24.76
20.8	1971	-25.99	-25.17
21.2	1971	-26.05	-25.27
21.6	1971	-26.01	-25.73
22.5	1972	-26.55	-25.84

(Continue of Table 4.2)

Radius (mm)	Age (Year)	$\delta^{13}C$ (permil,PDB) Raw Wood	$\delta^{13}C$ (permil,PDB) Cellulose
23.3	1972	-26.41	-25.73
23.8	1973	-27.20	-26.41
24.2	1974	-26.18	-25.39
24.9	1975	-26.56	-25.99
25.3	1976	-26.23	-25.57
25.5	1977	-25.80	-24.58
25.8	1978	-26.61	-25.26
26.1	1979	-26.21	-24.86
26.4	1980	-26.28	-25.22
26.6	1981	-25.65	-24.65
26.8	1982	-25.82	-24.89
27.1	1983	-25.79	-24.37
27.7	1984	-26.01	-24.54
28.3	1985	-25.30	-24.00
28.6	1986	-25.44	-24.14
28.9	1986	-25.42	-24.10
29.2	1987	-25.47	-24.13
29.5	1988	-26.05	-25.04
29.9	1989	-25.69	-25.00
30.3	1990	-26.30	-25.27
30.8	1991	-26.52	-25.23
31.2	1992	-26.76	-25.98
31.6	1993	-26.94	-26.12
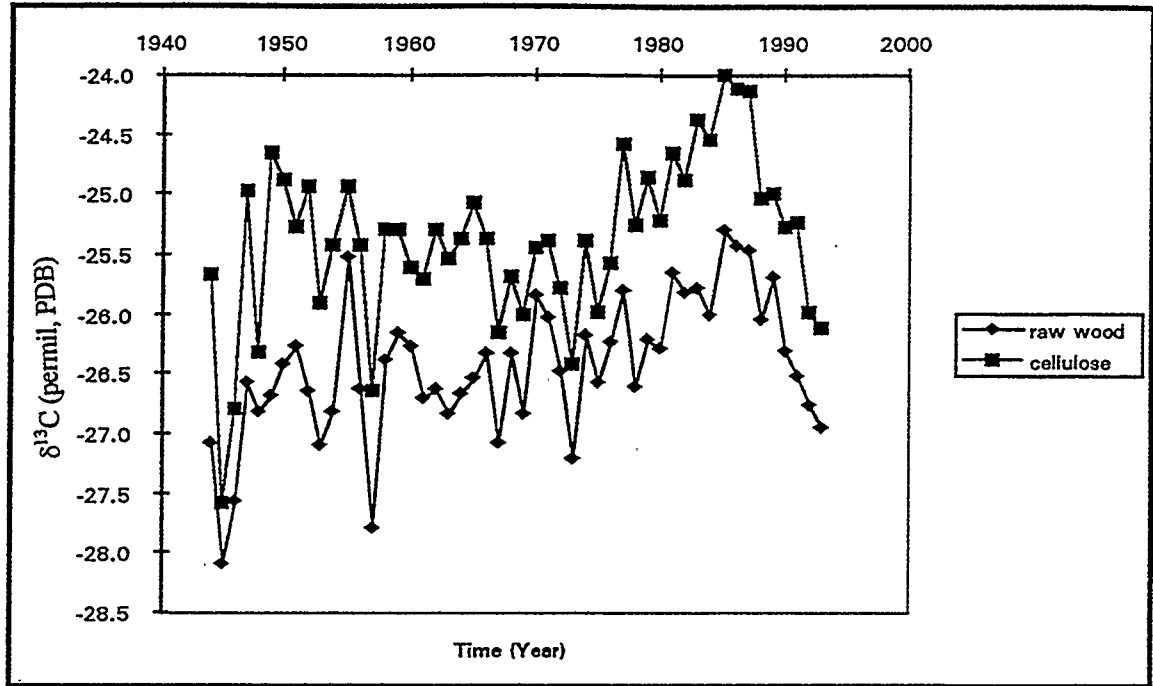
Fig. 4.2 $\delta^{13}C$ values versus age for raw wood and cellulose (the size of the symbols is consistent with the uncertainties in the stable isotope analyses).
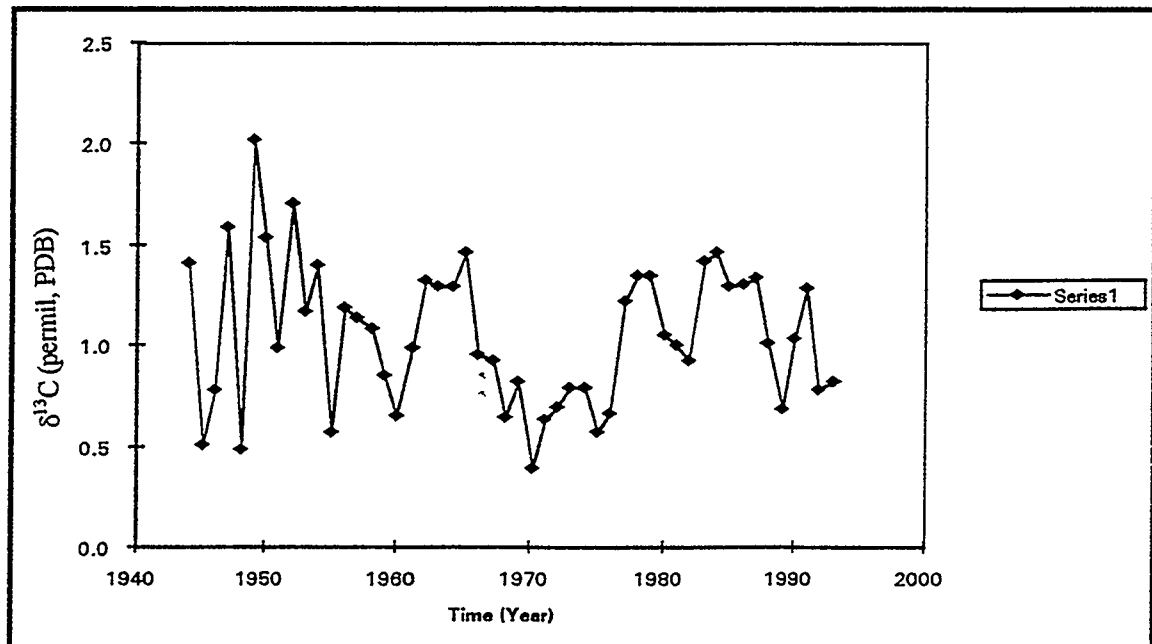
Fig. 4.3 Variations of the difference in $\delta^{13}C$ in raw wood and cellulose with age (Errors in $\delta^{13}C$ values are roughly the size of the symbol)

variation of the $\delta^{13}C$ values in raw wood samples. This would require knowledge about (1) environmental effects on every biochemical and physical process, and (2) dependence of $\delta^{13}C$ values on environmental parameters. So historically, cellulose has been preferred in stable isotope tree ring research to reduce the complexity of working with whole wood.

4.2.2 Correlation between the $\delta^{13}C$ values and annual precipitation

The annual precipitation in Death Valley is quite low (Table 4.1). An important question is whether the $\delta^{13}C$ values of tree rings reflect the variations of annual precipitation. From mathematical analyses of Fig. 4.4 and Fig. 4.5, it was found appropriate to separate the growth of tree into three different stages. The first stage is from 1944 to 1946 when the $\delta^{13}C$ values of tree rings are quite negative. During Stage II (from 1947 to 1967), the $\delta^{13}C$ values generally decreased (Fig. 4.5) and correlated positively to the annual precipitation. During later growth, the $\delta^{13}C$ values generally increased until about 1986 and then sharply decreased. Rather than define two stages before and after 1986, it was decided to consider one Stage, III, since throughout it, the $\delta^{13}C$ values of tree rings correlated inversely to the annual precipitation. As will be seen later, there are grounds for dividing Stage III into three intervals: IIIa, IIIb, and IIIc.

The data are discussed qualitatively in the next two sections and mathematical analyses provided thereafter.

4.2.2.a Short term response of the $\delta^{13}C$ values to the annual precipitation

Figs. 4.4 and 4.5 show the trends of the $\delta^{13}C$ values of tree rings and the annual precipitation respectively from 1944 to 1993. As seen, most peak values of $\delta^{13}C$ plotted from 1947 to 1967 coincide with many in the precipitation curve, e.g. $\delta^{13}C$ minima in 1948, 1953, and 1967, when the annual precipitation was also lower, and $\delta^{13}C$ maxima in 1949, 1958, and 1965, when the annual precipitation was high.

However, it is seen that after 1967, $\delta^{13}C$ minima in 1969, 1973, and 1988 (also for 1978 and 1980, where the difference between adjacent years is quite small), correspond to

high peaks in precipitation, e.g. maximum $\delta^{13}C$ values in 1971, 1977, and 1985 (also in years 1974, 1979 and 1981, where the difference between adjacent years is quite small), correspond to precipitation minima.

It can also be seen that the $\delta^{13}C$ value for the tree ring of a given year depends on not only the precipitation of that year but also those of previous years, i.e. a given $\delta^{13}C$ value is affected by previous precipitation. For example, the highest precipitation occurred in 1988. If only the effects of the current year were considered (inverse correlation during Stage III), a very low $\delta^{13}C$ value is expected for 1988. However, due to the low precipitation for the previous four years, the $\delta^{13}C$ value for this year is above the mean value. This is consistent with the observations of other investigations. Whereas the correlation between annual precipitation and tree ring $\delta^{13}C$ values may be poor, better correlation is found by the "running average" method e.g. Feng and Epstein (1996).
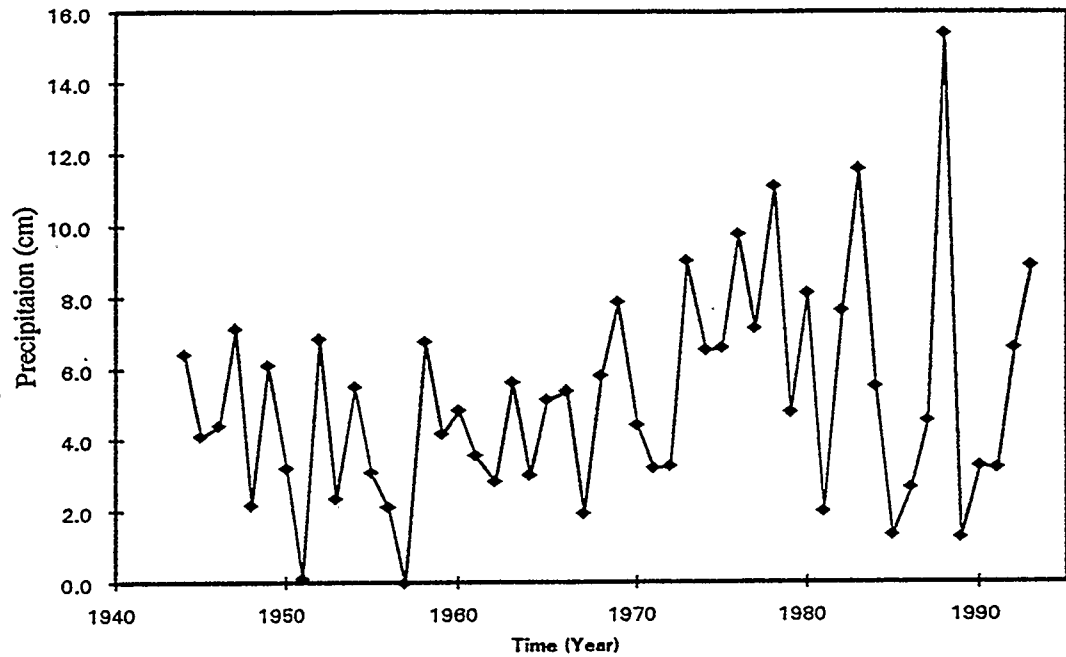
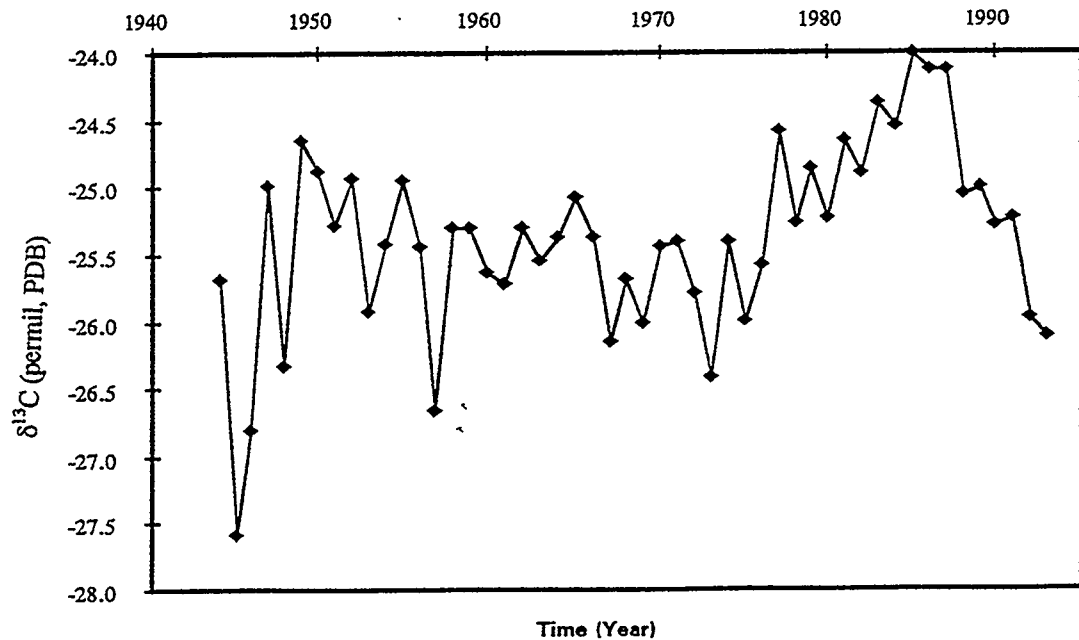Fig. 4.4 Annual precipitation in the Death Valley area.

Fig. 4.5 Variation of $\delta^{13}C$ values of tree rings in a *Tamarix aphylla* trunk, Death Valley, California. (Errors in $\delta^{13}C$ values are roughly the size of the symbol)

4.2.2.b Long-term response of the $\delta^{13}C$ values to precipitation

It is critical to decide the length of time in which the response of the $\delta^{13}C$ values of tree rings to any environmental parameter is the strongest. This time span depends on the plant species and environmental parameters such as climate, precipitation, amount of light etc. When studying the correlation between climate and the $\delta^{13}C$ values of tree rings of *Pinus longaeva* from White Mountain, California, Feng and Epstein (1995) used fifteen-year running averages of the $\delta^{13}C$ values. In this thesis, it was found that the $\delta^{13}C$ values of tree rings responded to the precipitation more strongly over a time-scale of 5 years. Therefore, five-year running averages of the $\delta^{13}C$ values and the annual precipitation were used to search for any correlations among precipitation, ring width, and stable isotope data.

The five year average of R (annual precipitation, the $\delta^{13}C$ value of tree ring or ring width) for a certain year x is defined as:

$$\overline{R}_x = (R_{x-2} + R_{x-1} + R_x + R_{x+1} + R_{x+2})/5 \tag{4.1}$$

Calculated values for the five year running averages of $\delta^{13}C$ values and annual precipitation are given in Table 4.4, using data from Table 4.1 and 4.2.

The long-term response of $\delta^{13}C$ to the precipitation is analyzed in the next sections mathematically.

Table 4.3 Five year running averages of precipitation and $\delta^{13}C$ values of cellulose (before correction and after correction for the effect of the change of $\delta^{13}C$ value and concentration of atmospheric CO_2)

Time (Year)	Hydro. P (cm)	Five Year Ave. $\delta^{13}C$ (permil, PDB) Before corrected	After Corrected
1946	4.87	-26.27	-26.27
1947	4.81	-26.07	-26.02
1948	4.63	-25.53	-25.44
1949	3.77	-25.22	-25.09
1950	3.71	-25.21	-25.04
1951	3.75	-25.13	-24.91
1952	3.62	-25.28	-25.02
1953	3.60	-25.30	-24.99
1954	4.00	-25.33	-24.98
1955	2.63	-25.67	-25.28
1956	3.51	-25.55	-25.11
1957	3.24	-25.52	-25.04
1958	3.59	-25.66	-25.13
1959	3.87	-25.71	-25.14
1960	4.43	-25.44	-24.83
1961	4.20	-25.49	-24.83
1962	3.97	-25.51	-24.80
1963	4.03	-25.40	-24.65
1964	4.60	-25.33	-24.53
1965	4.42	-25.50	-24.66
1966	4.46	-25.52	-24.64
1967	5.43	-25.65	-24.73
1968	5.28	-25.73	-24.76
1969	4.64	-25.73	-24.72
1970	4.92	-25.66	-24.60

(Continue of Table 4.3)

Time (Year)	Hydro. P (cm)	Five Year Ave Before Corrected	$\delta^{13}C$ (permil, PDB) After Corrected
1972	5.30	-25.68	-24.54
1973	5.75	-25.79	-24.60
1974	7.05	-25.83	-24.60
1975	7.82	-25.59	-24.31
1976	8.23	-25.36	-24.04
1977	7.87	-25.25	-23.89
1978	8.17	-25.10	-23.69
1979	6.62	-24.91	-23.46
1980	6.72	-24.98	-23.48
1981	6.82	-24.80	-23.26
1982	6.97	-24.73	-23.15
1983	5.62	-24.49	-22.86
1984	5.76	-24.38	-22.71
1985	5.14	-24.23	-22.52
1986	3.46	-24.37	-22.61
1987	2.60	-24.46	-22.65
1988	2.99	-24.71	-22.86
1989	3.10	-24.93	-23.04
1990	3.50	-25.30	-23.37

4.2.3 Long-term response of $\delta^{13}C$ to precipitation during Stage II

The five year running averages of the $\delta^{13}C$ values and the annual precipitation are plotted together versus time in Fig. 4.6 with their best fit parabolic curves. The precipitation decreased slightly to a minimum around 1955 and then noticeably increased. The $\delta^{13}C$ value tended to decrease until about 1960 after which it increased slightly. A number of peaks above and below the best fit curve for the $\delta^{13}C$ values coincide with similar peaks in precipitation.

The decreasing trend of the $\delta^{13}C$ values of tree rings must be considered in light of the fact that the tree carbon source - atmospheric CO_2 has decreased steadily in its $\delta^{13}C$ value in response to fossil fuel combustion. An estimate of this decrease is $0.046^o/oo$/annum (Keeling *et al.*, 1979; Mook *et al.*, 1983). Feng and Epstein (1995) concluded that 0.44 $^o/oo$ decrease per decade in the $\delta^{13}C$ value of cellulose can be attributed to the changes of the $\delta^{13}C$ value and concentration of atmospheric CO_2. Therefore, in this thesis, after 1946, a positive correction of $0.044^o/oo$ per annum was added cumulatively to the measured $\delta^{13}C$ values. The corrected data (Table 4.3) are presented in Fig. 4.7.

It turned out that the best fit curves for precipitation and $\delta^{13}C$ in Fig. 4.7 are almost "parallel". The $\delta^{13}C$ values have been plotted against precipitation in Fig. 4.8. The best linear fit is:

$$\delta^{13}C_{5\text{-ave}} = (0.35 \pm 0.06)\ P_{5\text{-ave}} - (26.27 \pm 0.24)\ , \qquad R^2 = 0.68 \qquad (4.2)$$

where $P_{5\text{-ave}}$ and $\delta^{13}C_{5\text{-ave}}$ are the five year running averages of the annual precipitation and the $\delta^{13}C$ value, respectively. R is significant at $\alpha = 0.01$.
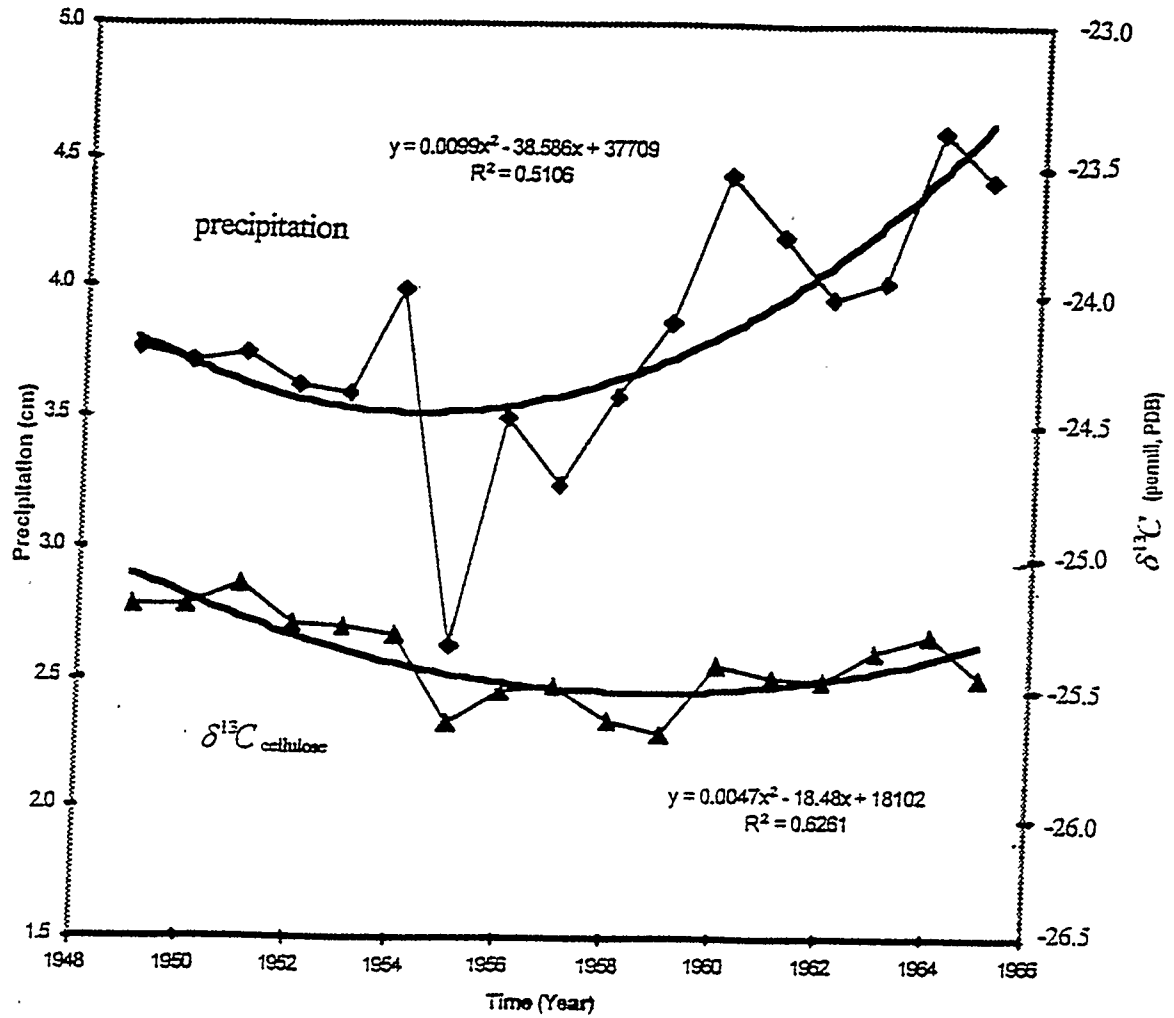
Fig. 4.6 Five year running average of precipitation and $\delta^{13}C$ values versus time for
Stage II (Errors in δ^{13}C values are roughly the size of the symbol).

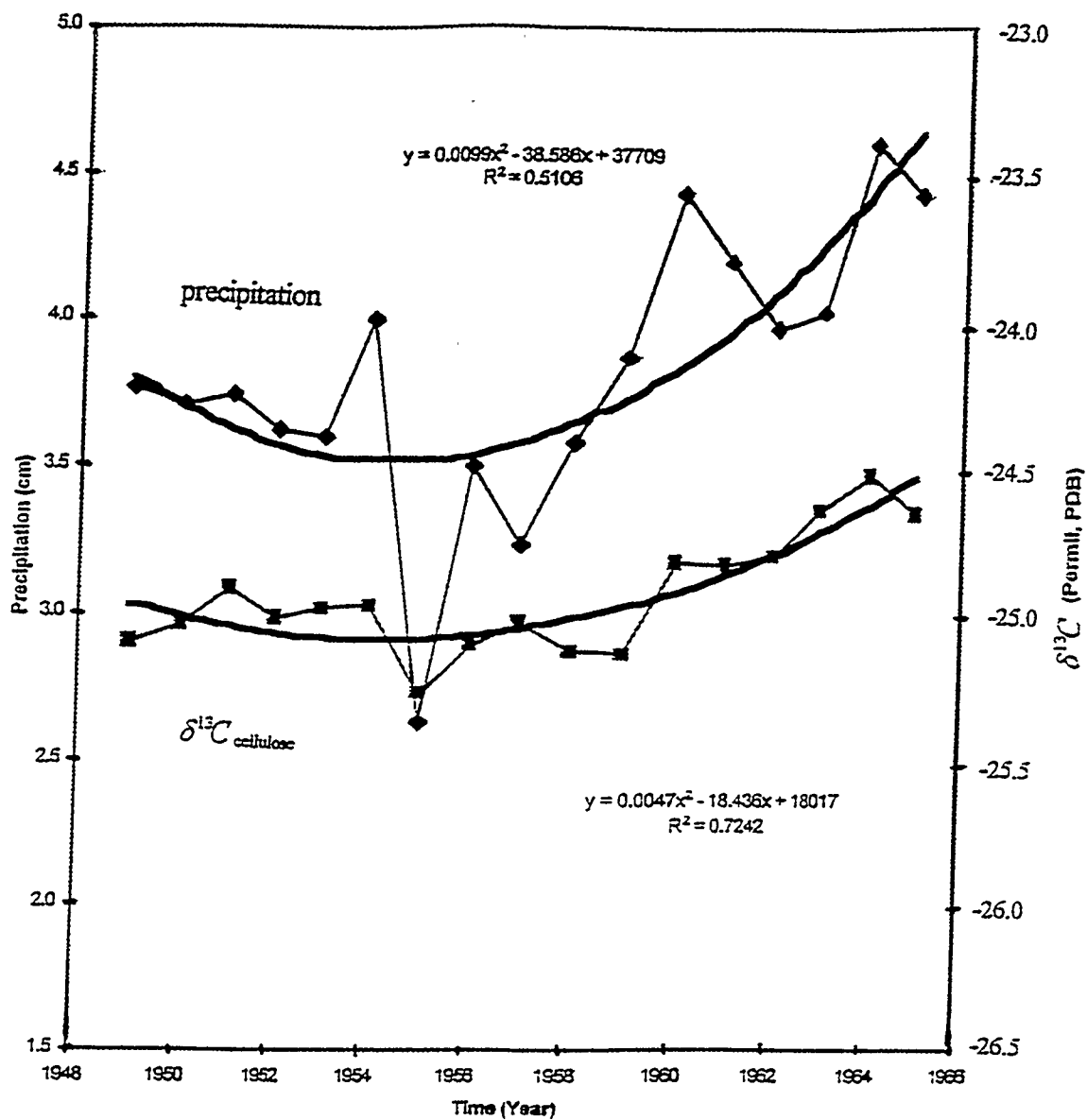**Fig. 4.7** Five year running averages of corrected $\delta^{13}C$ values and precipitation versus time for stage II (Errors in $\delta^{13}C$ values are roughly the size of the symbol).
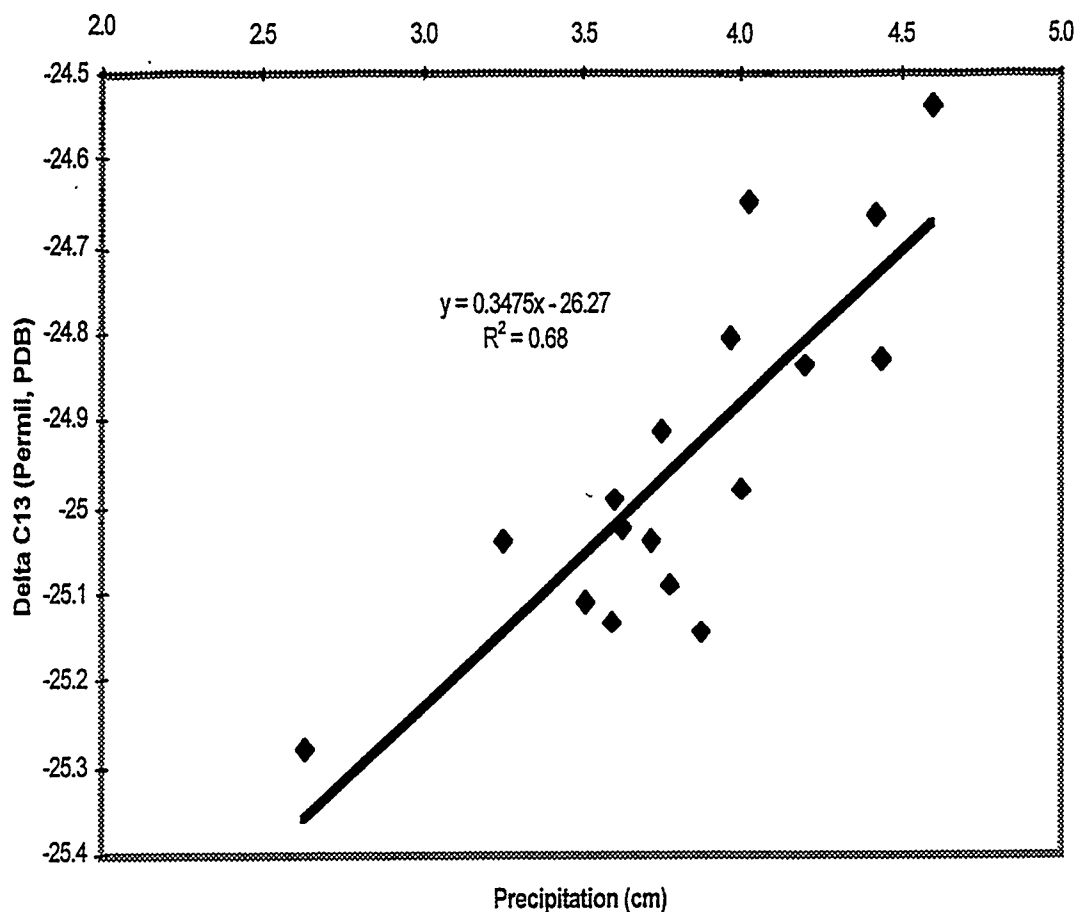
Fig. 4.8 Correlation between corrected $\delta^{13}C$ values and precipitation for Stage II (Errors in $\delta^{13}C$ values are roughly the size of the symbol).

4.2.4 Long-term response of $\delta^{13}C$ tò precipitation during Stage III

The third stage covers from 1967 to 1992. Five year running averages of precipitation and $\delta^{13}C$ values of cellulose are plotted against time in Fig. 4.9. If the effect of the changes of the $\delta^{13}C$ value and concentration of atmospheric CO_2 is considered as in Stage II, then the corrected data are as presented in Fig. 4.10. The corrected $\delta^{13}C$ values vs. precipitation are plotted in Fig. 4.11.
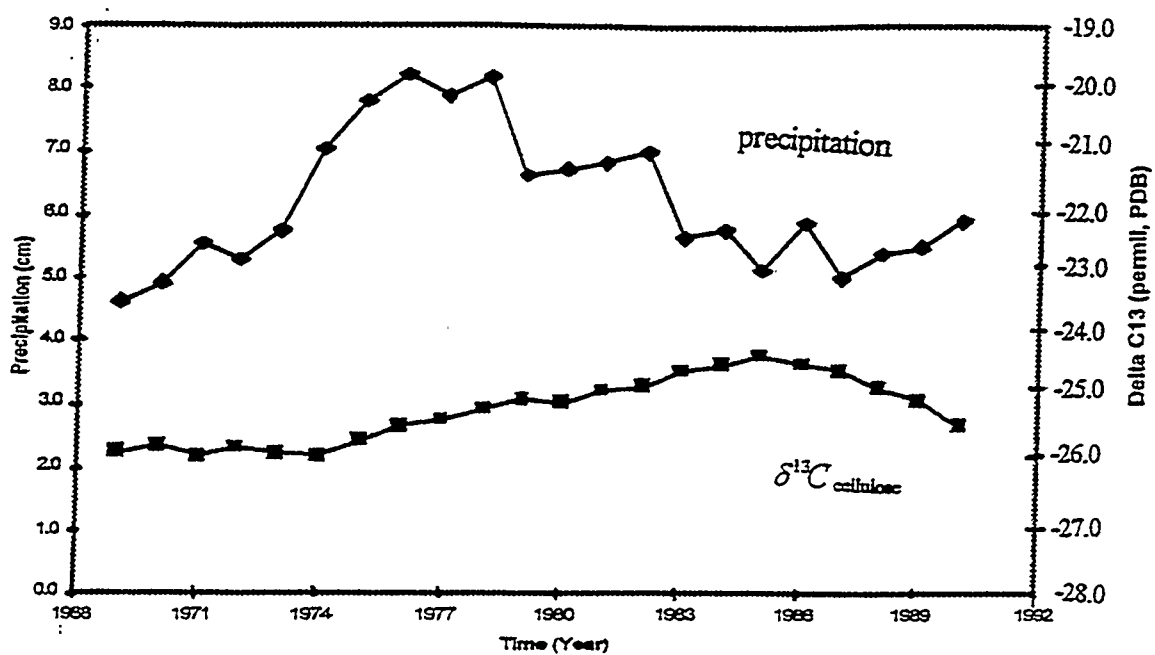
Fig. 4.9 Five year running average of precipitation and $\delta^{13}C$ vs. time for Stage III
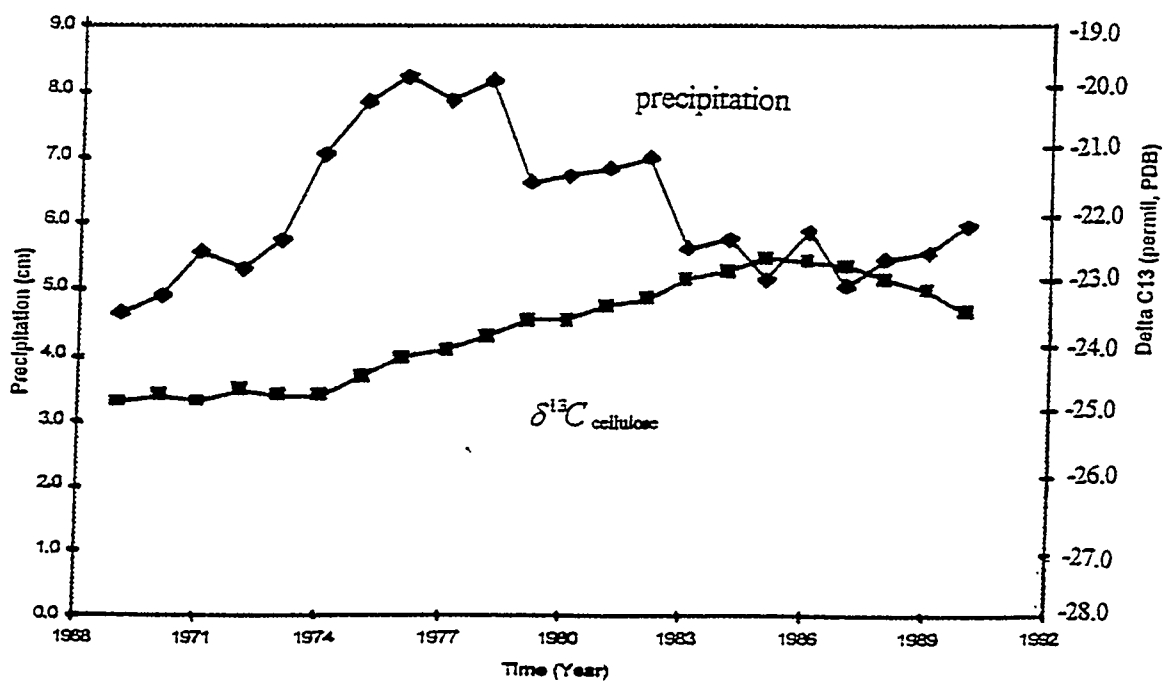
Fig. 4.10 Five year running average of precipitation and corrected $\delta^{13}C$ values vs. time for Stage III
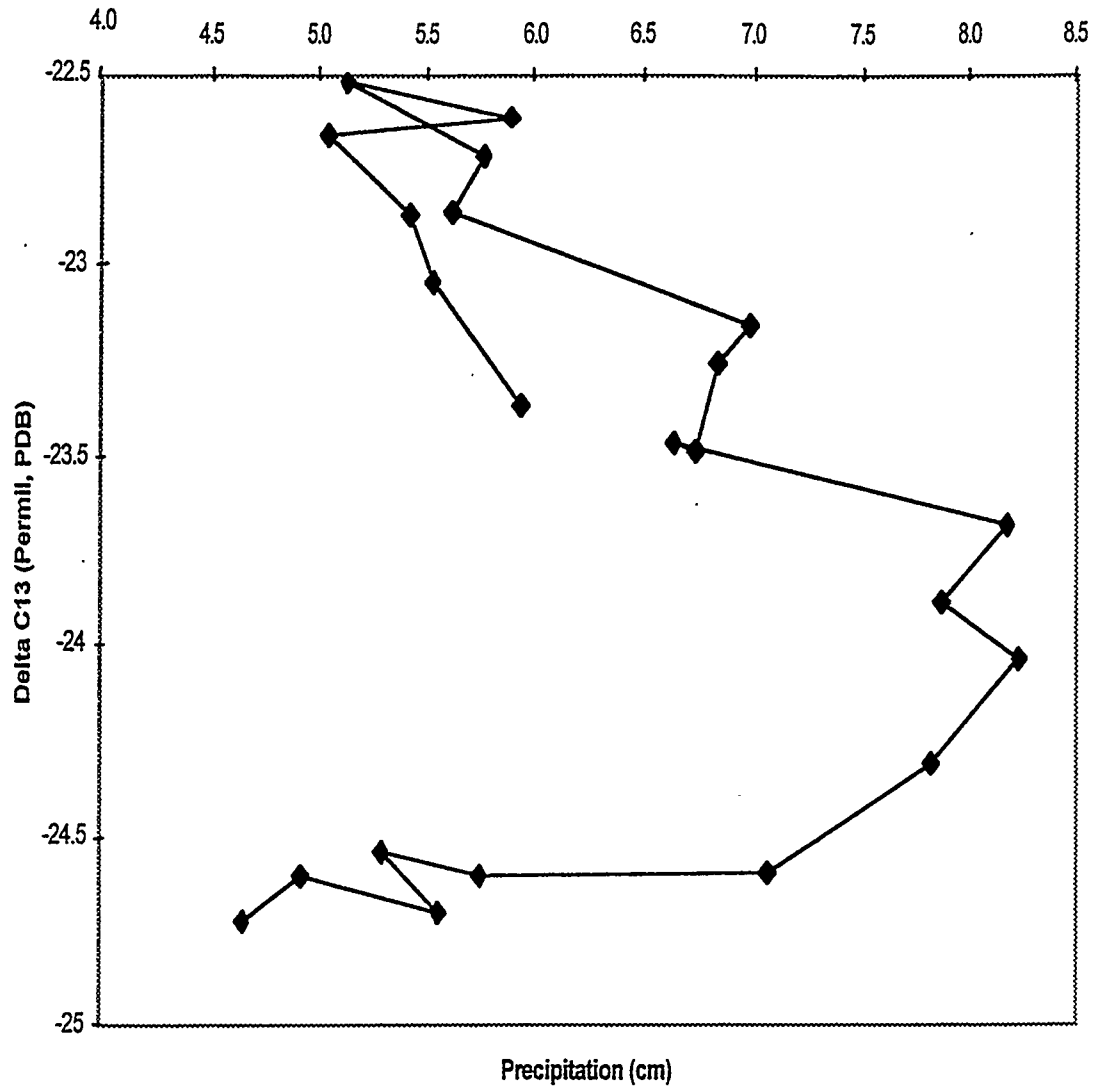
Fig. 4.11 Corrected $\delta^{13}C$ values versus precipitation for Stage III (Errors in $\delta^{13}C$ values are roughly the size of the symbol)

From Fig. 4.11, Stage III can be separated into three different intervals: IIIa, 1969-1976, where the $\delta^{13}C$ value increased with increasing precipitation, IIIb, 1977-1986, where the $\delta^{13}C$ increased with the decreasing precipitation, and IIIc: 1987-1990, where the $\delta^{13}C$ value decreased with the increasing precipitation. The corrected $\delta^{13}C$ value vs. precipitation plots are shown separately for each interval in Figs. 4.12, 4.13, and 4.14.
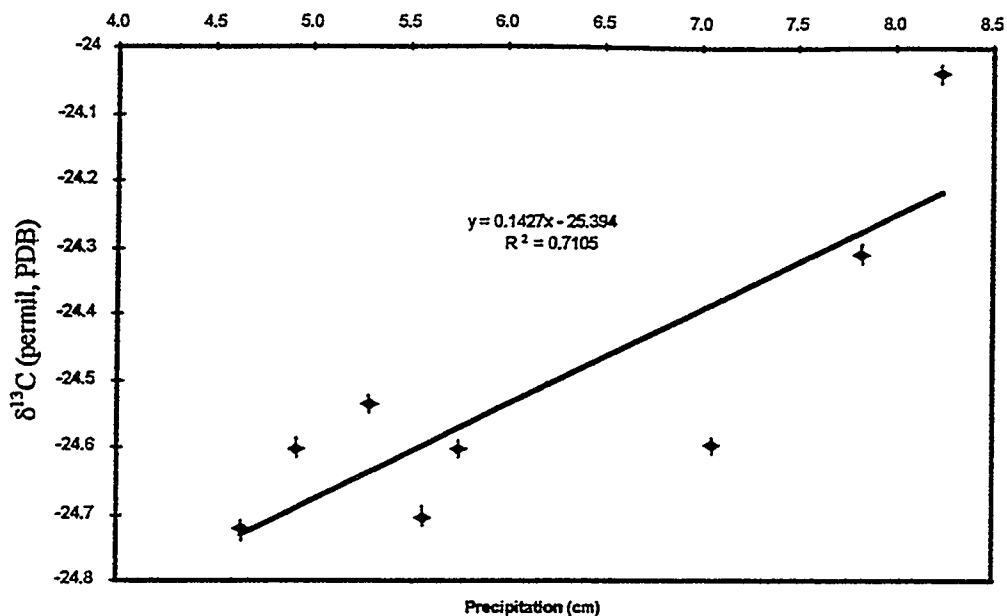
Fig. 4.12 Correlation between corrected $\delta^{13}C$ **values and precipitation for IIIa III**

(Error bars in $\delta^{13}C$ values as seen in figure)
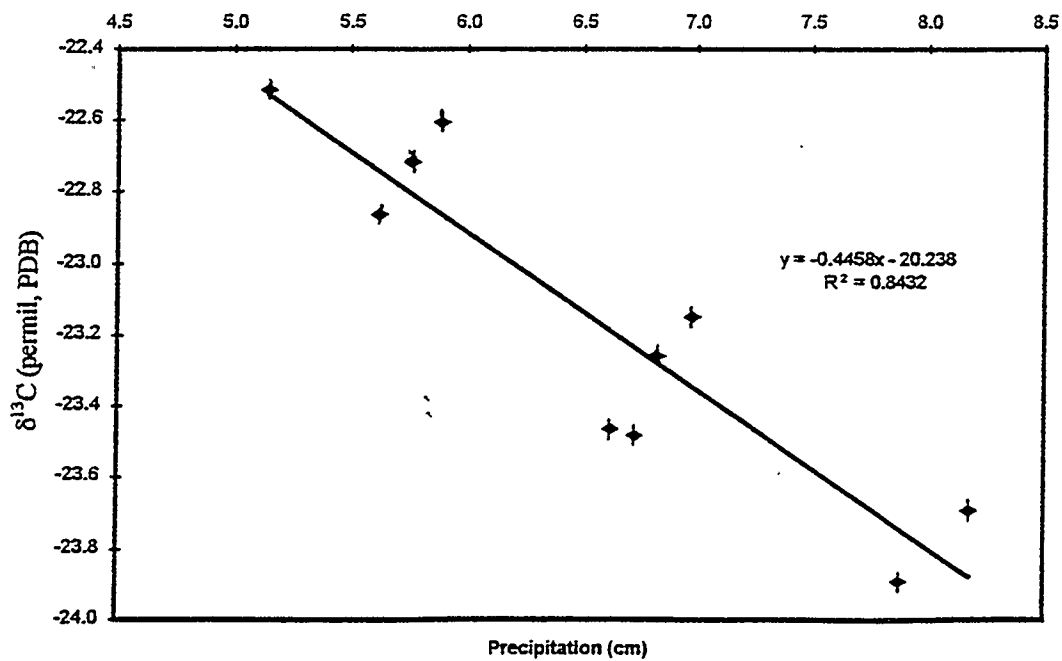
Fig. 4.13 Correlation between corrected $\delta^{13}C$ **values and precipitation for IIIb**

(Error bars in $\delta^{13}C$ values as seen in figure)
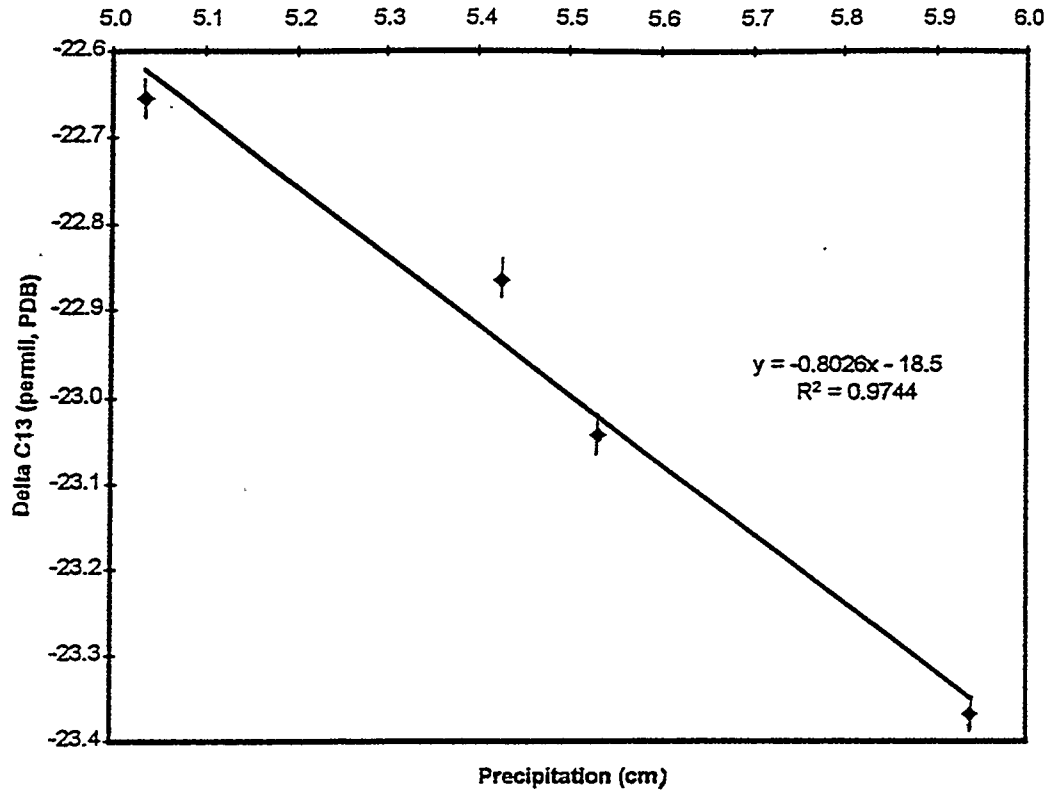
Fig. 4.14 Correlation between corrected $\delta^{13}C$ values and precipitation for IIIc (Error bars in $\delta^{13}C$ values as seen in figure)

The best linear fits for three intervals are:

IIIa $\delta^{13}C_{S\text{-ave}} = (0.14\pm0.04)\, P_{S\text{-ave}} \mp (25.39\pm0.23)$ $R^2 = 0.71$ (4.3)

IIIb $\delta^{13}C_{S\text{-ave}} = (-0.44 \pm 0.07)\, P_{S\text{-ave}} - (20.24 \pm 0.45)$ $R^2 = 0.84$ (4.4)

IIIc $\delta^{13}C_{S\text{-ave}} = (-0.80 \pm 0.09)\, P_{S\text{-ave}} - (18.58\pm 0.50)$ $R^2 = 0.97$ (4.5)

The best linear fits for IIIa, IIIb, and IIIc are plotted together in Fig. 4.15. R is significant at $\alpha = 0.01$ for IIIa, $\alpha = 0.01$ for IIIb, and $\alpha = 0.05$ for IIIc. The lines for IIIb
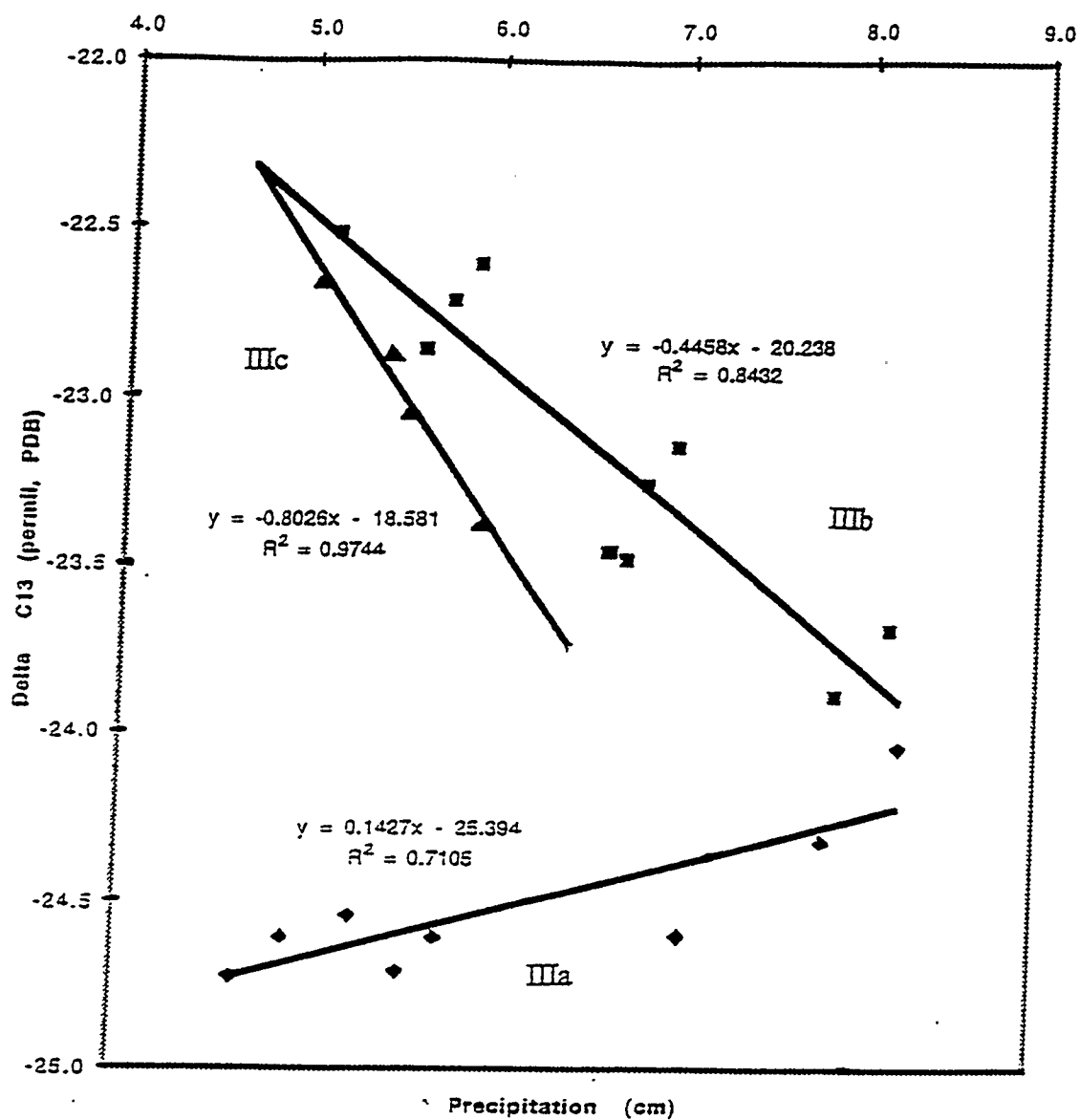
Fig. 4.15 Correlations between corrected $\delta^{13}C$ values and precipitation for three intervals in Stage III (Errors in $\delta^{13}C$ values are roughly the size of the symbol).

and IIIc intersect at the point 4.64 cm, -22.31 $^o/_{oo}$. Another possibility is to consider combining the data of IIIb and IIIc since both have the inverse dependence between $\delta^{13}C$ values and precipitation. In this case, the best linear fit (Fig. 4.16) is:

$$\delta^{13}C_{\text{S-ave}} = (-0.38 \pm 0.06) \, P_{\text{S-ave}} - (20.72 \pm 0.40) \qquad R^2 = 0.76 \qquad (4.6)$$
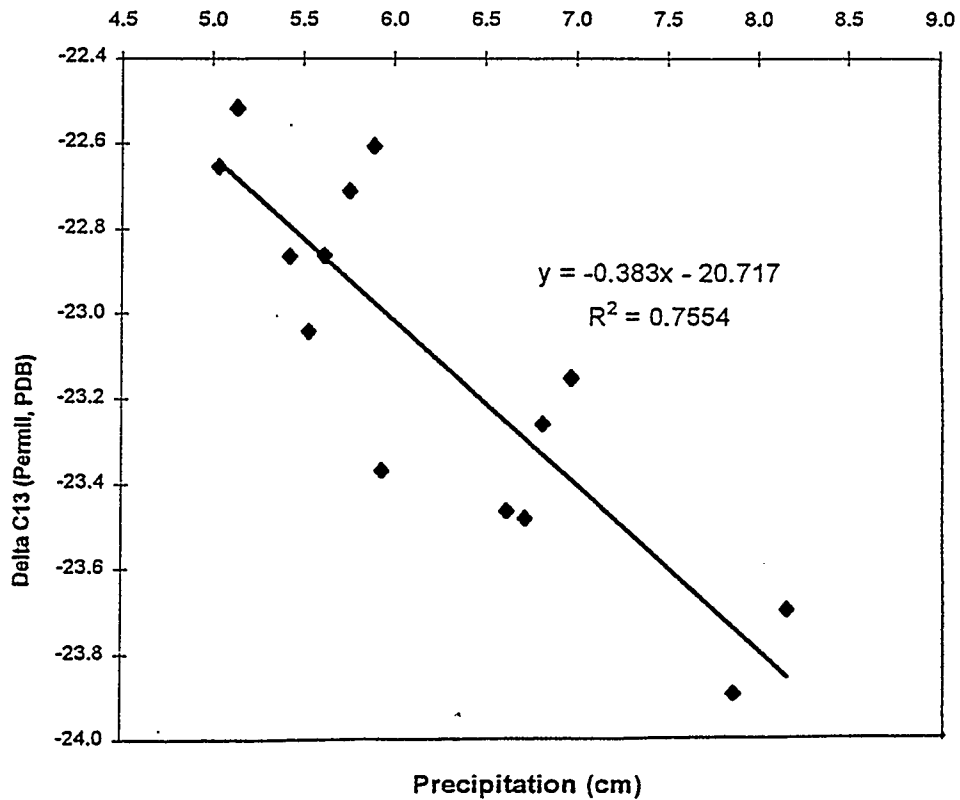
R is significant at $\alpha = 0.01$.

Fig. 4.16 Correlation between corrected $\delta^{13}C$ values and precipitation for combined data from intervals IIIb and IIIc (Errors in δ^{13}C values are roughly the size of the symbol).

4.3 Correlation between the Precipitation and Ring Width

The ring widths of the *Tamarix aphylla* trunk were measured in the Kananaskis Field Station of the University of Calgary by Kara Liane Webster. The data are given in Table 4.4.

No significant correlation was found between the precipitation and ring width for Stages I and II. The five year running averages of ring width vs. precipitation is plotted in Fig. 4.17.

The plot of ring width vs. precipitation is similar to the plot of $\delta^{13}C$ vs. precipitation for Stage III (compare Figs. 4.11 and 4.17). In Fig. 4.17, it can be seen that ring width increases with the increasing precipitation from 1969 to 1976 (as was found for corrected $\delta^{13}C$ vs. precipitation). In other words, the description of interval IIIa is appropriate for both $\delta^{13}C$ values and ring width. Ring width vs. precipitation for interval IIIa is plotted in Fig. 4.18. The best fit (R is significant at $\alpha = 0.01$) is:

$$\text{IIIa} \qquad RW_{5\text{-ave}} = (0.34 \pm 0.05)\, P_{5\text{-ave}} - (0.59 \pm 0.33) \qquad R^2 = 0.87 \qquad (4.7)$$

Proceeding with intervals IIIb and IIIc as defined for $\delta^{13}C$ data gives the following linear fits of ring width versus precipitation (Figs. 4.19 and 4.20):

$$\text{IIIb} \qquad RW_{5\text{-ave}} = (-5.67 \pm 1.32)\, P_{5\text{-ave}} + (48.02 \pm 8.67) \qquad R^2 = 0.70 \qquad (4.8)$$

$$\text{IIIc} \qquad RW_{5\text{-ave}} = (-14.37 \pm 6.18)\, P_{5\text{-ave}} + (87.89 \pm 33.94) \qquad R^2 = 0.73 \qquad (4.9)$$

R is significant at $\alpha = 0.01$ for IIIb and $\alpha = 0.20$ for IIIc.

Table 4.4 Raw values of ring widths (measured by Kara Liane Webster, in Kananaskis Field Station of the University of Calgary) and five year running average of ring width.

Time (Year)	Raw ring width (mm)	Five year ave. ring width (mm)
1946	N/A	N/A
1947	30.02	N/A
1948	11.12	N/A
1949	6.82	10.34
1950	1.79	4.78
1951	1.94	3.06
1952	2.24	2.19
1953	2.50	5.48
1954	2.46	7.31
1955	18.27	7.45
1956	11.07	7.45
1957	2.93	9.17
1958	2.51	5.67
1959	11.06	3.68
1960	0.80	3.28
1961	1.12	3.74
1962	0.93	1.76
1963	4.80	1.96
1964	1.16	3.58
1965	1.81	3.63
1966	9.22	2.97
1967	1.15	3.01
1968	1.52	2.83
1969	1.37	1.15
1970	0.88	1.24

(Continue of Table 4.4)

Time (Year)	Raw ring width (mm)	Five year ave. ring width (mm)
1971	0.85	1.15
1972	1.60	1.06
1973	1.08	1.11
1974	0.88	1.84
1975	1.15	1.89
1976	4.51	2.37
1977	1.86	2.80
1978	3.45	4.48
1979	3.02	5.23
1980	9.55	5.66
1981	8.29	10.72
1982	3.97	10.27
1983	28.76	11.20
1984	0.80	20.92
1985	14.17	21.24
1986	56.90	15.63
1987	5.58	15.75
1988	0.71	13.17
1989	1.37	3.92
1990	1.28	3.64
1991	10.70	N/A
1992	4.15	N/A

However, unlike $\delta^{13}C$ data, combining of intervals IIIb and IIIc does not give a good linear fit (The significance level was very low). This is also evident from the very different slopes and intercept of Eqs. 4.6 and 4.7.

The correlation lines for ring width and precipitation for three intervals are plotted in Fig. 4.21. The intersection for the best linear fits for IIIb and IIIc is 4.58 cm and 22.05 mm. It is noted that the precipitation value of 4.58 cm is close to that of 4.64 cm found at the intersection in the $\delta^{13}C$ versus precipitation plot. This is also close to the lowest precipitation during Stage III.

Fig. 4.17 Plot of ring width vs. precipitation for Stage III

$y = 0.3365x - 0.5941$
$R^2 = 0.8719$

Fig. 4.18 Correlation between ring width and precipitation for IIIa

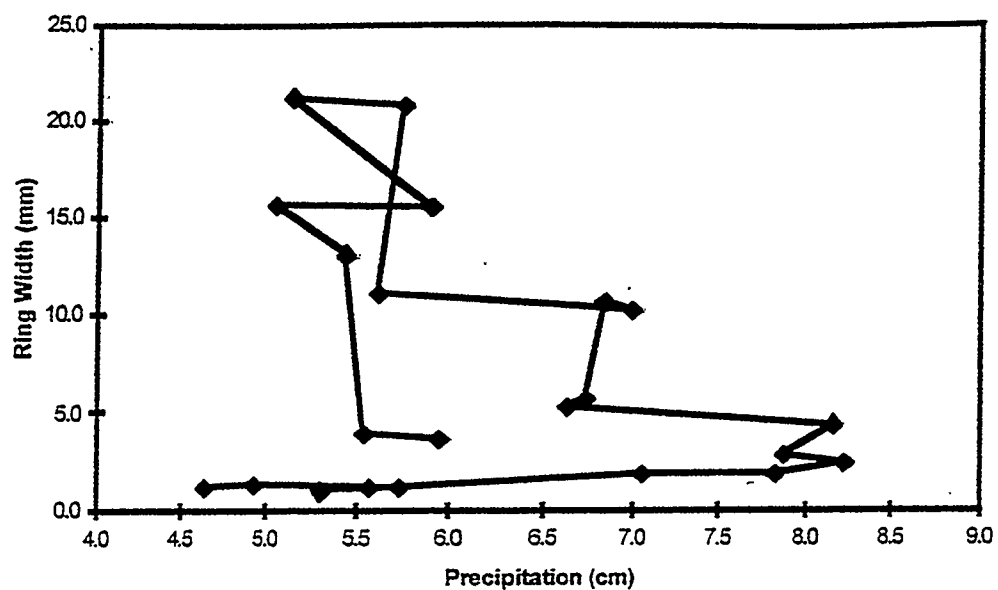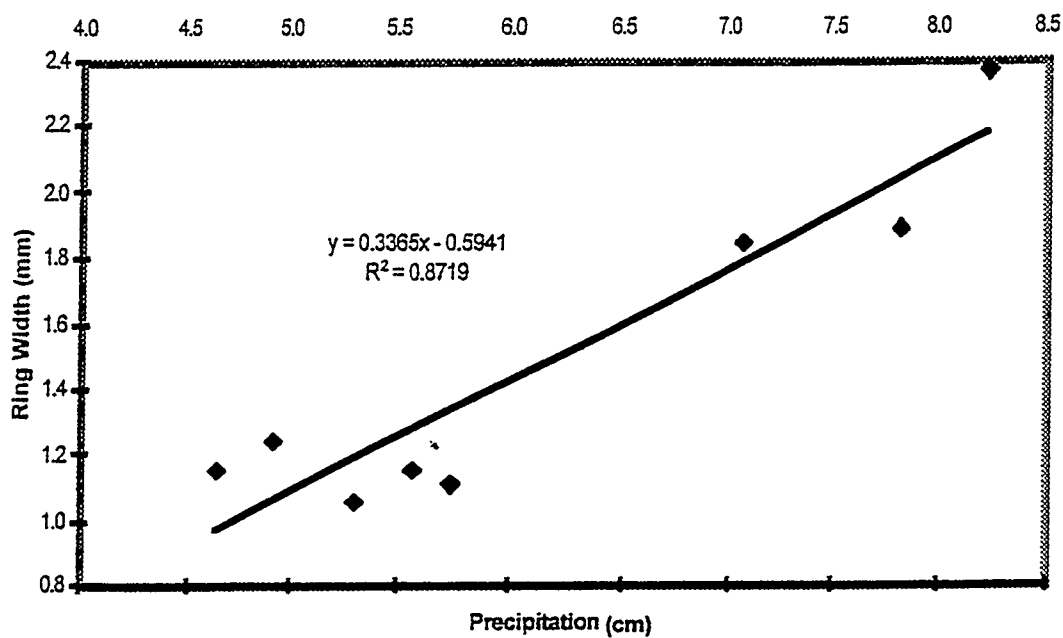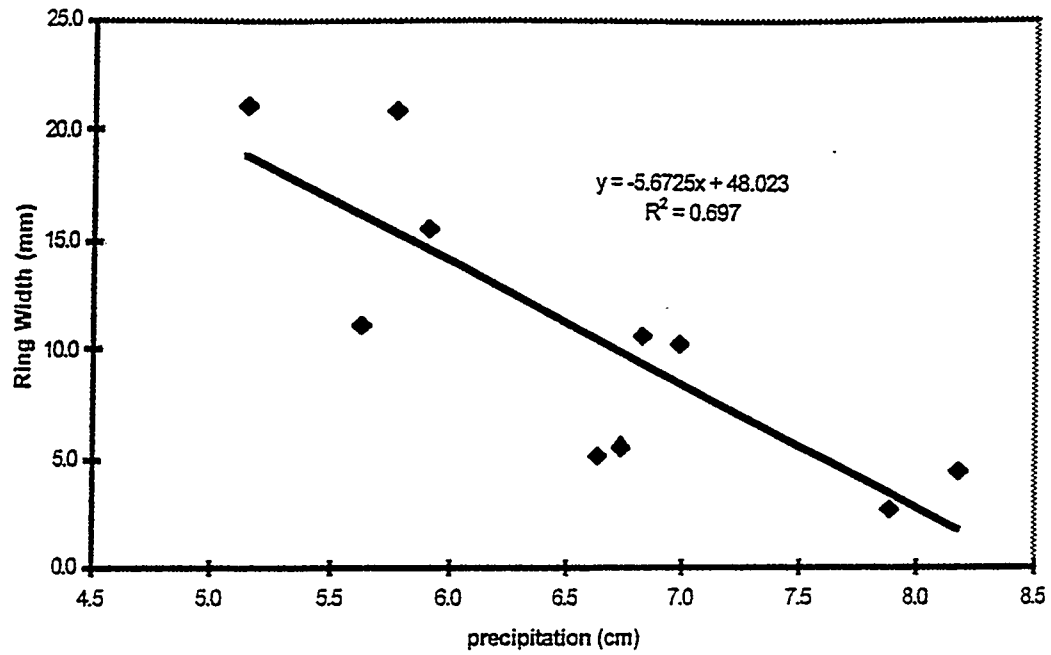Fig. 4.19 Correlation between ring width and precipitation for IIIb
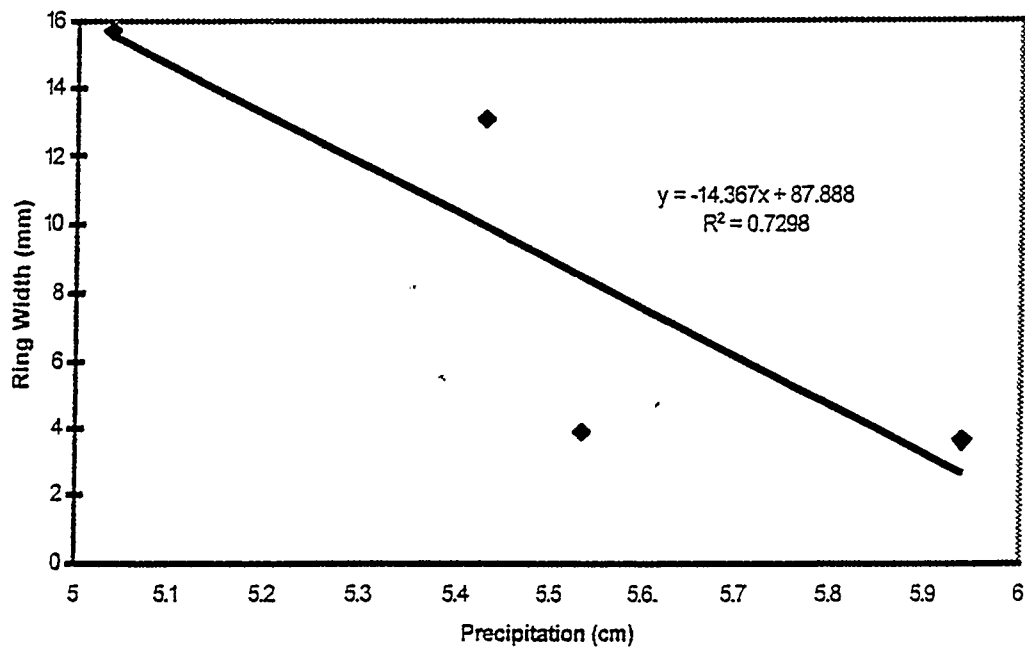
Fig. 4.20 Correlation between ring width and precipitation for IIIc
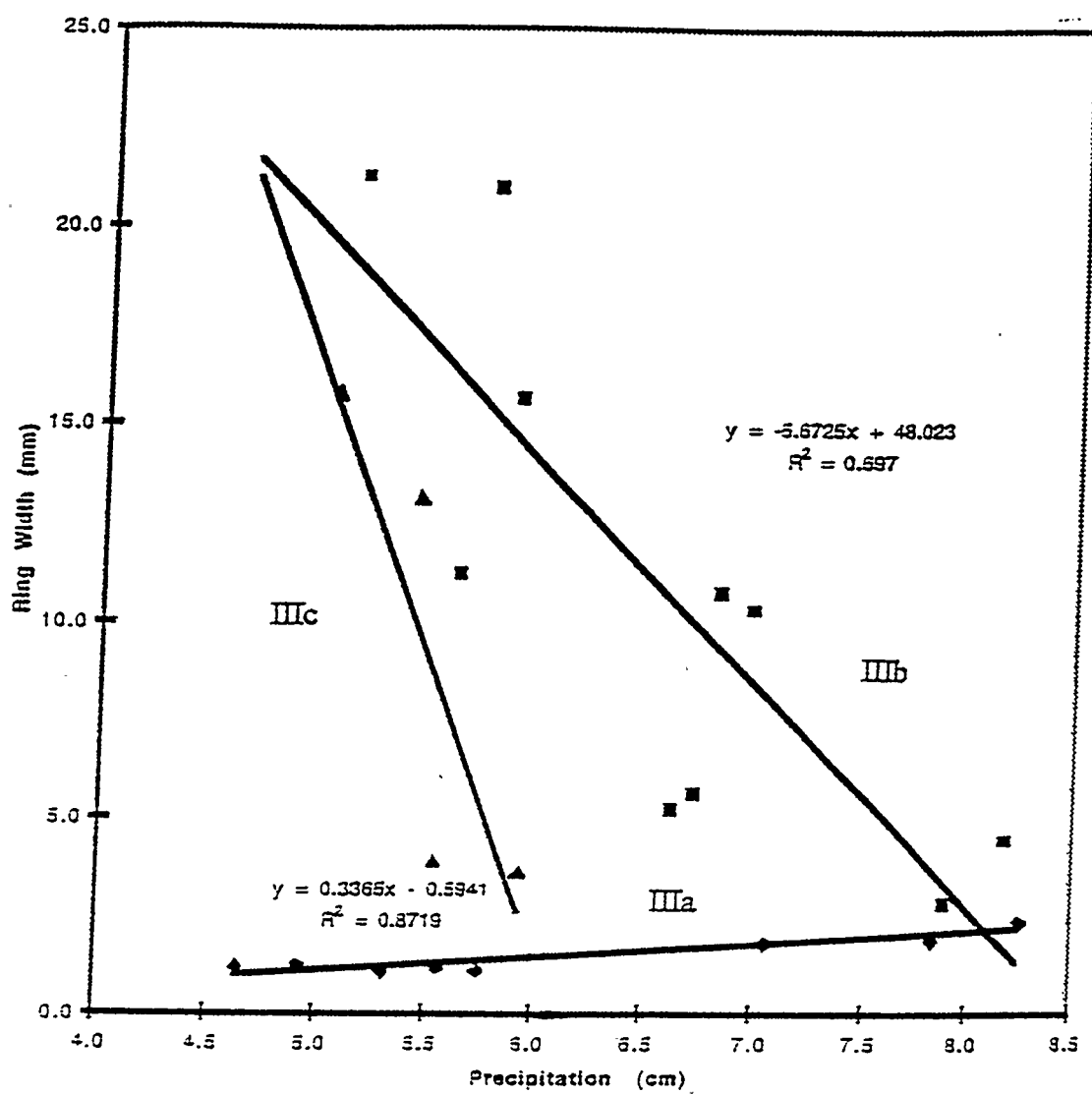
Fig. 4.21 Correlation between ring width and precipitation for Stage III

4.4 Correlation between the $\delta^{13}C$ Values and Ring Widths

No significant correlations were found between the ring width and the $\delta^{13}C$ values for Stage I and Stage II. The five year running averages of the ring width and the $\delta^{13}C$ value for stage III are plotted in Fig. 4.22. The ring width vs. $\delta^{13}C$ is plotted for the separate intervals of Stage III in Figs. 4.23, 4.24, and 4.25. The best linear fits for them are:

IIIa $\quad RW_{5\text{-ave}} = (1.81 \pm 0.46)\ \delta^{13}C + (45.93 \pm 11.16) \quad R^2 = 0.73 \qquad (4.10)$

IIIb $\quad RW_{5\text{-ave}} = (13.12 \pm 1.73)\ \delta^{13}C + (314.59 \pm 40.02) \quad R^2 = 0.88 \qquad (4.11)$

IIIc $\quad RW_{5\text{-ave}} = (18.52 \pm 6.51)\ \delta^{13}C + (434.76 \pm 149.58) \quad R^2 = 0.80 \qquad (4.12)$

R value is significant at $\alpha = 0.01$ for IIIa, $\alpha = 0.01$ for IIIb, and $\alpha = 0.10$ for IIIc. The correlation lines for the separate intervals of Stage III are plotted in Fig. 4.26. The intersection of the best fits for IIIb and IIIc is -22.01 $^0/_{00}$ and 25.94 mm. The value of -22.01 $^0/_{00}$ is close to that found at the intersection on the $\delta^{13}C$ versus precipitation plot, -22.31 $^0/_{00}$ (Fig. 4.15).

Fig. 4.22 Plot of ring width vs. corrected $\delta^{13}C$ for Stage III (Errors in $\delta^{13}C$ values are roughly the size of the symbol).

$$y = 1.8131x + 45.$$
$$R^2 = 0.7257$$
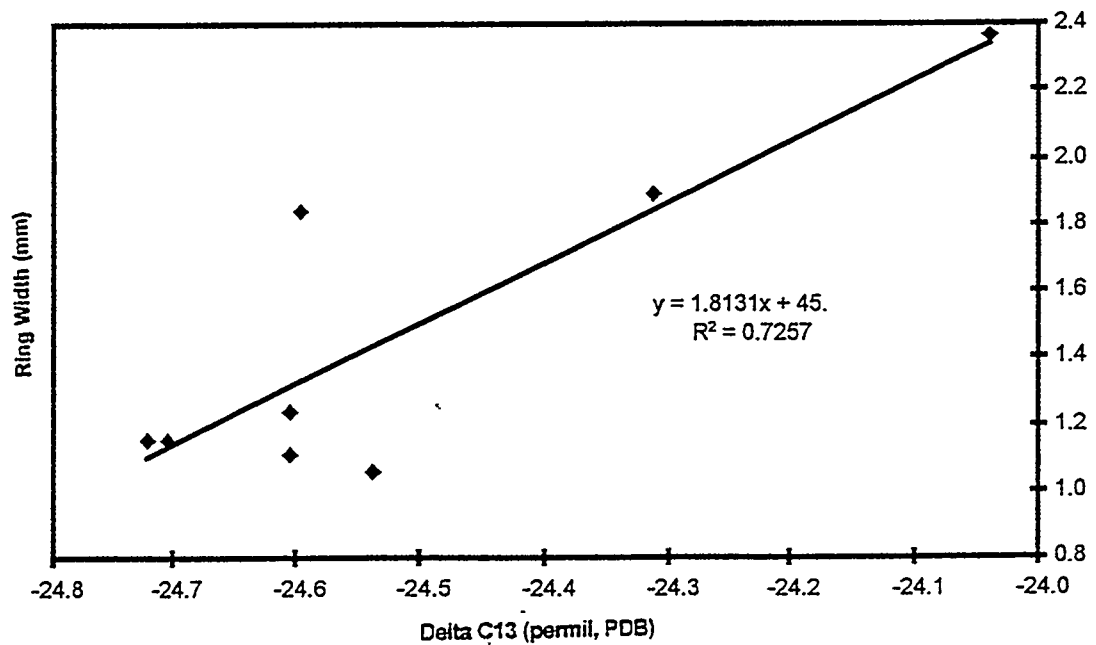
Fig. 4.23 Correlation between ring width and corrected $\delta^{13}C$ for IIIa (Errors in $\delta^{13}C$ values are roughly the double size of the symbol).
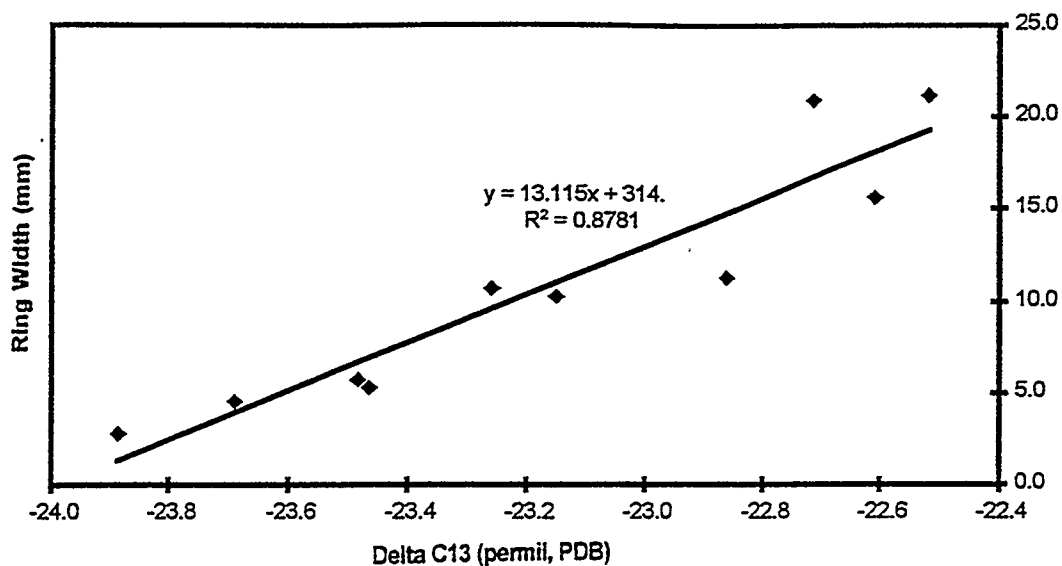
Fig. 4.24 Correlation between ring width and corrected $\delta^{13}C$ **for IIIb (Errors in** $\delta^{13}C$ **values are roughly the size of the symbol)**

The first chart shows:
$$y = 13.115x + 314.$$
$$R^2 = 0.8781$$
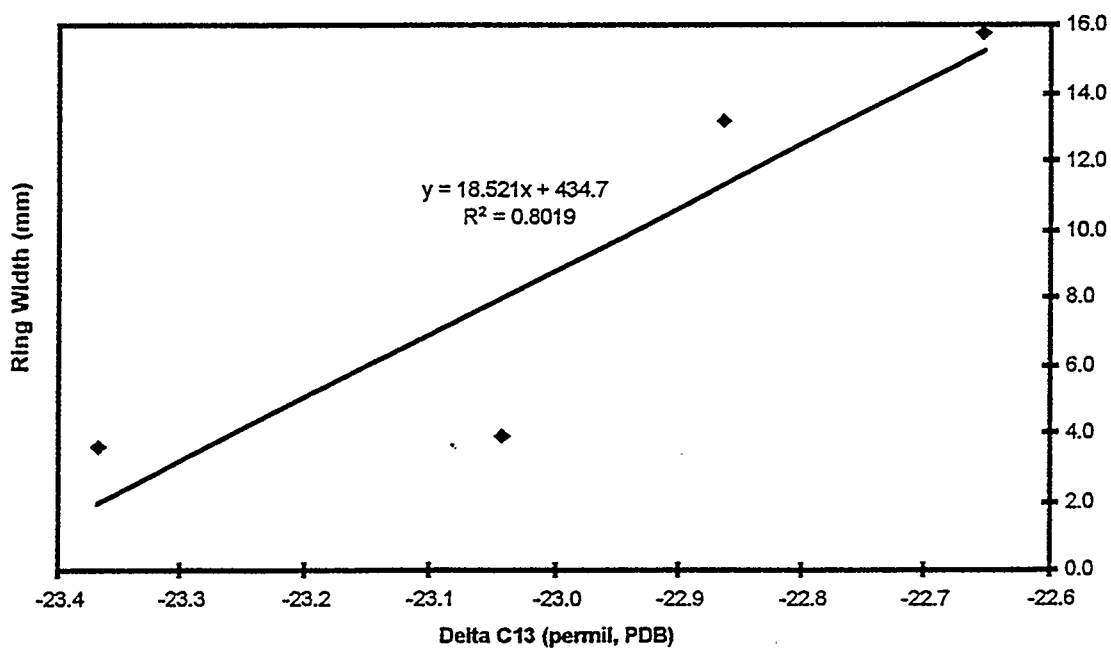
Fig. 4.25 Correlation between ring width and corrected $\delta^{13}C$ **for IIIc (Errors in** $\delta^{13}C$ **values are roughly the double size of the symbol)**

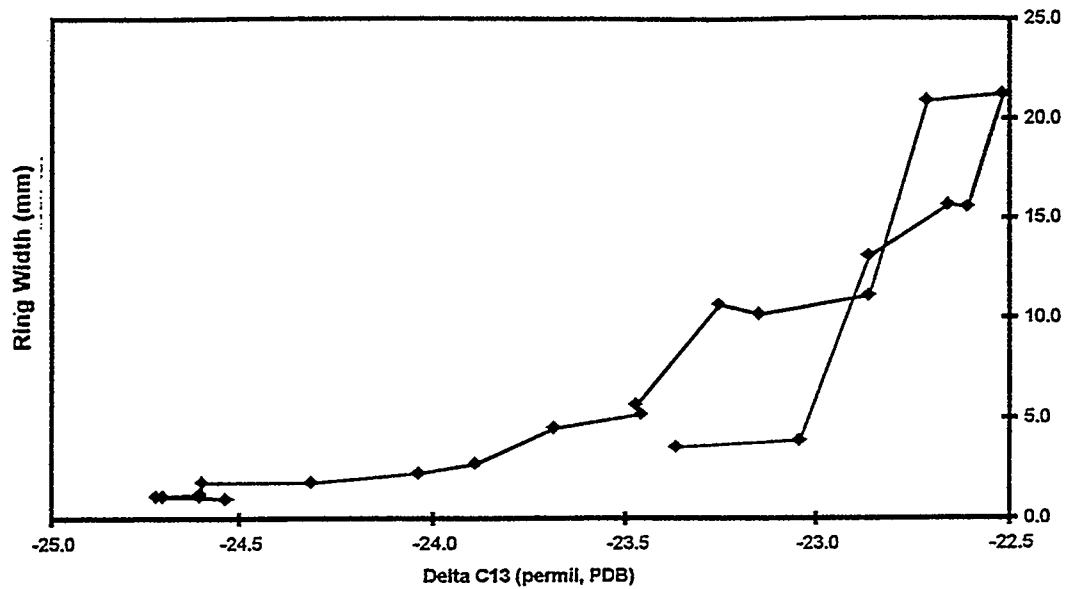The second chart shows:
$$y = 18.521x + 434.7$$
$$R^2 = 0.8019$$
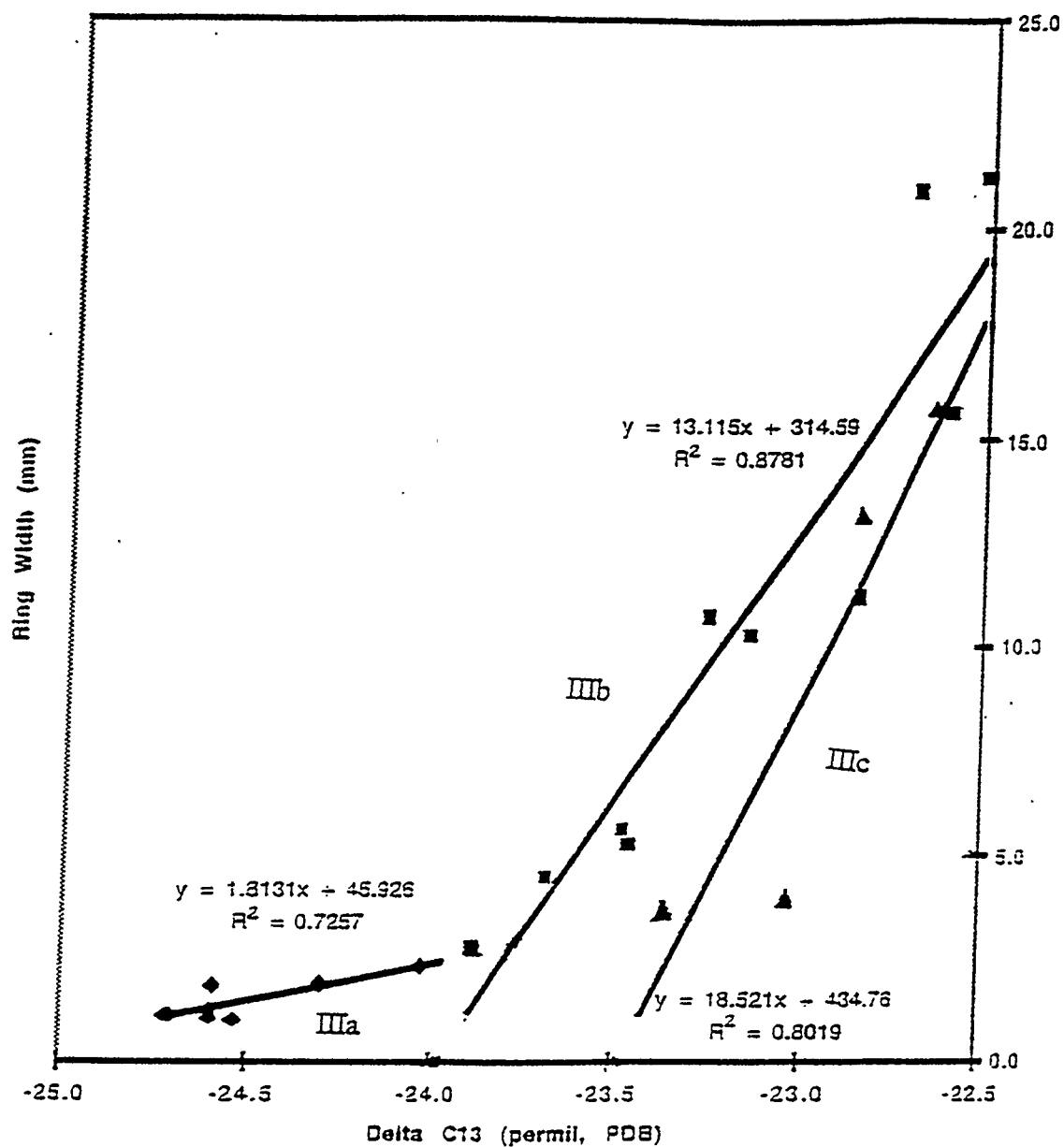
Fig. 4.26 Correlation between ring width and corrected $\delta^{13}C$ for Stage III (Errors in $\delta^{13}C$ values are roughly the size of the symbol).

4.5 Stable Oxygen Isotope Composition of Cellulose

The measured $\delta^{18}O$ values are given in Table 4.5. There are data gaps since the cellulose for 10 samples had been exhausted by repeated $\delta^{13}C$ measurements. The reproducibility of $\delta^{18}O$ measurement was poorer, possibly as high as $\pm 1^0/_{00}$. There is also suspicion that some high values (particularly near $+30^0/_{00}$) are not valid. Unfortunately, there was insufficient material for repeats on those samples. Any leakage of atmospheric O_2 into the nickel reactor could raise the $\delta^{18}O$ values. One possibility is that upon heating, micro-cracks open in the weld between the nickel tube and its nickel disk holder. In any case, the bulk of the data seems reasonable and permits qualitative interpretation.

The $\delta^{18}O$ values and precipitation are plotted along with their five year running averages against time in Fig. 4.27. There appears to be a general trend of decreasing $\delta^{18}O$ values with time, particular after 1970.

Table 4.5 The $\delta^{18}O$ values of *Tamarix aphylla* tree ring cellulose

Age (Year)	$\delta^{18}O$ cellulose (permil, V-SMOW)	Age (Year)	$\delta^{18}O$ cellulose (permil, V-SMOW)
1945	22.8	1967	21.1
1946	24.6	1968	28.1
1947	26.3	1969	20.8
1948	23.0	1970	25.6
1949	21.3	1971	26.4
1950	30.0	1973	19.8
1951	20.3	1974	19.8
1952	20.6	1976	25.1
1953	25.2	1977	20.8
1954	24.0	1978	23.6
1955	21.8	1979	22.6
1956	22.6	1980	19.9
1957	22.9	1981	21.2
1958	22.0	1982	19.5
1959	20.6	1983	24.1
1960	25.0	1984	21.5
1961	29.4	1986	18.7
1962	24.7	1990	16.8
1965	20.8	1991	18.2
1966	18.2	1992	20.1
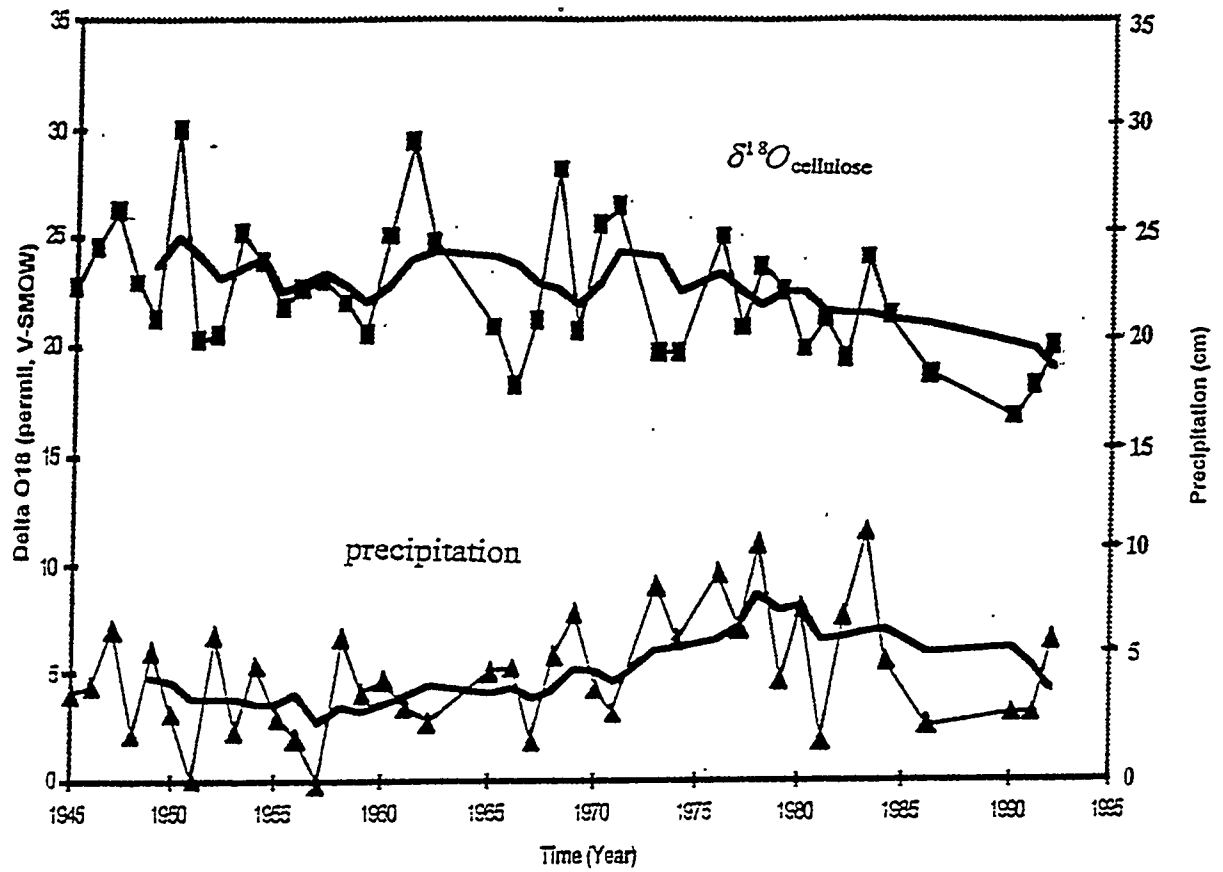
Fig. 4.27 Plot of $\delta^{18}O$ values for cellulose for *Tamarix aphylla* specimen, Death Valley, California and precipitation versus time

Chapter 5 Discussion

5.1 Water Sources for Tree Growth

For the whole earth, precipitation on average is dispersed four ways: (1) nearly half of the total returns directly to the atmosphere by evaporation, (2) a sixth of the total is returned to the atmosphere by transpiration, (3) one third discharges into the oceans, and (4) 1 or 2 percent enters the ground. However for the Death Valley area, more than 90 percent of precipitation returns to the atmosphere by evaporation, most of the remaining 10 percent also goes back to atmosphere by transpiration, no water enters an ocean, and finally little if any finds its way through the subsurface to a water table (Hunt, 1975).

Local precipitation has no significant effect on the water table in the Death Valley area, because groundwater is regionally recharged. A principal source seems to be the Spring Mountains, the range east of Death Valley. Rain and meltwater from snow recharge groundwater in Pahrump Valley. This escapes through many faults in the surrounding mountains, some moving to Furnace Creek via the Amargosa Desert (Hunt, 1975).

Therefore, the groundwater in the Death Valley area is assumed to be affected by precipitation in the Spring Mountains. During the lifetime of the *Tamarix aphylla* studied in this thesis, it is assumed that there was no correlation between the height of water table and the amount of local precipitation. Since nearly 100 percent of precipitation returns to atmosphere by evaporation and transpiration, it can be assumed that the local precipitation affects the local relative humidity in the short term. Also since nearly 10 percent of the precipitation returned to the atmosphere by transpiration, it is possible that the amount of precipitation affects the amount of water in the vadose zone (unsaturated zone above the water table).

5.2 Growth Stages

Yang *et al* (1996) studied the sulfur isotope composition of tree rings from the same slab used in this thesis research. They concluded that the tree growth could be divided into three different growth periods (Fig. 5.1). During the first stage, roots were solely in the vadose zone and soil water sulfate originated mainly from rain water. As more of the root network reached the water table, groundwater SO_4^{2-} with higher $\delta^{34}S$ values became increasingly supplied to the tree during the second stage. During the third mature tree stage, most of the root network reached the water table.

The response of carbon stable isotope data to precipitation, as described in chapter 4, independently of the study of Yang *et al.* (1996) also identified three growth stages. The first stage was from 1944 to 1946, the second from 1947 to 1967, and the third from 1967 to 1993. There are compelling reasons to further divide the third stage (Stage III) into three intervals.

In light of the findings with C-isotope data, one can re-evaluate the sulfur isotope data. The stages decided by Yang *et al.* (1996) were based on data for dissolved sulfate, the emphasis in the study being placed on hydrology. If one examines the data for total sulfur, which includes organic-S (Fig. 5.1), it can be argued that Stage III can be divided into three intervals which coincide with those deduced from the $\delta^{13}C$ data. $\delta^{34}S$ values increased from +15.3 $^0/_{00}$ to +17$^0/_{00}$ during interval IIIa. They decreased from +17$^0/_{00}$ to +16.3$^0/_{00}$ during interval IIIb, and then increased from +16.3$^0/_{00}$ to +17$^0/_{00}$ during interval IIIc.

Tamarix aphylla

YOUNG

MATURE

HIGH

Vadose Zone

WATER TABLE

LOW

(not to scale) Saturated Zone

I

II

III

$\delta^{34}S$ (o/oo V-CDT)

18

17

Some roots reach
saturated zone

16

All
roots
in
vadose
zone

15

14

13

IIIa

IIIb

IIIc

Most roots reach
saturated zone

1940   1950   1960   1970   1980   1990
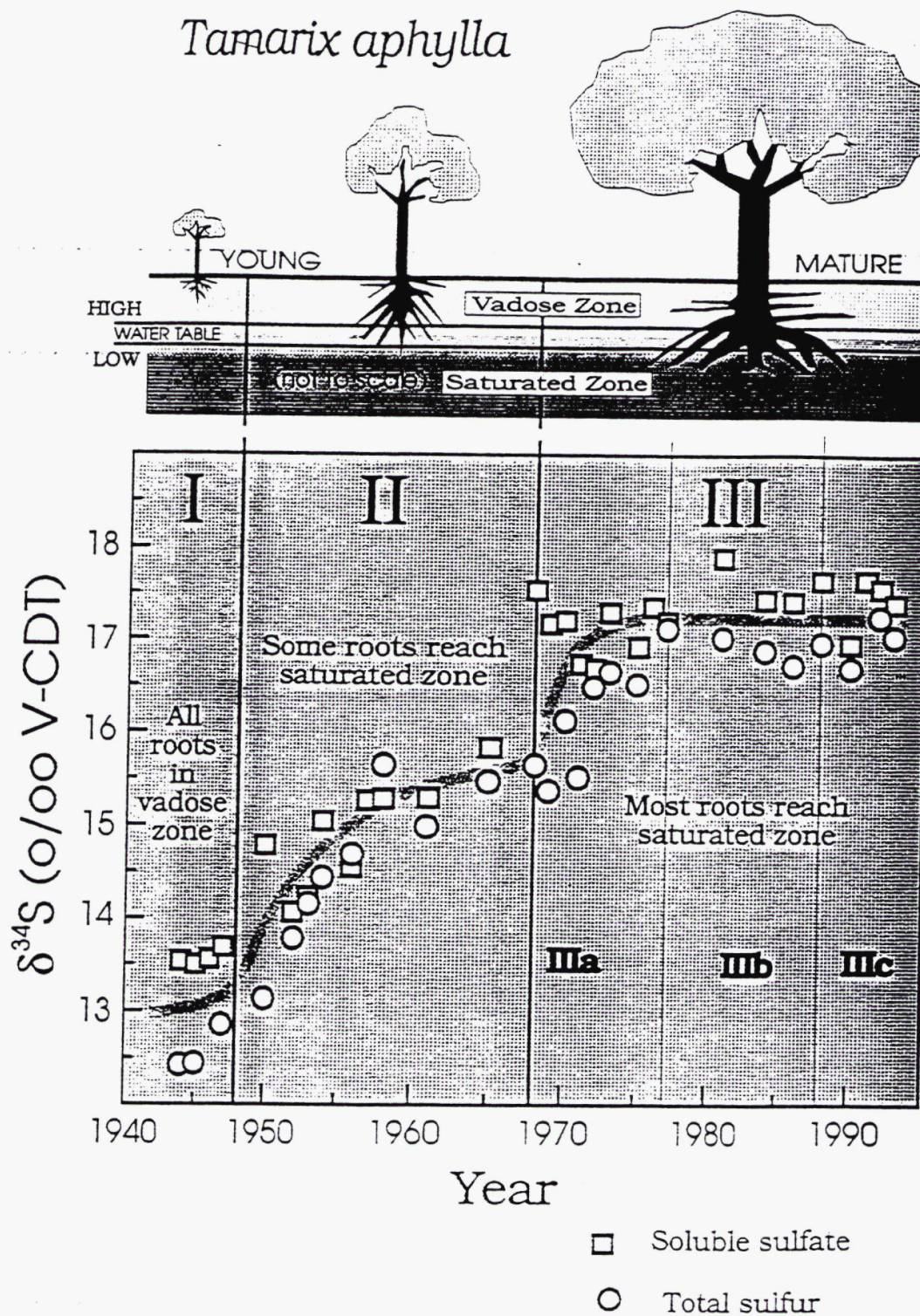
Year

□   Soluble sulfate

○   Total sulfur

Fig. 5.1 $\delta^{34}S$ values versus year of tree ring growth, and their relationships to water sources, sulfate sources and growth for *Tamarix aphylla*, Death Valley, California (after Yang *et al.* 1996)

5.3 Theoretical Relationships between Physiological Parameters and $\delta^{13}c$ Values

The following relationship can be derived from Eq. 2.19 by rearrangement;

$$\frac{A}{gC_a} = 1 + (\delta^{13}C_{cell} - \delta^{13}C_{atm} + a) / (b - a) \qquad (5.1)$$

where A is the CO_2 assimilation rate, g is leaf conductance, and C_a (c_a in Equation 2.19) is the concentration of atmospheric CO_2. For the left side of Equation 5.1 to be unit-less, C_a is expressed as the partial pressure of CO_2 divided by the total pressure, or an equivalent ratio. From the measured $\delta^{13}C_{cell}$ values, $\dfrac{A}{gC_a}$ can be estimated if values are assumed for "a" and "b".

In the following discussion, Stage I is omitted because of the short time duration, few samples, and the very negative $\delta^{13}C$ values which must reflect early growth phenomena, e.g. since early foliage is close to the ground, soil CO_2 could play a larger (yet minor) role in photosynthesis than is the case for more mature higher foliage.

For Stage II and Stage III, five year running averages of the $\delta^{13}C_{cell}$, corrected for decreasing $\delta^{13}C$ value and increasing concentration of atmospheric CO_2 due to fossil fuel burning, are used in Eq. 5.1. Based on discussion in Chapter 2, "a" is set at 4.4, "b" at 27, and $\delta^{13}C_{atm}$ at $-6.7^0/_{00}$.

5.3.1 Stage II

As seen in chapter 4, the five year running averages of the corrected $\delta^{13}C_{cell}$ values, during Stage III respond inversely and linearly to the amount of precipitation (R^2

= 0.66). Conversely, one could assume a linear relationship and estimate the changes in atmospheric CO_2 over this time.

$\dfrac{A}{gC_a}$ values calculated from $\delta^{13}C_{cell}$ values using Eq. 5.1, are plotted against precipitation in Fig. 5.2. The linear fit, which is derivable from Eq. 4.2, is:

$$\frac{A}{gC_a} = (0.015 \pm 0.003)\, P_{5\text{-ave}} + (0.329 \pm 0.010) \qquad R^2 = 0.68 \qquad (5.2)$$

R is significant at $\alpha = 0.01$. The unit for the slope is cm^{-1}.

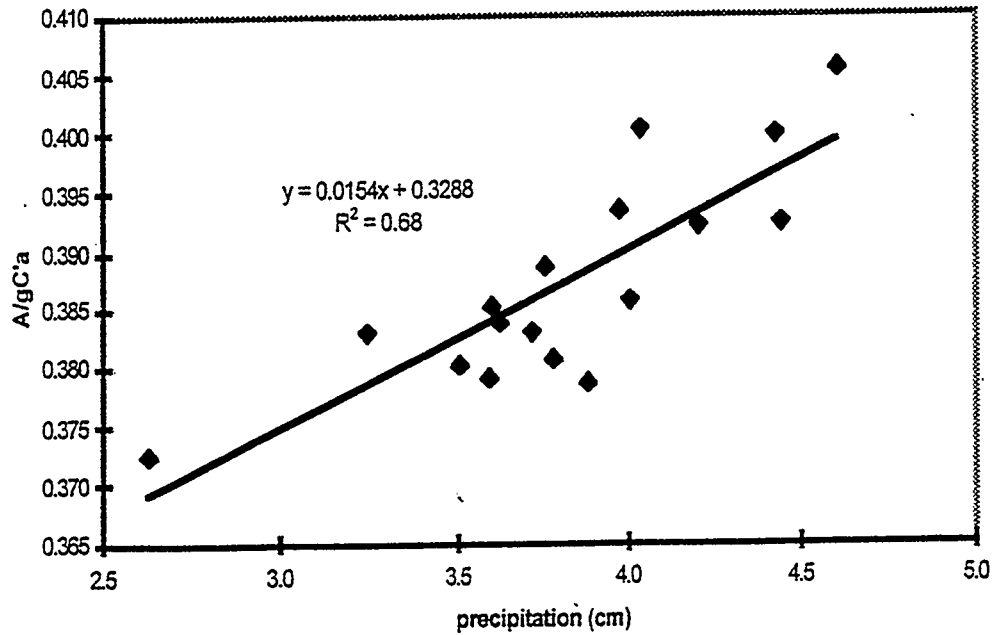Fig. 5.2 Plot of $\dfrac{A}{gC_a}$ vs. precipitation for Stage II.

Since the effect of the changes in $\delta^{13}C$ and concentration of the atmospheric CO_2 has been corrected, C_a can be considered to be a constant. Therefore, there is a linear positive correlation between $\dfrac{A}{g}$ and precipitation.

The linear positive correlation between $\dfrac{A}{g}$ and precipitation means the fractional increase of A is larger than that of g with increasing precipitation. This can be explained as follows: During Stage II growth, it is assumed that most of the roots of the tree were in the vadose zone, and water in this zone comes mainly from precipitation. Therefore the tree was growing under water stress (drought stress). For the tree to survive in such an arid environment, it is likely that the stomatal apertures were very sensitive to the water availability, and in turn , the amount of precipitation. Increase in stomatal aperture with increasing precipitation would be conducive to higher transpiration rates and larger leaf conductance, g. This in turn would increase the photosynthesis and CO_2 assimilation rates.

5.3.2 Stage III

Proceeding with Stage IIIa, IIIb, and IIIc as done with Stage II gives the following linear relationships (Fig.5.3):

IIIa $\dfrac{A}{gC_a}= (0.006 \pm 0.002)\,P_{5\text{-ave}} + (0.368 \pm 0.010)$ $R^2 = 0.71$ (5.3)

IIIb $\dfrac{A}{gC_a}= (-0.020 \pm 0.003)\,P_{5\text{-ave}} + (0.596 \pm 0.020)$ $R^2 = 0.84$ (5.4)

IIIc $\dfrac{A}{gC_a}= (-0.036 \pm 0.004)\,P_{5\text{-ave}} + (0.669 \pm 0.022)$ $R^2 = 0.97$ (5.5)

These equations are derivable from Eqs. 4.2, 4.3, and 4.4. R is significant at $\alpha = 0.01$, 0.01, and 0.05 respectively. The units for the slopes are cm^{-1}.

On the basis of sulfur isotope data, it was concluded that during the third stage, most of the tree roots had reached the water table. The groundwater is the main water source for tree growth and its availability is not influenced markedly by local precipitation. Hagemeyer and Waisel (1989) showed that the stomatal aperture of *Tamarix aphylla* did not change much with changes in the relative humidity of the ambient atmosphere. They found that in *in vitro* experiments, the transpiration rate was negatively correlated with relative humidity over a wide range of NaCl concentrations. If, as suggested by the above studies, the leaf conductance, g, remained constant with varying amounts of precipitation, then A responded linearly and inversely to the amount of local precipitation during intervals IIIb and IIIc. Since the relative humidity of Death Valley is determined by the amount of precipitation (about 100 % of the precipitation returns to the atmosphere), then lower transpiration rates are expected with higher precipitation. The assimilation rate of CO_2, A, has been found to increase with higher transpiration rates in laboratory studies with several species (Mott and Parkhurst, 1991). This in turn implies a linear negative correlation between A and the amount of precipitation as found for intervals IIIb and IIIc (Equations. 5.4 and 5.5).

In contrast, for interval IIIa, the $\dfrac{A}{gC_a}$ value correlated positively with the amount of precipitation as found for Stage II (although the slope for the latter is much higher). This supports other evidence that interval IIIa is transitional between Stage II and interval IIIb.
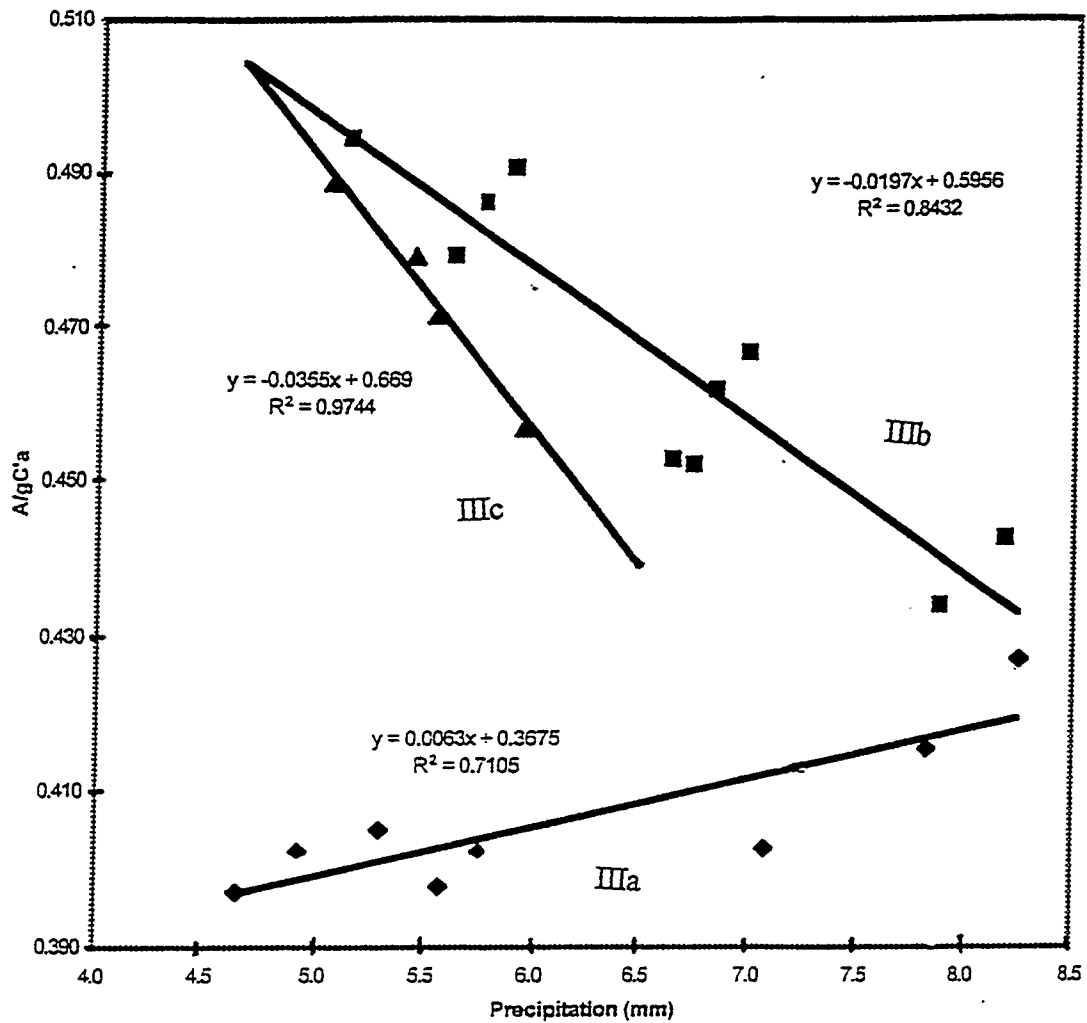
Fig. 5.3 Plot of $\dfrac{A}{gC_a}$ vs. precipitation for the Stage III.

5.4 Ring Width

When under water stress during stage II, it is likely that the tree invested most of its carbon into roots. In this way, the tap roots would reach the water table as early as possible. Masle *et al* (1987) showed that the ratio of plant carbon mass to leaf area increased markedly with increasing soil strength (i.e., the mechanical resistance of the soil

to deformation by roots). They concluded that this is mainly because of a greater investment of carbon into roots than into shoots. Masle and Passioura (1987) analyzed the response of the shoot to the soil strength. Their experiment showed that both stomatal conductance and shoot growth responded similarly when the soil strength was increased by soil density or decreasing water content.

Greater investment of carbon into the growth of roots can explain why no significant correlation was found between the ring width and the $\delta^{13}C_{cell}$ value or precipitation during Stage II

For considering the ring width variations during Stage III, equation 2.19 is rewritten as:

$$\delta^{13}C_{cell} - \delta^{13}C_{atm} = -b + \frac{b-a}{gC_a} A \qquad (5.6)$$

If the ring width is considered to be proportional to A, the CO_2 assimilation rate, then theoretically, positive linear correlation is expected between $\Delta\delta = (\delta^{13}C_{cell} - \delta^{13}C_{atm})$ and ring width. $\Delta\delta$ values are plotted against ring width for Stage III in Fig. 5.4. The linear fits for the three intervals in Stage III are:

IIIa $\Delta\delta = (0.40 \pm 0.10) RW_{5-ave} - (18.41 \pm 0.16)$ $R^2 = 0.73$ (5.7)

IIIb $\Delta\delta = (0.07 \pm 0.01) RW_{5-ave} - (17.18 \pm 0.11)$ $R^2 = 0.88$ (5.8)

IIIc $\Delta\delta = (0.04 \pm 0.02) RW_{5-ave} - (16.68 \pm 0.16)$ $R^2 = 0.80$ (5.9)

R value is significant at $\alpha = 0.01$ for IIIa, $\alpha = 0.01$ for IIIb, and $\alpha = 0.10$ for IIIc. The units for the slopes are mm^{-1}.
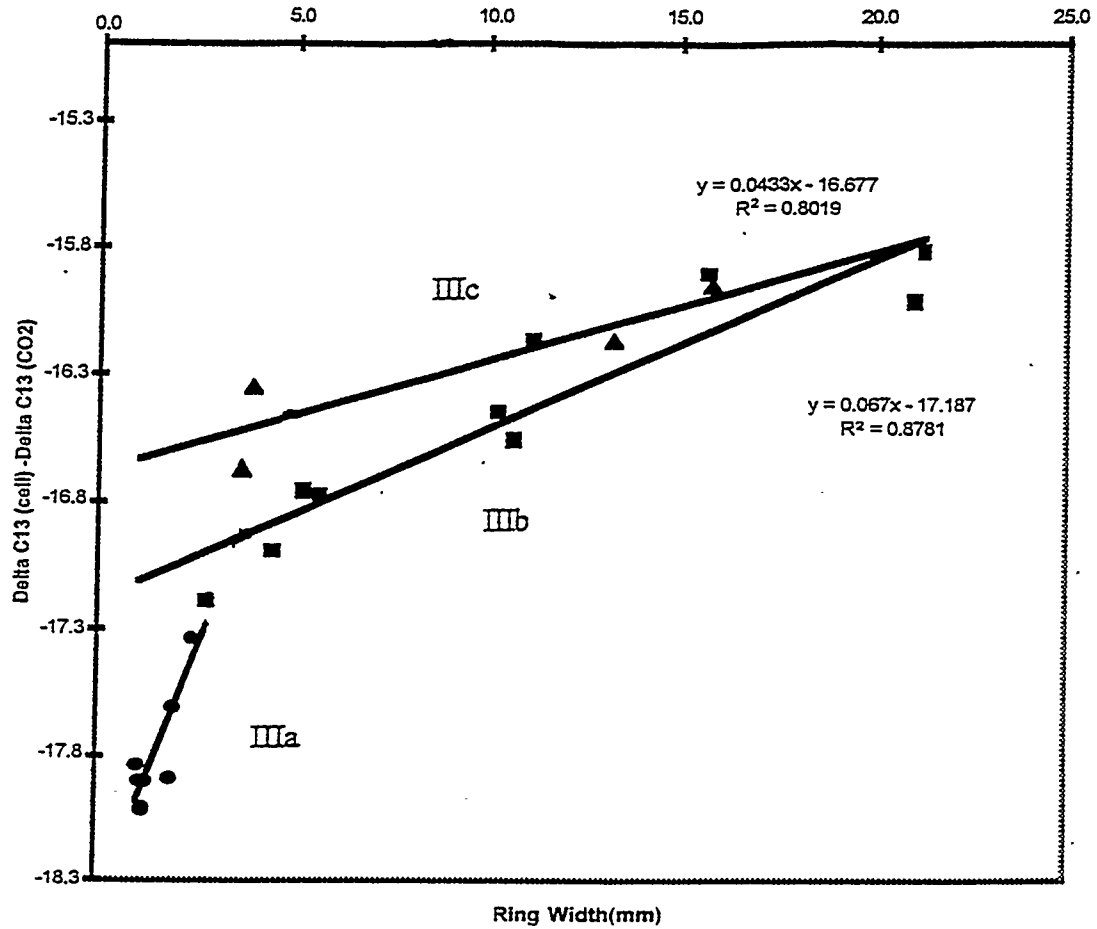
Fig. 5.4 Plot of ($\delta^{13}C_{\text{S-ave}}$ - $\delta^{13}C_{\text{atm}}$) **vs. ring width for IIIa, IIIb, and IIIc of Stage III**

5.5 Comparison of Stage II and Stage III

The slope found for $\dfrac{A}{gC_a}$ vs. $P_{\text{S-ave}}$ is 0.015 cm^{-1} for stage II, and steadly decreased to negative values, 0.006 cm^{-1}, -0.020 cm^{-1}, and -0.036 cm^{-1} for intervals IIIa, IIIb, and IIIc respectively. Both A and C_a varied with the amount of precipitation during stage II, but C_a can be considered as constant.with A varying with precipitation during intervals IIIb and IIIc.

The behavior during IIIa is intermediate to the above cases and is probably better described as a transition between Stage II and intervals IIIb and IIIc of Stage III. The $\delta^{34}S$ data for total sulfur support this interpretation (Fig. 5.1).

5.6 Stable Oxygen Isotope Data

Using the growth stages defined by $\delta^{13}C$ (and $\delta^{34}S$) data, it is seen that the five year running averages of $\delta^{18}O$ values varied little during Stage II and IIIa (Fig. 4.27). Although they generally decreased with time during IIIb and IIIc, there is a minimum at the beginning of IIIa which is difficult to explain. It is also noted that the spread in measured $\delta^{18}O$ values is much larger in Stage II than in Stage III and it appears to decrease during Stage III. The average $\delta^{18}O$ value during Stage II is $+23^o/_{oo}$ and $+21^o/_{oo}$ during IIIa and IIIb.

The $\delta^{18}O$ value of cellulose is mainly influenced by the $\delta^{18}O$ values of water sources and by the ambient humidity (Epstein et $al.$, 1977). The $\delta^{18}O$ values for the precipitation in the Death Valley area ranged from -6 to $-5^o/_{oo}$ in the summer and -11 to -8.3 $^o/_{oo}$ in the winter. The $\delta^{18}O$ values of spring waters were consistently near $-13^o/_{oo}$ (data provided by Wenbo Yang). The lower value of the latter relates to regional recharge, the main source being snowmelt in the Spring Mountains. The decreasing $\delta^{18}O$ values of cellulose during Stage III is consistent with derivation of more water from the more ^{18}O-depleted groundwater. It is seen that $(\delta^{18}O_{cellulose})_{min} - \delta^{18}O_{Spring}$ is about $(+17 - (-13))^o/_{oo}$, or $+30^o/_{oo}$. This is in agreement with the value of $+27 \pm 3^o/_{oo}$ described in Chapter 2. A larger value would seem reasonable in view of extensive evapotranspiration. During early growth, the $\delta^{18}O$ value of cellulose was influenced more by water in the vadose zone and in turn local precipitation which evaporates extensively. The smaller spread in $\delta^{18}O$ values in Stage III as compared to Stage II is consistent with going from

the vadose source where higher variability in $\delta^{18}O$ values is expected to the groundwater source with a more constant $\delta^{18}O$ value (since it is not subjected to extensive evaporation).

Fig. 5.5 shows that *Tamarix aphylla* in Death Valley, California, is distinguishable from the same species in Israel (Yakir *et al.*, 1994). The average $\delta^{18}O$ and $\delta^{13}C$ values for *Tamarix aphylla* in Death Valley are $22.5 \pm 3.0^0/_{00}$ and $-25.4 \pm 0.7^0/_{00}$ respectively. A Tamarix tree growing recently in central Israel had an average $\delta^{18}O$ value of $+28.8 \pm 0.6^0/_{00}$ and average $\delta^{13}C$ value of $-24.5 \pm 0.9^0/_{00}$. The lower $\delta^{18}O$ value in Death Valley is ascribed to the lower $\delta^{18}O$ values in precipitation and groundwater.

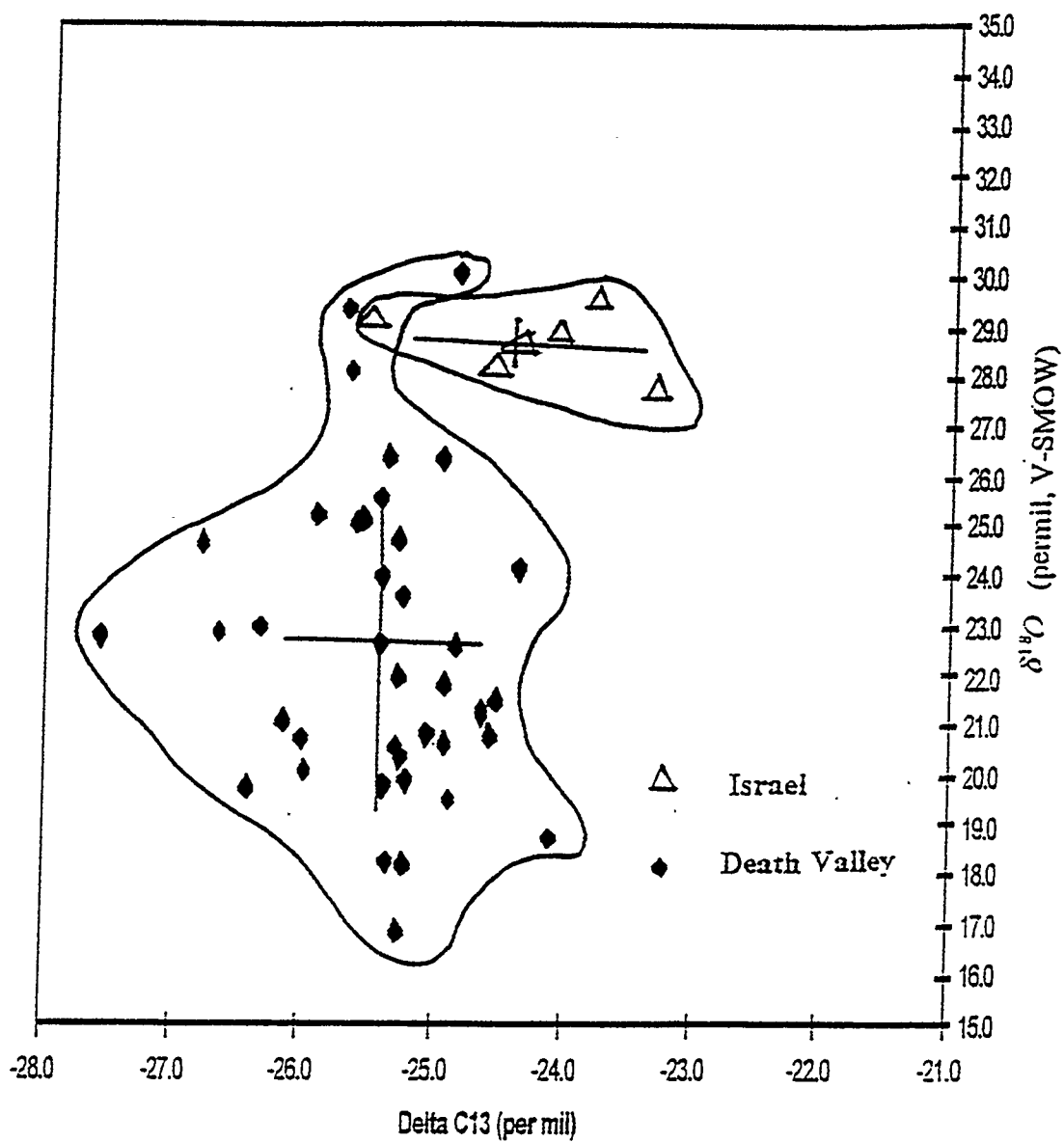**Fig. 5.5** Plot of the $\delta^{18}O$ values vs. the $\delta^{13}C$ values of cellulose from Tamarix trees from Death Valley and Israel

Chapter 6 Conclusions

There have been a variety of equations developed in the literature to relate the $\delta^{13}C$ of plant cellulose to climatic parameters. Examples are:

Coniferous trees, North America (after Stuiver and Braziunas, 1987)

$$\delta^{13}C = 0.32 \pm 0.06 \;(^0C, \text{July}) + b \qquad\qquad r = 0.81$$

$$\delta^{13}C = - \, 0.060 \pm 0.011 \;(\%, \text{RH}) + c \qquad\qquad r = 0.81$$

Abies alba, Black Forest (Lipp *et al.*, 1991)

$$\delta^{13}C = 0.33 \;(\text{T}, \, ^0C, \text{August}) - 26.2^0/_{00} \qquad\qquad r = 0.72$$

$$\delta^{13}C = - \, 0.11 \;(\text{RH}, \%, \text{August}) + 2.4^0/_{00} \qquad\qquad r = - \, 0.83$$

$$\delta^{13}C = - \, 0.0046 \;(\text{P}, \text{mm}, \text{August}) - 21.0^0/_{00} \qquad\qquad r = - \, 0.68$$

Pinus Coulteri, San Dimas Experimental Forest, California, USA (Feng and Epstein, 1995)

$$\delta^{13}C = -21.4 - 1.04\exp(\,0.02 \;(\text{Year} - 1940)) + 2.25 \; \exp(-0.04\text{P})$$

Taiwan fir, Southern Taiwan (Sheu *et al.*, 1995)

$$\delta^{13}C = - \, 0.46 \;(\text{T}, \, ^0C) - 20.22^0/_{00} \qquad\qquad r = 0.562$$

where $\delta^{13}C$ and T are three year running averages of $\delta^{13}C$ values and mean May-October temperature.

Tamarix jordanis, Israel (Lipp *et al.*, 1996)

$$\delta^{13}C = - \, 0.23(\text{RH}, \%) - 12.23^0/_{00} \qquad\qquad r^2 = 0.96$$

For many years, it has been recognized that trees show different behavior during early growth than when more mature. The $\delta^{13}C$ values of early tree ring cellulose increase with age (e.g. Feng and Epstein, 1995; also this thesis). This can be ascribed to the canopy effect whereby CO_2 produced from decaying litter with more negative $\delta^{13}C$ values is used in photosynthesis. The length of this stage, which can be as large as 50

years, depends on the surrounding plant density and air turbulence. The effects are minimized for tree growth in an environment with lower plant density and high turbulence. Shiu *et al* (1995) pointed out that the response of tree-ring $\delta^{13}C$ to climatic and/or environmental changes must be performed on trees during stable growth. They reasoned that the $\delta^{13}C$ values may be affected by the canopy effect during juvenile growth and a stomatal conductance reduction with tree age.

Prior to this thesis, it appears that researchers have not divided tree ring records into stages on the basis of stable isotope and other data. It became clear from the $\delta^{13}C$ values of cellulose of *Tamarix aphylla* from Death Valley, California, and their relationships with other parameters, that the tree could be best described in terms of three different growth stages: Stage I (1944-1946), Stage II (1947-1967), and Stage III (1967-1992). These stages are consistent with those of Yang *et al* (1996) which are based on the $\delta^{34}S$ values of tree rings from the same trunk. Furthermore, measured values of parameters in this thesis suggest that Stage III should be separated into three intervals (IIIa, IIIb, IIIc). A re-examination of the trends of $\delta^{34}S$ values for total sulfur of the tree ring (Fig. 5.1) confirms the appropriateness of this further sub-division.

The high frequency variations in the measured $\delta^{13}C$ values of cellulose can be explained by the changes in the amount of precipitation, whereas the long term trend is explained by the changes of the $\delta^{13}C$ value and concentration of atmospheric CO_2. The latter effect on the measured $\delta^{13}C$ values can be corrected by accumulative addition of $0.044^0/_{00}$ per year. This was done prior to comparison of the carbon isotope data with other parameters.

Correlations are found between the five year running averages of the corrected $\delta^{13}C$ values and precipitation:

II $\delta^{13}C_{\text{5-ave}} = (0.35 \pm 0.06)\,P_{\text{5-ave}} - (26.27 \pm 0.24)$ $R^2 = 0.68$ (6.1)

IIIa $\delta^{13}C_{\text{5-ave}} = (0.14 \pm 0.04)\,P_{\text{5-ave}} - (25.39 \pm 0.23)$ $R^2 = 0.71$ (6.2)

IIIb $\delta^{13}C_{\text{5-ave}} = (-\,0.44 \pm 0.07)\,P_{\text{5-ave}} - (20.24 \pm 0.45)$ $R^2 = 0.84$ (6.3)

IIIc $\delta^{13}C_{\text{5-ave}} = (-\,0.80 \pm 0.09)\,P_{\text{5-ave}} - (18.58 \pm 0.50)$ $R^2 = 0.97$ (6.4)

Correlations between ring width and precipitation are:

IIIa $RW_{\text{5-ave}} = (0.34 \pm 0.05)\,P_{\text{5-ave}} - (0.59 \pm 0.33)$ $R^2 = 0.87$ (6.5)

IIIb $RW_{\text{5-ave}} = (-\,5.67 \pm 1.32)\,P_{\text{5-ave}} + (48.02 \pm 8.67)$ $R^2 = 0.70$ (6.6)

IIIc $RW_{\text{5-ave}} = (-\,14.37 \pm 6.18)\,P_{\text{5-ave}} - (87.89 \pm 33.94)$ $R^2 = 0.73$ (6.7)

and correlations for $\delta^{13}C$ and ring width are:

IIIa $RW_{\text{5-ave}} = (1.81 \pm 0.46)\,\delta^{13}C_{\text{5-ave}} + (45.93 \pm 11.16)$ $R^2 = 0.73$ (6.8)

IIIb $RW_{\text{5-ave}} = (13.12 \pm 1.73)\,\delta^{13}C_{\text{5-ave}} + (314.59 \pm 40.02)$ $R^2 = 0.88$ (6.9)

IIIc $RW_{\text{5-ave}} = (18.52 \pm 6.51)\,\delta^{13}C_{\text{5-ave}} + (434.76 \pm 149.58)$ $R^2 = 0.80$ (6.10)

Comparison of the above equations with those at the beginning of this chapter suggests that the quality of the data of this study are comparable to those reported by others in the literature.

During Stage II, most roots of *Tamarix aphylla* are in the vadose zone. The main water source is the local precipitation. The stomatal apertures should be sensitive to the amount of precipitation during this stage since the tree is under water stress (drought

stress). It is concluded from the current study that the ratio of CO_2 assimilation rate, A, to stomatal conductance, g, increases with the amount of precipitation during this stage.

Groundwater is the main water source for the tree during Stage III. Since there is enough water available for the tree growth, the stomatal aperture size does not change much with the amount of precipitation. So g can be considered to be constant during the intervals IIIb and IIIc, whereas interval IIIa could be considered to be transitional between Stage II and IIIb. Calculations in Section 5.4 suggest that the stomatal aperture size increases by a factor of 6 to 10 in going from Stage II to IIIb. The different slopes for equations 5.4 and 5.5 corresponding to intervals IIIb and IIIc may be due to heterogeneous stomatal behaviors as described for many species by Mott et al. (1991).

In summary, one can conclude that this particlar *Tamarix aphylla* responded differently during successive growth stages. Multiple parameters ($\delta^{13}C$ and $\delta^{18}O$ values of cellulose, ring width, $\delta^{34}S$ values of tree rings, and local precipitation) were used to deduce the history of the tree's behavior. Water availability was a major factor in influencing the tree's response to various parameters. It was concluded by several arguments that the source of water changed from being solely vadose for the younger tree to dominantly groundwater during later stages.

References

Baum B. R. (1978) *The Genus Tamarix*. The Israel Academy of Sciences and Humanities, Jerusalem.

Berry J. A., Osmond C. B., and Lorimer G. H. (1978) Fixation of ^{18}O during photorespiration. *Plant Physiol*. **62**, 739-742.

Bender, M. M. (1968) Mass spectrometric studies of carbon-13 variations in corn and other grasses. *Radiocarbon* **10**, 468-472.

Bender, M. M. (1971) Variations in the $^{13}C/^{12}C$ ratios of plants in relation to the pathway of photosynthetic carbon dioxide fixation. *Phytochemistry* **10**, 1239-1244.

Bigeleisen, J. (1949) The relative reaction velocities of isotopic molecules. *J. Chem. Phys.* **17**, 675-678.

Bigeleisen, J. and Mayer, G.M. (1947). Calculation of equilibrium constants for isotopic exchange reactions. *J. Chem. Physics.* **15**. No. 5, 261-267.

Brenninkmeijer, C.A.M. and Mook, W.G. (1981) A batch process for direct conversion of organic oxygen and water to CO_2 for $^{18}O/^{16}O$ analysis. *Int. J. Appl. Rad. Isot.* **32**, 137-141.

Burk R. L. and Stuiver M. (1981) Oxygen isotope ratios in trees reflect mean annual temperatures, and humidity. *Science* **211**, 1417-1419.

Cowan I. R. (1977) Stomatal behavior and environment. *Advances in Botanical Research* **4**, 117-228.

Craig, H. (1953). The geochemistry of the stable carbon isotopes. *Geochim. Cosmochim. Acta* **3**, 53-92.

Deines P. (1980) The isotopic composition of reduced organic carbon. In *Handbook of Environmental Isotope Geochemistry* (ed. P. Fritz and J. Ch. Fontes), pp. 329-406. *The Terrestial Environment A*. **Vol. 1**, Elsevier.

Deleens E., Ferhi A., and Queiroz O. (1983) Carbon isotope fractionation by plants using the C4 pathway. *Physiol. Veg.* **21**, 897-905.

DeNiro M. J. and Epstein S. (1979) Relationship between oxygen isotope ratios of terrestrial plant cellulose, carbon dioxide and water. *Science* **204**, 51-53.

DeNiro M. J. and Epstein S. (1981) Isotope composition of cellulose from aquatic organisms. *Geochim. Cosmochim. Acta*, **42**, 495-506.

Dequasie, H. L. and Grey, D. C. (1970) Stable isotopes applied to pollution studies. *Mer. Lab.*, Dec. 1970, pp. 19-27.

Edwards, T. W. D., W. M. Buhay, R. J. Elgood, and H. B. Jiang (1994) An improved nickel-tube pyrolysis method for oxygen isotope analysis of organic matter and water. *Chemical Geology* **114**, 179-183.

Ehleringer J. R. (1989) Carbon isotope ratios and physiological processes in aridland plants. In *Stable Isotopes in Ecological Research* (ed. R. W. Rundel et al.), pp. 41-54. *Ecological Studies* **68**, Springer-Verlag.

Epstein S., Thompson P., and Yapp C. J. (1977) Oxygen and hydrogen isotopic ratios in plant cellulose. *Science* **198**, 1209-1215.

Epstein, S., C. J. Yapp, and J. H. Hall (1976) The determination of D/H ratios of non-exchangeable hydrogen in cellulose extracted from aquatic and land plants. *Earth planet. Sci. Letters* **30**, 241-51.

Eyring H. (1935) The activated complex in chemical reactions. *J. Chem. Phys.* 107-116.

Farmer, J. G. and Baxter, M. S. (1974) Atmospheric carbon dioxide levels as indicated by the stable isotope record in wood. *Nature* **247**, 273-275.

Farquhar G.D. (1983) On the nature of carbon isotope discrimination in C_4 species. *Aust. J. Plant Physiol.* **10**, 205-26.

Farquhar G. D., O'Leary M. H., and Berry J. A. (1982) On the relationship between carbon isotope discrimination and the intercellular carbon dioxide concentration of leaves. *Aust. J. Plant Physiol.* **9**, 121-137.

Farquhar G. D., and von Caemmerer S. (1982) Modelling of photosynthetic response to environmental conditions. In Physiological Plant Ecology 11 (Eds. O. L. Lange, P. S. Nobel, C. B. Osmond and H. Ziegler) *Encycl. Plant Physiol.* New series. **Vol 12B**, (Springer-Verlag: Heidelberg).

Farquhar, G. D., von Caemmerer, S., and Berry, J. A. (1980). A biochemical model of photosynthetic CO_2 assimilation in leaves of C_3 species. *Planta* **149**, 78-90

Farquhar G. D., Hubick K. T., Condon A. g., and Richards R. A. (1989a) Carbon isotope fractionation and plant water-use efficiency. In *Stable Isotopes in Ecological Research* (ed. R.W. Rundel et al.), pp. 21-40. Ecological Studies 68, Springer-Verlag.

Farquhar G.D., Ehleringer J.R., and Hubick K. T. (1989b) Carbon isotope discrimination and photosynthesis. *Annu. Rev. Plant. Physiol. Plant Mol. Biol.* **40**, 503-537.

Feng Xiaohong and Epstein S. (1995) Carbon isotopes of trees from arid environments and implications for reconstructing atmospheric CO_2 concentration. *Geochim. Cosmochim. Acta* **59**, 2599-2608.

Ferhi A. and Letolle R. (1977) Transpiration and evaporation as the principal factors in oxygen isotope variations of organic matter in land plants. *Physiol. Veg.* **15**, 363-370.

Freyer, H. D. and Wiesberg, L. (1973) ^{13}C- decrease in modern wood due to the large-scale combustion of fossil fuels. *Naturwissenschaften* **60**, 517-518.

Freyer, H. D. and Wiesberg, L. (1975) Anthropogenic carbon-13 decrease in atmospheric carbon dioxide as recorded in morden wood. In: *Isotope Ratios as Pollutant Source and Behavior Indicators*. IAEA, Vienna, pp. 49-62.

Friedli H., Lötscher H., Oeschger H., Seigenthaler U., and Stauffer B. (1986) Icecore record of the $^{13}C/^{12}C$ ratio of atmospheric CO2 in the past two centuries. *Nature* **324**, 237-238.

Galimov, E. M. (1976) Variations of the carbon cycle at present and in the geological past. In: J. O. Nriagu (Editor), *Environmental Biogeochemistry, 1. Carbon , Nitrogen, Phosphorous, Sulfur and Selenium Cycles*. pp. 3-11.

Gonfiantini R., Gratziu S., and Tongiorgi E. (1965) Oxygen isotopic composition of water in leaves. pp. 405-410. In *Isotope and Radiation in Soil-Plant-Nutrition Studies*. International Atomic Energy Commission, Vienna.

Gray, J. and P. Thompson (1976) Climatic information of $\delta^{18}O$ and δD in tree rings. *Nature, Lond.* **271**, 93-4.

Gray, J. and P. Thompson (1977) Climatic information from O^{18}/O^{16} analysis of cellulose, lignin and whole wood from tree rings. *Nature, Lond.* **270**, 708-9.

Greitner, C. S., Winner, W. E. (1988) Increases in $\delta^{13}C$ values of radish and soybean plants caused by ozone. *New Phytol.* **108**, 489-94.

Grinsted, M. J., A. T. Wilson, and C. W. Ferguson (1979) $^{13}C/^{12}C$ ratio variations in *Pinus longaeva* (Bristlecone Pine) cellulose during the last millennium. *Earth Planet. Sci. Letters* 42, 251-253.

Guy, R. D., Reid, D. M. and Krouse, H.R. (1980) Shifts in carbon isotope ratios of two C_3 halophytes under natural and artificial conditions. *Oecologia (Berlin)* 44, 241.

Guy R.D., Warner P.G., and Reid D.M. (1989) Stable carbon isotope ratio as an index of water-use efficiency in C_3 holophytes - possible relationship to strategies for osmotic adjustment. In *Stable Isotopes in Ecological Research* (ed. R.W. Rundel et al.), pp. 55-75. *Ecological Studies* 68, Spring-Verlag.

Green, J. W. 1963. Wood Cellulose. *Methods in Carbohydrate Chemistry, Volume III,Cellulose*. 9-21.

Hagemeyer J. and Waisel Y. (1989) Influence of NaCl, $Cd(NO_3)_2$ and air humidity on transpiration of *Tamarix aphylla*. *Physiol. Plant* 75, 280-284.

Hamilton J. K., and Quimby G. R. (1957) The extractive power of lithium, sodium, and potassium hydroxide solutions for the hemicelluloses associated with wood cellulose and holocellulose from Western Hemlock. *Tappi*, **Vol. 40, No. 9**, 781-786.

Hattersley P. W. (1982) $\delta^{13}C$ values of C_4 types in grass. *Aust. J. Plant Physiol.* 9, 139-54.

Hunt Charles B. (1975) *Death Valley: Geology, Ecology, Archaeology*. University of California Press.

Jasen, H. S. (1962) Depletion of carbon-13 in young Kauri trees. *Nature* 196, 84-85.

Keeling, C. D. (1958) The concentration and isotopic abundances of atmospheric carbon dioxide in rural areas. *Geochim. Cosmochim. Acta* 13, 322-334.

Keeling J. E. (1989) Stable carbon isotopes in vernal pool aquatics of differing photosynthetic pathways. In *Stable Isotopes in Ecological Research* (ed. R.W. Rundel *et al.*), pp. 76-81. Ecological Studies 68, Springer-Verlag.

Keeling, C. D., Mook, W. M., Tans, P. P. (1979) Recent trends in the $^{13}C/^{12}C$ ratio of atmospheric carbon dioxide. *Nature* 277, 121-23.

Keeling C. D. *et al.* (1989) A three-dimensional mode of atmospheric CO_2 transport based on observed winds: 1. Analysis of observational data. In *Aspects of Climate Variability in the Pacific and the Western Americas* (ed. D. H. Perterson); *Geophys. Mono* **55**, 165-236.

LaMarche, V.C. (1973) Holocene climatic variations inferred from treeline fluctuations in the White Mountains, California. *Quat. Res.* **3**, 632-660.

Lesaint C, Merlivat L, Bricout J, Fontes J. C., and Gautheret R. (1974) Sur la composition en isotopes stables de l'eau de la tomate et du maïs. C. R. *Acad. Sci. Paris Ser.* D **278**, 2925-2930.

Libby, L. M. (1972) Multiple thermometry in paleoclimate and historic climate. *J. Geophys. Res.* **77**, 4310-17.

Lipp J., Trimborn P., Fritz P., Moser H., Becker B., and Frenzel B. (1991) Stable isotopes in tree ring cellulose and climatic change. *Tellus* **43B**, 322-330.

Lipp J., Trimborn P., Edwards T., Waisel Y., and Yakir (1996) Climatic effects on the $\delta^{18}O$ and $\delta^{13}C$ of cellulose in the desert tree *Tamarix jordanis*. *Geochim Cosmochim Acta* (Revised and resubmitted April, 1996).

Martin B., Bytnerowicz A., and Thorstenson Y. R. (1988) Effects of air pollutants ($\delta^{13}C$) of leaves and wood, and on leaf injury. *Plant Physiol.* **88**, 218-23.

Masle J. and Farquhar G. D. (1988) Effects of soil strength on the relation of water-use efficiency and growth to carbon isotope discrimination in wheat seedlings. *Plant Physiol.* **86**, 32-38.

Masle, J. and Passioura, J. B. (1987) Effects of soil strength on the growth of wheat seedlings. *Aust. J. Plant Physiol.* **14**, 6-20.

Mason, E. A., and Marrero, T. R. (1970). The diffusion of atoms and molecules. *Adv. At. Mol. Phys.* **6**, 155-232.

Mayer, B., Legge, A. H., and Krouse, H. R. (1994) Private Communication of Unpublished Data, The University of Calgary.

Melander, L., and Saunders, W. H. (1979). *'Reaction Rates of Isotopic Molecules.'* (John Wiley and Sons: New York.)

Mook, W. G., Koopmans, M., Carter, A. F., Keeling, C. D. (1983) Seasonal, latitudinal, and secular variations in the abundance of isotopic ratios of atmospheric carbon dioxide. 1. Results from land stations. *J. Geophys. Res.* **88**, 10915-33.

Mott K. A., and Parkhurst D. F. (1991) Stomatal responses to humidity in air and helox. *Plant, Cell and Environment* **14**, 509-515.

O'Leary, M. H. (1978). Heavy atom isotope effects in enzyme-catalyzed reactions. In *'Transition States of Biochemical Processes'*. (Eds R. Gandour and R. L. Schowen.) pp. 285-316. (Plenum New York.)

O'Leary M. H. (1981) Carbon isotope fractionation in plants. *Phytochemistry* **20**,553-567.

O'Leary M. H. (1988) Carbon isotopes in photosynthesis. *BioScience* **3**, 328-336.

Park, R., and Epstein, S. (1960). Carbon isotope fractionation during photosynthesis. *Geochim Cosmochim. Acta* **21**, 110-26.

Pearman, G. I., R.J. Francey, and P.J.B. Fraser (1967) Climatic implications of stable carbon isotopes in tree rings. *Nature, Lond* **260**, 771-773.

Peisker M. (1985) Modelling carbon metabolism in C_3-C_4 intermediate species. 2. Carbon isotope discrimination. *Photosynthetica* **19**, 300-11.

Rebello, A. and Wagener, K. (1976) Evaluation of ^{12}C and ^{13}C data on atmospheric CO_2 on the basis of a diffusion model for ocean mixing. In: J. O. Nriagu (Editor), *Environmental Biogeochemistry, 1. Carbon, Nitrogen, Phosphoros, Sulfur and Selenium Cycles.* pp. 13-23.

Reibach P. H., Benedict C. R. (1977) Fractionation of stable carbon isotopes by phosphoenolpyruvate carboxylase from C_4 plants. *Plant Physiol.* **59**, 564-68.

Robinson T. W. (1965) Introduction, spread and areal extent of saltcedar (*Tamarix*) in the Western States. Geological Survey Professional Paper 491-A, United States Government Printing Office, Washington.

Seemann, J. R., Critchley, C. (1985) Effects of salt stress on growth, ion content, stomatal behavior and photosynthesis. *Oecologia* **69**, 305-8.

Sheu David D., Kou P., Chiu C.-H., and Chen M. J. (1996) Variability of tree-ring $\delta^{13}C$ in Taiwan fir: Growth effect and response to May-October temperatures. *Geochimica et Cosmochimica Acta* Vol. **60**, No. **1**, pp. 171-177.

Smith B. N. and Epstein S. (1970) Biogeochemistry of the stable isotopes of hydrogen and carbon in salt marsh biota. *Plant Physiol.* **46**, 738.

Smith, B. N. and Epstein, S. (1977) Two categories of $^{13}C/^{12}C$ ratios for higher plants. *Plant Physiol.* **47**, 380-384.

Sternberg L. and DeNiro M. J. (1983) Biogeochemical implications of the isotopic equilibrium fractionation factor between the oxygen atoms of acetone and water. *Geochim. Cosmochim. Acta* **47**, 2271-2274.

Sternberg L. and DeNiro M. J., and Keeley J.E. (1984) Hydrogen, oxygen and carbon isotope ratios of cellulose from submerged aquatic crassulacean acid metabolism and non-crassulacean acid metabolism plants. *Plant Physiol.* **76**, 68-70

Sternberg L. S. L., DeNiro M. J., Sloan M. E., and Black C. C. (1986a) Compensation point and isotopic characteristics of C_3/C_4 intermediates and hybrids in *Panicum*. *Plant Physiol.* **80**, 242-245.

Sternberg L. S. L., DeNiro M. J., and Savidge R. A. (1986b) Oxygen isotope exchange between metabolites and water during biochemical reactions leading to cellulose synthesis. *Plant Physiol.* **82**, 423-427.

Stuiver M., and Braziunas T. F. (1987) Tree cellulose $^{13}C/^{12}C$ isotope ratios and climatic change. *Nature* **328**, 58-60.

Thomas, R. J. (1977) Wood: structure and chemical composition. *ACS symposium series Wood Technology: Chemical Aspects*, 1-23.

Tregunna, E. B., Smith, B. N., Berry, J. A. and Downton, W. J. S. (1970) Some methods for studying the photosynthetic taxonomy of the angiosperms. *Can. J. Bot.* **48**, 1209-1214.

Urey, H.C. (1947). The thermodynamic properties of isotopic substances. *J. Chem. Soc.* 562-581.

Yakir D., Issar A., Gat J., Adar E., Trimborn P., and Lipp J. (1994) ^{13}C and ^{18}O of wood from the Roman Siege rampart in Masada, Israel (AD 70-73): Evidence for a less arid climate for the region. *Geochima et Cosmochima Acta* **58**, 3535-3539.

Yang Wenbo, Spencer R. J., and Krouse H. R. (1996) Stable sulfur isotope hydrogeochemical studies using desert shrubs and tree rings, Death Valley, California, USA. *Geochima et Cosmochimica Acta* (in press).